Evolution of Carbonation in Cement Blends with Incorporation of Activated Low-Kaolinite mix layer Clays: Insights into Hydrate phase assemblage, C-A-S-H Structure and Porosity

Sahar Iftikhar[a], Ingemar Löfgren[a,b], Joao Figueira[c], Helen Jansson[a], Jelke Dijkstra[a] and Arezou Babaahmadi[a]

(a) Chalmers University of Technology, Department of Architecture and Civil Engineering, Gothenburg, Sweden

(b) Thomas Concrete, Gothenburg, Sweden

(c) Department of Chemistry, Scilife Lab, Umeå University, Umeå, 90187, Sweden

Corresponding author: Sahar Iftikhar

Authors	E-Mail	Postal address
Sahar Iftikhar	Sahar.iftikhar@chalmers.se	Chalmers University of Technology Department of Architecture and Civil Engineering SE-412 96 Gothenburg, Sweden
Ingemar Löfgren	ingemar.lofgren@c-lab.se	C-lab, Thomas Concrete Group Ringogatan 12, SE-417 07 Gothenburg, Sweden
Joao Figueira	joao.figueira@umu.se	Department of Chemistry, Scilife Lab, Umeå University, Umeå, 90187, Sweden
Helen Jansson	helen.jansson@chalmers.se	Chalmers University of Technology Department of Architecture and Civil Engineering SE-412 96 Gothenburg, Sweden
Jelke Dijkstra	jelke.dijkstra@chalmers.se	Chalmers University of Technology Department of Architecture and Civil Engineering SE-412 96 Gothenburg, Sweden
Arezou Baba Ahmadi	arezou.ahmadi@chalmers.se	Chalmers University of Technology Department of Architecture and Civil Engineering SE-412 96 Gothenburg, Sweden

Preprint not peer reviewed

This preprint research paper has not been peer reviewed. Electronic copy available at: https://ssrn.com/abstract=6205146

Evolution of Carbonation in Cement Blends with Incorporation of Activated Low-Kaolinite mix layer Clays: Insights into Hydrate phase assemblage, C-A-S-H Structure and Porosity

Sahar Iftikhar[a], Ingemar Löfgren[a,b], Joao Figueira[c], Helen Jansson[a], Jelke Dijkstra[a] and Arezou Babaahmadi[a]

(a) Chalmers University of Technology, Department of Architecture and Civil Engineering, Gothenburg, Sweden

(b) Thomas Concrete, Gothenburg, Sweden

(c) Department of Chemistry, Scilife Lab, Umeå University, Umeå, 90187, Sweden

Highlights

- Carbonation mechanisms in low-kaolinite 2:1 clay binder differ fundamentally from OPC and LC³ systems.
- Aluminum incorporation and polymerization of C–A–S–H govern resistance to deep decalcification.
- AFm phases provide intermediate buffering once portlandite is depleted in clay-rich binders.
- Carbonation-induced pore coarsening is controlled by hydrate chemistry and gel maturity rather than solely CH availability.
- Extended curing enhances carbonation resistance due to evolution of C-A-S-H despite lower portlandite content.

Abstract

Low-kaolinite clays represent a globally abundant resource for reducing clinker content, yet their durability under carbonation remains poorly understood. This study examines the carbonation behavior of a 2:1 mixed-layer clay blended binder (30% replacement of OPC), focusing on changes in hydrate assemblage, C–A–S–H structure, and pore network. To isolate carbonation effects, drying was decoupled from CO_2 exposure, and the influence of curing duration was assessed to account for the slow pozzolanic reaction. Results show that carbonation follows the typical sequence of CH depletion, AFm/AFt destabilization, and C–A–S–H decalcification, but its severity depends strongly on curing. Extended curing promoted AFm formation, increased Al incorporation into C–A–S–H, and densified the microstructure, reducing decalcification (Ld ≈ 34% vs. 92% in short-cured samples) and limiting pore coarsening. These findings highlight that carbonation resistance in low-kaolinite systems is governed primarily by hydrate chemistry and

Preprint not peer reviewed

This preprint research paper has not been peer reviewed. Electronic copy available at: https://ssrn.com/abstract=6205146

microstructural maturity rather than portlandite content, underscoring the importance of curing protocols for durable implementation.

Keywords: low-kaolinite, carbonation, hydrate phase assemblage, C–A–S–H decalcification, pore structure evolution

1. Introduction

The growing focus on sustainable construction has driven increased interest in the use of supplementary cementitious materials (SCMs) as partial clinker replacements [1, 2], offering a practical way to lower emissions while maintaining comparable performance. As traditional SCMs such as fly ash and slag become increasingly scarce, attention has shifted towards more abundant resources, particularly clays and limestone, which can be sourced worldwide and activated through calcination to provide significant pozzolanic reactivity. This shift has driven the development of limestone–calcined clay systems (LC^3), which combine calcined clay and limestone to achieve high reactivity and reduce clinker content by up to 50% while maintaining mechanical and durability performance [3-9]. Much of the early LC^3 research has centered on calcined clays containing at least 40% kaolinite, as kaolinite readily transforms into highly reactive metakaolin upon calcination and promotes the formation of carboaluminate phases that enhance strength and durability. [10, 11]. The hydration and durability of the traditional SCMs as well as kaolinitic clays is well studied [12-17]. However, such high-kaolinite clays are not representative of the majority of global clay deposits, most global clay resources contain less than 40% kaolinite and are instead dominated by a mix of less reactive 2:1 clay minerals and other non-clay minerals often considered impurities [18] . The widespread occurrence of these clays makes them promising candidates for future SCMs, but their full potential pertaining to durability is not yet explored. Several studies have investigated the activation and hydration of 2:1 clays [19-24] while only a few have focused on their durability aspects [25, 26].

Carbonation is a degradation mechanism that occurs across all exposure classes and often governs the long-term performance of cementitious materials. While it has been extensively studied in the context of reinforcement depassivation, its influence on the hydrated cementitious matrix remains insufficiently explored in modern low-clinker and clay-based binders. This process is one of the most influential physicochemical processes affecting both the phase assemblage and pore structure of hydrated binders. When atmospheric CO_2 diffuses through the pore network, it reacts with calcium-bearing phases such as portlandite (CH), calcium silicate hydrate (C–S–H), unhydrated clinker (C_3S and C_2S), and hydrated aluminate phases including AFm and AFt [27-29]. These reactions predominantly produce calcite [30, 31], with minor occurrences of other calcium carbonate polymorphs such as aragonite and vaterite [15, 17, 32-34]. However, the hydrate assemblage produced by low-kaolinite 2:1 clays differs fundamentally from that

Preprint not peer reviewed

This preprint research paper has not been peer reviewed. Electronic copy available at: https://ssrn.com/abstract=6205146

of LC^3. Because of their limited kaolinite content, these clays supply less reactive aluminium, resulting in negligible AFm formation with reduced buffer capacity. Instead, most of the aluminium becomes incorporated into the C-A-S-H. Such differences in hydrate chemistry suggest that 2:1 clay–based binders may carbonate through pathways different from both OPC and LC^3 systems.

The mechanisms governing carbonation are strongly influenced by binder chemistry. These mechanisms, although reasonably well-understood for OPC, become even more intricate in blended binders. In ordinary Portland cement (OPC), carbonation is governed primarily by the reaction of CO_2 with portlandite [28], however, in blended binders, particularly those with lower-calcium content, such 2:1 calcined clays, the limited CH availability due to dilution and pozzolanic reactions [35] shifts carbonation toward the C–S–H phase. The carbonation of low-Ca/Si C–S–H leads to the formation of amorphous silica gel, where the extent of shrinkage or densification depends on the Ca/Si ratio and the amount of bound water within the gel structure [27, 36]. The loss of bound water during carbonation can trigger local shrinkage, resulting in pore coarsening instead of refinement [37]. This behaviour is especially relevant for binders with illitic or smectitic clays, which tend to form low-Al, low-Ca/Si C-A-S-H, possessing distinct chemistry and stability compared to OPC. Consequently, the combined effects of reduced portlandite availability and altered hydrate composition are expected to strongly influence phase assemblage.

In addition, carbonation drives dissolution–precipitation processes that modify microstructure and transport properties. In OPC systems, carbonation of CH commonly leads to pore refinement due to the larger molar volume of $CaCO_3$ [27, 29, 30] whereas carbonation of C–S–H follows a more complex decalcification–polymerization pathway that forms amorphous silica gel [3,10–12]. The resulting molar volume change depends strongly on the initial Ca/Si ratio, the water content of the silica gel, and the degree of hydration [38, 39]. Consequently, carbonation can both refine or coarsen the microstructure depending on the initial Ca/Si ratio, water content in the silica gel, and the degree of hydration [27].

Not only the binder composition but also the moisture state of the material is decisive in determining carbonation behavior. Even in the absence of CO_2, exposure to moderate relative humidity can significantly alter cement paste microstructure. Studies have shown that drying at 55–70% RH leads to gradual coarsening of the pore network due to collapse of fine pores, while the overall porosity remains relatively constant [35, 40]. Such microstructural changes influence transport properties [17, 38, 41, 42] and therefore affect how carbonation proceeds. Moreover, the moisture content of the paste itself plays a decisive role in carbonation as at very high saturation, CO_2 ingress is hindered by water-filled pores [43], while at low saturation the lack of water limits CO_2 dissolution. Thus, drying not only modifies the pore structure but also conditions the balance between gas

Preprint not peer reviewed

This preprint research paper has not been peer reviewed. Electronic copy available at: https://ssrn.com/abstract=6205146

transport and chemical reaction, ultimately shaping the kinetics and mechanisms of carbonation. In addition, studies have shown that temperature [44-46], and CO_2 concentration [32, 47-49] have an impact on carbonation.

Based on our previous work on the activation and hydration behavior of low-kaolinite 2:1 clays by Hazarika et al. [23, 24], the present study examines how such binders respond to carbonation. Specifically, we examine (i) changes in hydrate phase assemblage, (ii) the structure and chemistry of C–A–S–H, and (iii) the evolution of pore size distribution. To isolate carbonation effects, they are separated from drying-induced changes and evaluated by how curing duration influences microstructure and subsequent carbonation behavior by a multi-technique approach. X-ray diffraction (XRD) was used to identify the evolution of the hydrate phase assemblage, while Thermogravimetric analysis (TGA) provided quantitative insight into carbonate formation and CH consumption. ^{29}Si and ^{27}Al solid-state nuclear magnetic resonance (NMR) analyses were employed to examine changes in the C-A-S-H structure, including silicate polymerization and aluminum incorporation. Mercury intrusion porosimetry (MIP) was performed to assess the pore structure and its refinement or coarsening under both drying and carbonation conditions.

2. Materials

The materials used in this study are Ordinary Portland Cement (OPC) and Calcined Clay (C). The chemical composition obtained from inductively coupled plasma atomic emission spectroscopy (ICP-AES) of OPC and calcined clay is given in

Table 1. The primary blend investigated in this study incorporates 30% clay as a replacement for OPC. In earlier work [24], several replacement levels were assessed, and while higher substitutions also produced strengths comparable to OPC, the 30% level was chosen for the present study. This choice, we believe, provides a balanced system with sufficient pozzolanic reactivity while retaining an adequate amount of portlandite (CH), which is a critical factor for studying carbonation mechanisms. Mortars were cast to study pore structure evolution and pastes were used for phase assemblage and C-S-H modifications. The binder-to-aggregate ratio was kept at 1:3, and the water-to-cement ratio was 0.50. The paste samples were rotated for 24 hours after casting to minimize the risk of segregation between the binders and water. OPC was cured for 28 days, whereas for clay two curing regimes of 28 days (30C) and 100 days (30CLC) was employed in order to investigate the effect of curing time on evolution of carbonation. The binder compositions and curing durations are summarized in Table 2. They were then subjected to pre-carbonation curing at a temperature of (20 ± 2)°C and a relative humidity of (57 ± 3)% for 14 days. Following this, the samples were exposed to carbon dioxide in a carbonation chamber with a carbon dioxide concentration of (3.0 ± 0.5)% by volume, also maintained at (20 ± 2)°C temperature and (57 ± 3)% relative humidity, in accordance with EN 12390-12:2020 [50]. To decouple drying effects from carbonation, companion

Preprint not peer reviewed

This preprint research paper has not been peer reviewed. Electronic copy available at: https://ssrn.com/abstract=6205146

samples of each mix were kept under identical temperature and relative humidity conditions i.e. (20 ± 2) °C and (57 ± 3) % RH without CO_2 exposure. Sample designations are defined as follows: MR refers to month-dried reference samples, MC refers to month-carbonated samples, and Undried samples which were analyzed in the hydrated state immediately after curing

The planned carbonation durations were 1, 2, 4, and 6 months. At each interval, samples were taken out of the carbonation chamber and saw-cut into 1 cm x 2 cm size approximately, and the carbonation depth was measured using a pH indicator spray. Following this, the samples underwent a combined solvent exchange and vacuum oven drying procedure. The samples were immersed in isopropanol for 5 days, with the solvent replaced daily to ensure complete water removal. Subsequently, the samples were dried in vacuum oven at 30 °C for 2 days. Once these steps were completed, the samples were prepared for specific pore structure analysis, C-S-H structure evolution and hydrate phase assemblage experiments. For Nuclear Magnetic Resonance (NMR), Thermogravimetric Analysis (TGA) and X-ray Diffraction (XRD), the paste samples are manually ground in a mortal and then sieved to achieve a particle size of less than 75 µm. These samples were stored in a vacuum-sealed desiccator until the XRD analysis was conducted. For Mercury Intrusion Porosimetry (MIP), the samples are cut into pieces measuring 2-8 mm before being sent for testing.

Table 1. Chemical composition of ordinary Portland cement and calcined clay

wt.%	SiO_2	Al_2O_3	Fe_2O_3	CaO	MgO	Na_2O	K_2O	TiO_2	SO_3	MnO	P_2O_5	SrO	BaO	LOI	Total
OPC	19.60	4.50	3.00	62.20	3.50	0.27	1.01	-	3.50	-	-	-	-	2.50	100.08
C	51.80	18.35	9.55	1.32	3.34	1.70	4.42	0.87	-	0.11	0.15	0.01	0.08	8.15	99.86

Table 2. Binder composition and curing durations

Sample Designation	SCM	Curing
OPC	-	28 days
30C	30% Clay	28 days
30CLC	30% Clay	100 days

Preprint not peer reviewed

This preprint research paper has not been peer reviewed. Electronic copy available at: https://ssrn.com/abstract=6205146

3. Methods

3.1. X-ray diffraction

XRD was conducted on carbonated as well as uncarbonated pastes, to study the effect of carbonation on hydrate phase assemblage of OPC and 30C blends. Bruker D8 Discover was used with 2 theta ranges 5^o – 60^o with step size 0.02^o, time per step 0.8 s. To identify the phases DIFFRAC.EVA V5.2 software was used.

3.2. Thermogravimetric Analysis

Thermogravimetric analyses were performed on a Mettler Toledo TGA/DSC 3+ under nitrogen purge (flow 50 mL min^{-1}). Approximately 8–10 mg of powdered sample was loaded into alumina pans and heated from 20 to 1000 °C at a constant heating rate of 10 °C min^{-1}. Using STARe v20 mass losses were evaluated over 40–520 °C (hydrate water), 400–500 °C (CH), and 520–820 °C ($CaCO_3$). CH and $CaCO_3$ contents were calculated from respective mass losses using stoichiometric factors and expressed as % weight relative to the mass at 520 °C. The deconvolution of the TGA curves was performed using Origin software, and the amounts of ettringite and AFm were quantified by integrating the area under the corresponding mass-loss peaks; a representative example of the deconvolution procedure is provided in the Supplementary Data. Ettringite was evaluated using the center-of-gravity region between 80–90 °C, while AFm was quantified from the 110 – 140 °C and 230 – 260 °C interval.

3.3. ^{29}Si and ^{27}Al Nuclear Magnetic Resonance (NMR)

The modifications in C-S-H structure due to carbonation were studied by magic angle spinning (MAS) Nuclear Magnetic Resonance (NMR). All ^{29}Si and ^{27}Al MAS NMR experiments were conducted at 298 K using a Bruker 4 mm MAS BB/1H probe. Powdered samples (~0.09–0.12 g) were packed into 4 mm zirconia rotors for analysis. The ^{29}Si MAS NMR spectra was acquired using high-powered proton decoupling (HPDEC) with a spinning rate of 7.5 kHz. A total of 2500 scans were accumulated using a 3 µs pulse (~45° flip angle) and a relaxation delay of 30 s. The 27Al HPDEC MAS NMR spectra was obtained at a spinning rate of 11 kHz with 2048 scans, using a 4µs pulse (~65° flip angle) and a relaxation delay of 0.8 s. For both nuclei SPINAL64 proton decoupling was employed with a 1H-field strength of 50 kHz [51].

Peak deconvolution was performed using the Interactive Peak Fitting (IPF) software, version 13.2.0.0 [52], which operates within the MATLAB environment (version 2024b). A combination of Lorentzian and Gaussian functions was used for curve fitting. The software automatically determined the optimal mixing ratio between the two profiles during the fitting process based on the number of peaks manually selected by the user. The relative intensities of Q^n species and structural characteristics of C-S-H phase were evaluated from the deconvoluted ^{29}Si MAS NMR spectra. The structural parameters of C-

Preprint not peer reviewed

This preprint research paper has not been peer reviewed. Electronic copy available at: https://ssrn.com/abstract=6205146

S-H average chain length (CL), silicate chain length (CL_Si) and Al/Si molar ratio for Al are incorporated into silicate chains of the C-S-H structure using following equations adapted from [53].

$$CL = \frac{2[\mathrm{Q}^1 + \mathrm{Q}^2 + \frac{3}{2}\mathrm{Q}^2(1Al)]}{\mathrm{Q}^1} \quad (1)$$

$$CL\_Si = \frac{2[\mathrm{Q}^1 + \mathrm{Q}^2 + \mathrm{Q}^2(1Al)]}{\mathrm{Q}^1 + \mathrm{Q}^2(1Al)} \quad (2)$$

$$\frac{Al}{Si} = \frac{\mathrm{Q}^2(1Al)}{2[\mathrm{Q}^1 + \mathrm{Q}^2(1Al) + \mathrm{Q}^2]} \quad (3)$$

The level of decalcification *(L_d)* was evaluated by comparing the relative intensities related to C-S-H (Q_b^n and Q_a^n) before and after carbonation respectively using the following equation and is given in Figure 5(e) [54]:

$$L_d = \left(1 - \frac{Q_a^1 + Q_a^2}{Q_b^1 + Q_b^2}\right) x\ 100 \quad (4)$$

Semi quantitative degree of silicate polymerization is simply calculated by using the following equation adopted from [54] and is given in Figure 5(f).

$$\frac{B}{A} = \left(\frac{Q^3 + Q^4}{Q^1 + Q^2}\right) \quad (5)$$

3.4. Mercury Intrusion Porosimetry

Mercury intrusion porosimetry was performed using a Micromeritics AutoPore V 9620 instrument. The instrument is capable of applying pressures in the range of 0.001–414 MPa, corresponding to a calculated pore diameter range of approximately 0.003–800 μm. The pore diameter was calculated using the Washburn equation.

$$r = -\frac{2\gamma cos\theta}{P} \quad (6)$$

where *r* is the pore radius, γ is the surface tension of mercury (0.485 N·m⁻¹), θ is the contact angle (130°), and *P* is the applied pressure. The calculation assumes cylindrical pore geometry and non-wetting conditions, meaning that smaller pores require higher intrusion pressures. High-resolution data were collected with intrusion and extrusion volume precision better than 0.1 μL.

Preprint not peer reviewed

This preprint research paper has not been peer reviewed. Electronic copy available at: https://ssrn.com/abstract=6205146

4. Results and discussion

The following sections presents and discusses the results in relation to the research questions, aiming to provide a coherent and logically structured interpretation of the findings.

4.1. How does carbonation affect the hydrate phase assemblage in binders with incorporation of low kaolinite mix layer activated clays in comparison to traditional OPC systems?

The combined XRD–TGA analysis provides insight into how carbonation alters the hydrate phase assemblage. XRD patterns of OPC, 30C, and 30CLC pastes are shown in Figure 1(a, b & c). For each system, samples carbonated for 1, 2, 4, and 6 months are included alongside their respective uncarbonated reference samples at equivalent ages. Figure 2 illustrates the complementary TGA based quantification of CH (Figure 2a), hydrate water (Figure 2b), and calcite contents (Figure 2c) in OPC, 30C, and 30CLC pastes, comparing undried, reference (MR), and carbonated (MC) samples. In addition, Figure 3(a) illustrates how ettringite evolves under carbonation, whereas Figure 3(b) depicts the corresponding evolution of AFm.

4.1.1. Hydrate phase assemblage prior to carbonation

In Undried hydrated state OPC, 30C and 30CLC the major crystalline phases identified include portlandite (CH) at 2θ 18^{o} , 28.6° and 34 ^{o}[55, 56] , corresponding to the (001) and (002) crystallographic planes, respectively. Ettringite (Et) appeared at 2θ 9.1^{o} [55] and Afm phases commonly represented by monosulfoaluminate or hemicarboaluminate, are detected around 2θ 11.3° [55]. These peak positions confirm the presence of CH, AFt, and AFm in all three systems, and are consistent with hydrate assemblages reported for OPC [57] and LC^{3} binders [10, 58, 59].

TGA provides complementary quantitative information about the phase assemblage. In undried hydrated state, OPC showed highest portlandite content in comparison to 30C and 30CLC [60]. This reduced portlandite content in clay blended binders is attributed mainly to two factors. First, the dilution effect reduces the absolute amount of clinker in these blended systems, limiting the potential for portlandite formation. Second, the calcined smectite–illite clay exhibits significant pozzolanic reactivity, the reactive aluminosilicates consume CH as they react to form additional C–A–S–H gels [3, 61]. The CH contents of 30C and 30CLC are very similar, with only a slightly higher CH content observed in 30C. This small reduction in CH for 30CLC can be attributed to continued, but limited, pozzolanic reaction during the extended curing period, resulting in minor additional consumption of portlandite[23, 62]. This indicates that the majority of the pozzolanic reaction is already completed by 28 days of curing, such that prolonged curing does not lead to substantial further reductions in CH content. As noted in previous studies,

Preprint not peer reviewed

This preprint research paper has not been peer reviewed. Electronic copy available at: https://ssrn.com/abstract=6205146

calcined 2:1 layered aluminosilicates such as smectite and illite react with water and portlandite to form additional C–A–S–H with a lower Ca/Si ratio [30, 63, 64], which reduces the quantity and crystallinity of CH and AFm phases in the system. Although these clays exhibit slower pozzolanic kinetics than kaolinite [11], their reactivity persists over time. Consequently, extended curing in 30CLC primarily enhances the degree of hydration and promotes continued hydrate evolution and microstructural refinement, rather than significant additional CH consumption. The reduced formation of crystalline AFm phases can be attributed to the incorporation of Al into the C–A–S–H gel during ongoing hydrate development [24].

Hydrate water also varies among the systems, reflecting differences in their degree of hydration and enabling direct comparison between the binders. OPC exhibits the highest bound water, consistent with its higher degree of hydration. The 30C binder shows lower hydrate water, reflecting the limited hydration achievable after 28 days, whereas 30CLC contains a higher hydrate water content than 30C, approaching that of OPC and demonstrating the influence of prolonged curing.

The deconvoluted DTG signals reveal clear differences in aluminate hydrate distribution among the three systems. The largest ettringite (AFt) peak area is observed in 30C, consistent with active early-age aluminate hydrate formation. In contrast, 30CLC exhibits the highest AFm peak area, reflecting the expected progression of hydration due to prolonged curing, where part of the AFt has converted to AFm and additional aluminum has been incorporated into the C–A–S–H gel. OPC shows intermediate amounts of both AFt and AFm. These distinctions highlight how curing duration and pozzolanic reactions govern the evolution of aluminate hydrates even prior to drying or carbonation.

4.1.2. Effect of drying de-coupled from carbonation on hydrate phase assemblage

In the dried state, the XRD patterns of OPC, 30C, and 30CLC show that the characteristic reflections of the main hydrate phases including portlandite (CH), ettringite (AFt), and AFm appear at the same 2θ positions as in the undried samples. Drying does not introduce any new crystalline phases, indicating that the primary hydration products formed under sealed curing conditions remain stable and structurally preserved. Consistent with this observation, TGA analysis shows no measurable change in CH content upon drying, confirming that portlandite is not significantly affected by exposure to 20 °C and 57% RH. When exposed to drying, a slight reduction in hydrate water is observed at 1MR across all binders. This initial decrease is attributed to the removal of physically bound and weakly held gel water. It is well established that when the relative humidity drops below approximately 75–80%, hydration reactions effectively halt, limiting further bound-water development and influencing the measurable degree of hydration [40]. Beyond 1MR, the hydrate water content remains relatively stable at 2MR, 4MR, and

Preprint not peer reviewed

This preprint research paper has not been peer reviewed. Electronic copy available at: https://ssrn.com/abstract=6205146

6MR, indicating that the remaining bound water is structurally incorporated within the C–A–S–H and other hydrates and is therefore less sensitive to drying at the applied relative humidity.

4.1.3. Effect of carbonation coupled with drying on hydrate phase assemblage

Carbonation of OPC pastes leads to significant changes in the mineralogical composition, as reflected in the XRD patterns of the MC samples (Figure 1a). In carbonated OPC the main type of carbonation product formed is calcite at 2Θ = 29.4o. Upon exposure to carbon dioxide for 1 to 6 months the Figure 1(a), gradual calcite formation and CH depletion particularly in 4MC and 6MC can be observed. Although calcite is the major representative peak, weak shoulders or broad peaks appear in the 2θ range of 26.6° to 27.2°, which can be attributed to the formation of vaterite (110) and aragonite (111, 021) [65] in 4MC and 6MC samples suggesting that prolonged exposure to CO2 is facilitating the formation of polymorphs of calcite. Calcium carbonate is the principal reaction product of carbonation which can precipitate in three calcite polymorphs including calcite, aragonite and vaterite. Among these calcite is the most stable one whereas aragonite and vaterite are metastable phases that may gradually transform into calcite over time [30].

In comparison with OPC, the blended binder 30C exhibits a modified carbonation behavior as shown in Figure 1b, majorly because of lower initial CH content available and pozzolanic activity of clay. The primary CH peak at 2Θ = 18^{o} progressively becomes less intense with carbonation exposure from 1 to 6 months. The major calcite peak appears at 2Θ = 29.4^{o,} also secondary peaks emerge in the 24–30° 2θ range, which can be attributed to the formation of vaterite (e.g., 24.9° & 27.2°) and aragonite (e.g., 26.2° & 33.1°) simultaneously. Similar to 30C, carbonation exposure of 30CLC (Figure 1c) leads to a substantial attenuation of the portlandite (CH) reflections at 2θ 18.0° and 34.1°, with these peaks becoming barely distinguishable by 4MC and nearly absent at 6MC. On the other hand, in the case of OPC, CH peak is still visible even in 6-month carbonated sample. In addition to that, besides calcite 30CLC shows more prominent aragonite and vaterite peaks.

In case of 30C CH peak is nearly disappeared by 4 months of carbonation, which is attributed to insufficient hydration limited pozzolanic reactivity, leaving more unreacted CH and less refined microstructure making the system vulnerable to CO_2. In contrast the 30CLC system retained CH at 4 months. In the 30C and 30CLC systems, ettringite disappears after six months of carbonation, coinciding with the complete consumption of portlandite (CH). This simultaneous loss indicates that the pore solution pH has dropped below approximately 10, the threshold at which ettringite becomes unstable and decomposes under these conditions [30, 66].

Preprint not peer reviewed

This preprint research paper has not been peer reviewed. Electronic copy available at: https://ssrn.com/abstract=6205146

TGA results corroborate the XRD results and show the evolution of portlandite (CH) content during carbonation in the two binder systems investigated (Figure 2a). While CH consumption is observed in both systems, the carbonation kinetics differ substantially. In OPC, a significant reduction in CH is evident at 1MC; however, CH levels remain comparatively stable between 1MC and 4MC, indicating a sustained buffering capacity against carbonation. A further decrease in CH content is observed at 6MC. In contrast, the calcined-clay binder exhibits a more progressive and continuous reduction in CH with increasing carbonation duration. CH depletion occurs earlier in 30C, whereas prolonged curing in 30CLC delays, but does not prevent CH consumption, with complete depletion observed by 4MC in 30C and by 6MC in 30CLC. The earlier loss of CH in the calcined-clay systems results in a more rapid decline in pore solution alkalinity, thereby promoting earlier destabilization of AFt and AFm phases and advancing C–A–S–H decalcification relative to OPC.

With carbonation (1MC to 6MC), a gradual decrease in hydrate water (Figure 2b) was observed in all binders. This reduction results from the decalcification and destabilization of hydrates during carbonation, where bound water is released as hydrates convert into carbonate phases. The decrease was more pronounced in the calcined clay systems, particularly 30C, which had lower overall hydrate stability compared to OPC. Part of this water loss can also be attributed to the decomposition of ettringite, which becomes unstable under the lower pH conditions associated with carbonation.

The evolution of ettringite and AFm after six months of carbonation exposure is quantified in Figure 3a, and Figure 3b, respectively. After six months of carbonation (6MC), however, both AFt and AFm decrease sharply in all systems. In 30C and 30CLC, ettringite is almost completely consumed, and AFm is reduced to a minor fraction of its original quantity. The XRD patterns show that AFt reflections disappear almost entirely in these binders, and only OPC retains a faint ettringite signal after prolonged exposure. These observations are consistent with the known carbonation pathways of sulfoaluminate hydrates: ettringite carbonates to aragonite and an amorphous alumina–silica gel, AFm phases decalcify to calcite with an alumina-rich residue, and carbonation of C–A–S–H produces a mixture of aragonite and vaterite [67]. Accordingly, the emergence and intensification of aragonite and vaterite peaks in the 4MC and 6MC XRD patterns of the clay-blended binders reflect the progressive decomposition of AFt and AFm and the onset of C–A–S–H carbonation. The extent to which these phases decompose differs markedly between OPC and the calcined-clay binders. The much stronger depletion of AFt and AFm in 30C and 30CLC can be attributed to their lower initial CH content, which limits their pH-buffering capacity during carbonation. As CH is consumed earlier in these systems, the pore solution pH drops more rapidly, accelerating the destabilisation of sulfoaluminate hydrates and exposing C–A–S–H to carbonation sooner than in OPC. However, following the carbonation sequence described in RILEM TC 281-CCC, AFm and AFt carbonate after

Preprint not peer reviewed

This preprint research paper has not been peer reviewed. Electronic copy available at: https://ssrn.com/abstract=6205146

CH but before deep C–S–H decalcification [13]. Thus, the higher initial AFm and AFt contents in the calcined-clay binders especially in the more matured 30CLC system provide an intermediate carbonation “sink,” allowing these phases to react first and thereby delaying the onset of aggressive C–A–S–H decalcification. This mechanistic buffering effect is consistent with the NMR results presented in the next section, where earlier signatures of Si and Al polymerization appear in 30C than in 30CLC, indicating that the richer sulfoaluminate content in 30CLC affords temporary protection to the C–A–S–H gel during the early stages of carbonation.

In both binder systems, calcite formation shows an increasing trend with carbonation ages (Figure 2c). At 1, 2, and 4 months of carbonation, calcite formation in 30C is consistently higher than in both OPC and 30CLC. In contrast, 30CLC exhibits the lowest calcite content across almost all ages, which can be attributed to its denser pore structure and the reduced availability of CH for carbonation. By 6 months, however, OPC shows the highest calcite formation, reflecting its greater CO_2 uptake capacity at later ages due to the initially higher CH availability.

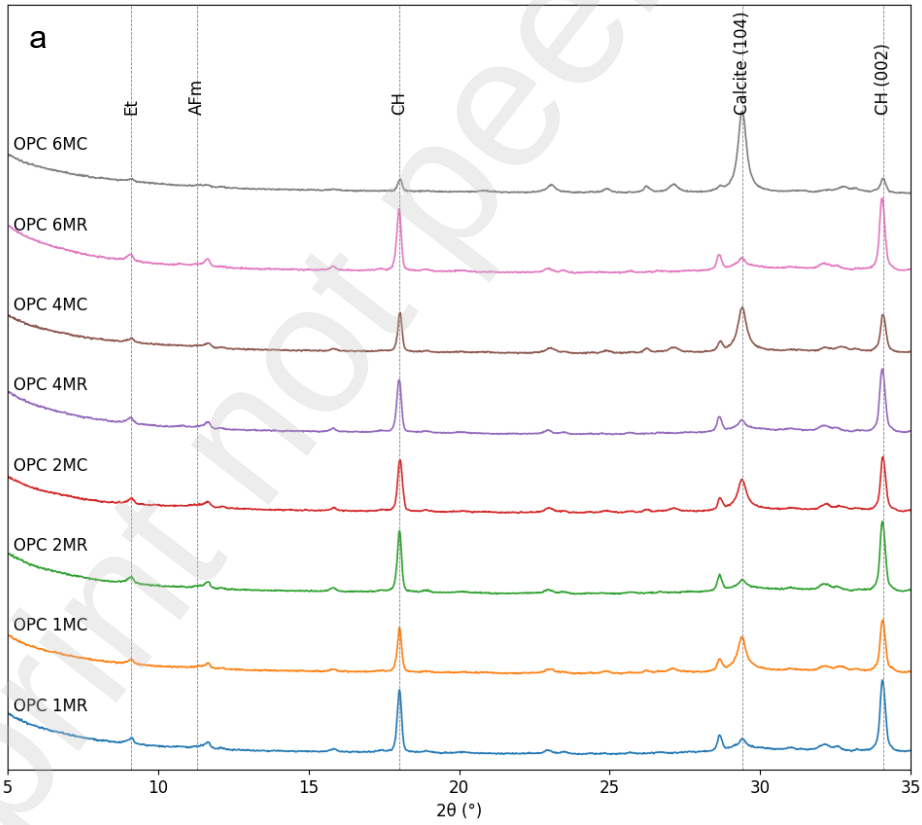

Preprint not peer reviewed

This preprint research paper has not been peer reviewed. Electronic copy available at: https://ssrn.com/abstract=6205146

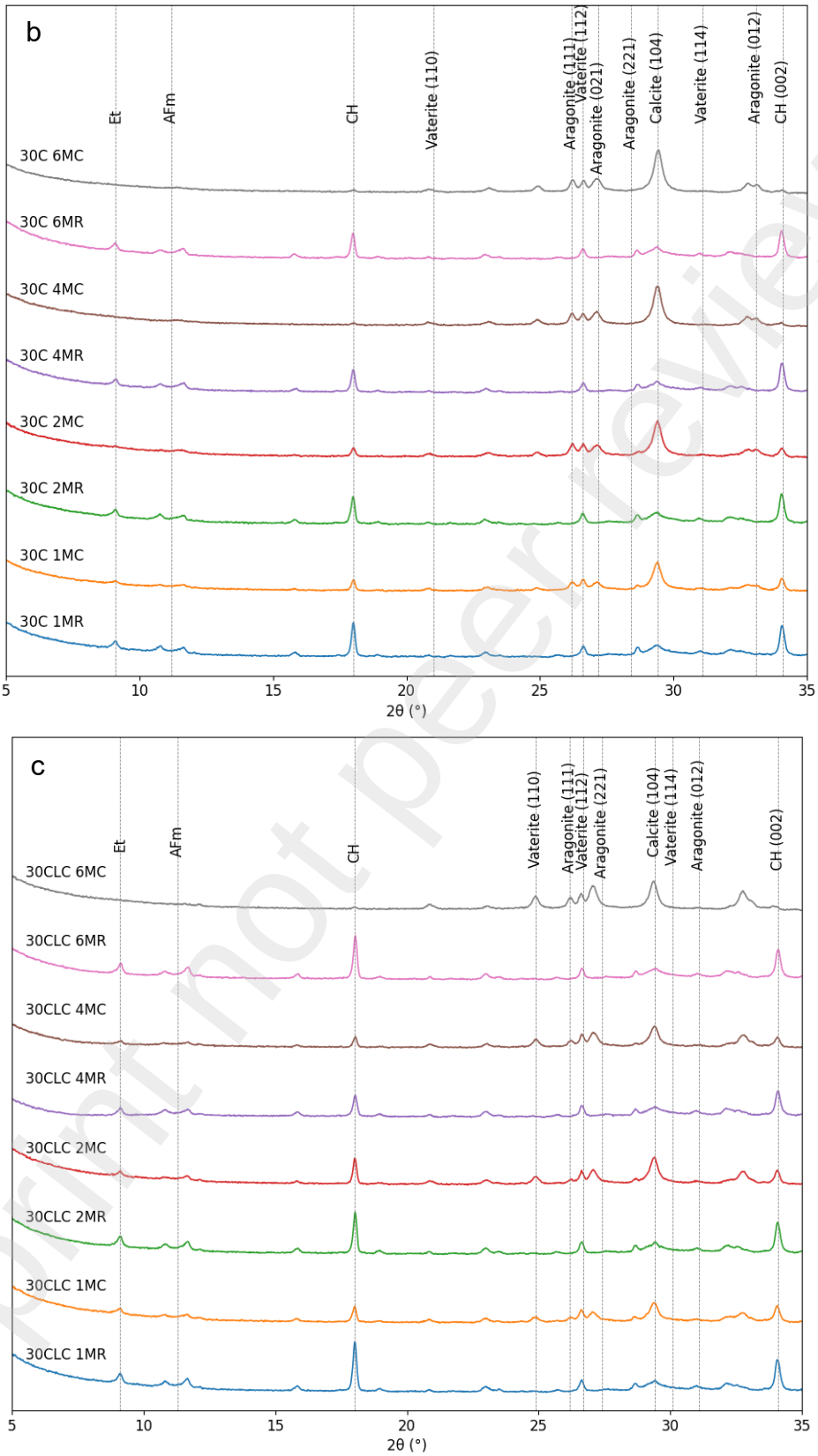

Figure 1. XRD hydrate phase evolution under carbonation and drying over one four and six months (a) OPC. (b) 30C & (c) 30CLC.

Preprint not peer reviewed

This preprint research paper has not been peer reviewed. Electronic copy available at: https://ssrn.com/abstract=6205146

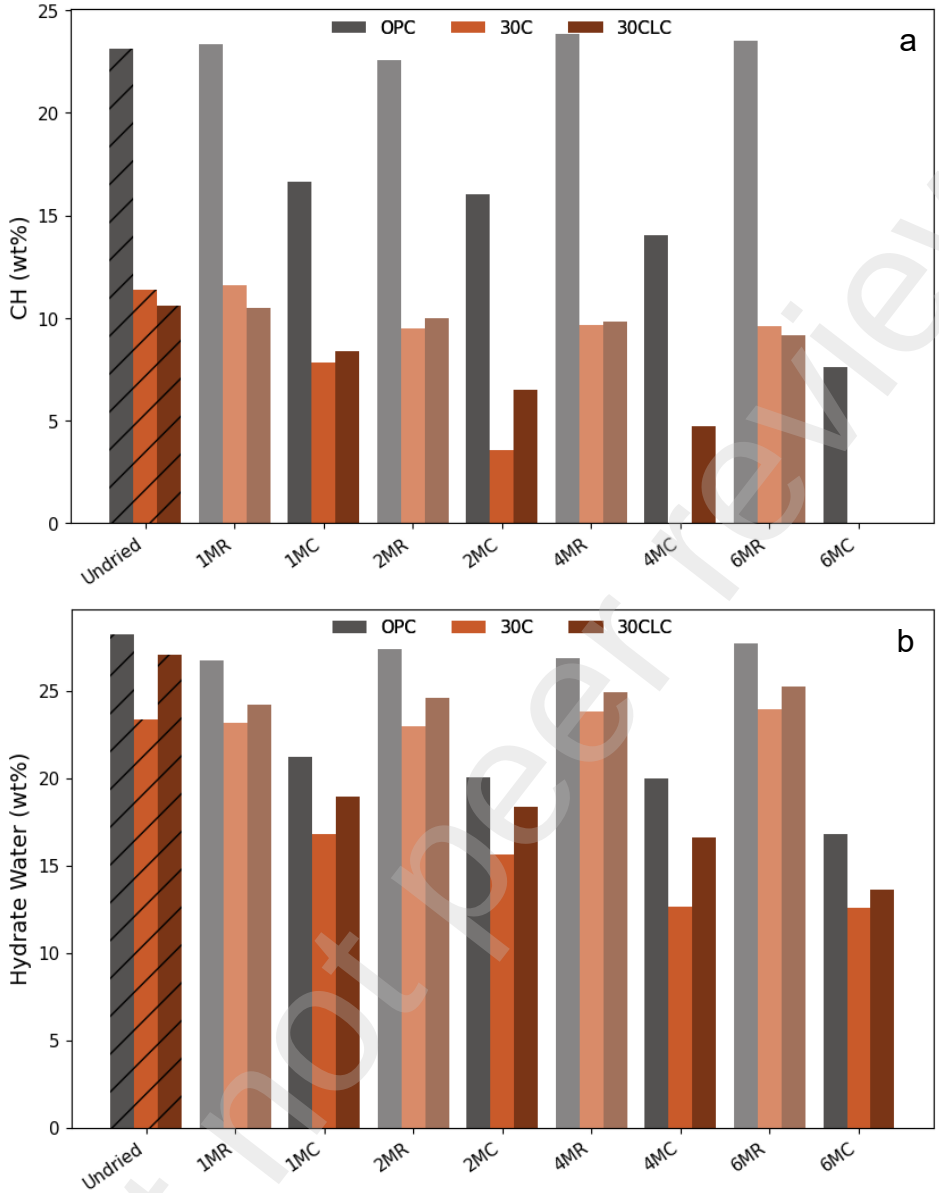

Preprint not peer reviewed

This preprint research paper has not been peer reviewed. Electronic copy available at: https://ssrn.com/abstract=6205146

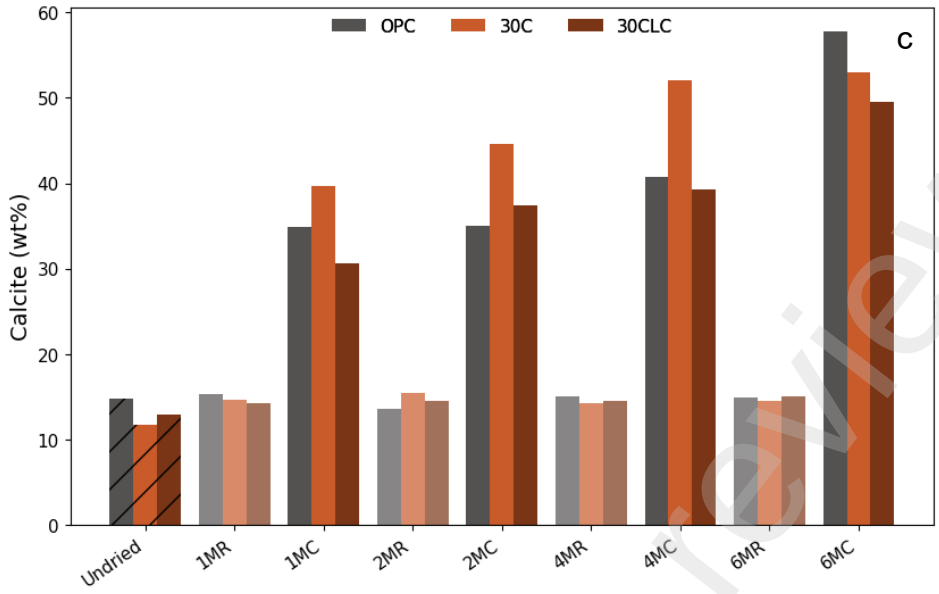

Figure 2. TGA of Uncarbonated and carbonated OPC, 30C and 30CLC. (a) % CH, (b)% Hydrate water & (c)% Calcite.

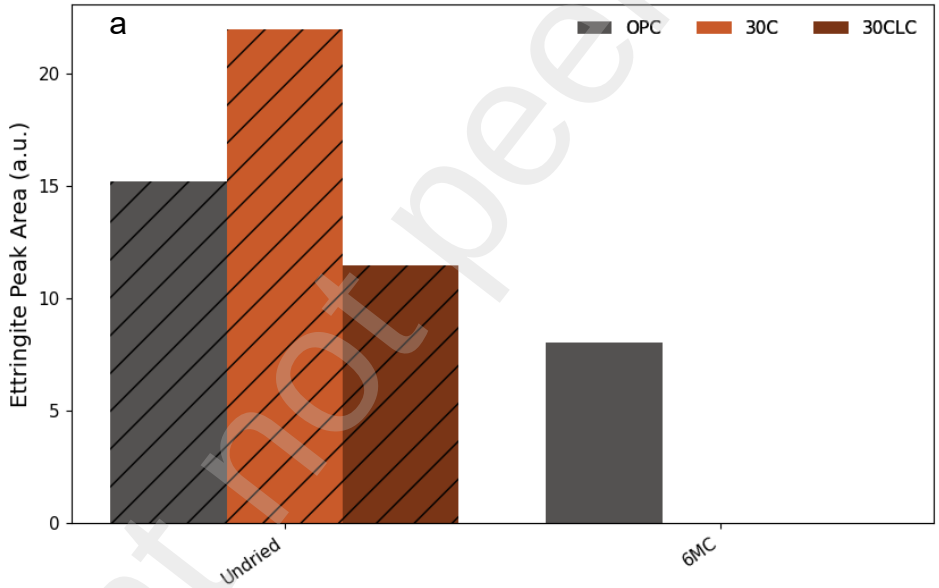

Preprint not peer reviewed

This preprint research paper has not been peer reviewed. Electronic copy available at: https://ssrn.com/abstract=6205146

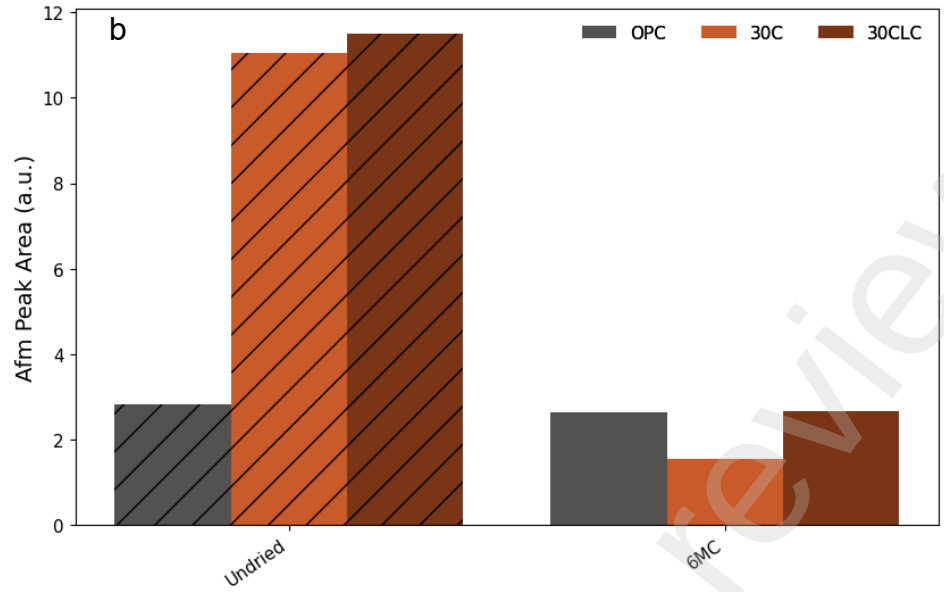

Figure 3. TGA of Undried and carbonated OPC, 30C and 30CLC. (a) Ettringite & (b) AFm.

4.2. Does carbonation cause any structural modifications of C–A-S–H and are these similar in OPC systems compared to when low kaolinite mix layer activated clays are incorporated?

The structural modification of C–A–S–H was investigated using ^{29}Si MAS NMR spectra of OPC, 30C and 30CLC are shown in Figure 4 (a, b & c). To facilitate interpretation of the spectral changes, key structural parameters of the C–S–H were quantified, including the chain length (Figure 5b), silicate chain length (SiCL; Figure 5d) and Al/Si molar ratio (Figure 5c), which reflects the degree of Al incorporation into the silicate chains of the C–S–H structure. The degree of decalcification (Ld) is presented in Figure 4(e), while a semi-quantitative evaluation of silicate polymerization, expressed as the bridging-to-paired tetrahedra ratio (B/A), is shown in Figure 4(f).

4.2.1. C-A-S-H structure prior to carbonation stage

In the undried OPC sample (Figure 4a), the dominant resonance at −78.5 ppm corresponds to Q^1, representing silicon atoms in the C–S–H chain-end sites [68], while the shoulder around −84.5 ppm corresponds to Q^2, associated with chain-middle groups [69]. A resonance centered at −81.5 ppm is attributed to $Q^2(1Al)$, reflecting partial substitution of Si by Al in the silicate framework [70]. The relative Q^n intensities are given in Figure 5(a). For both 30C (Figure 4b) and 30CLC (Figure 4c) binders, Q^1 appears near −78.7 ppm, Q^2 between −84.0 and −84.4 ppm, and $Q^2(1Al)$ around −81.5 ppm. However, notable differences in peak intensities indicate changes in the relative abundance of local silicate environments within the C–(A)–S–H structure. The 30C sample, cured for 28 days, displays a $Q^1/Q^2(1Al)$ distribution similar to OPC, suggesting a C-A-S-H structure with limited early Al incorporation. In contrast, the 30CLC system,

Preprint not peer reviewed

This preprint research paper has not been peer reviewed. Electronic copy available at: https://ssrn.com/abstract=6205146

cured for 56 days, exhibits reduced Q^1 intensity and a marked increase in $Q^2(1Al)$, indicating enhanced substitution of Si by Al and greater silicate chain connectivity. These observations suggest that extended curing promotes further development and polymerization of the C–A–S–H gel network in the presence of low-reactivity calcined clay. C-A-S-H at zero carbonation stage. At zero carbonation stage, for the undried samples, distinct differences in the C–A–S–H nanostructure are observed between OPC, 30C, and 30CLC. OPC-Undried exhibits a chain length (CL ≈ 4.4), silicate chain length (SiCL ≈ 2.7), and a low Al/Si ratio (≈ 0.12), characteristic of Ca-rich C–S–H with limited silicate polymerization and minimal Al incorporation. Notably, CL values for OPC-Undried and 30C-Undried are essentially identical, indicating that 28 days of curing is insufficient for the calcined clay system to significantly modify the C–S–H chain structure. This suggests that pozzolanic reaction and Al incorporation in 30C are still limited at this early age. In contrast, 30CLC-Undried shows a markedly higher CL (≈ 7.9), nearly double that of OPC, together with the highest Al/Si ratio (≈ 0.21). This indicates substantially enhanced Al incorporation into the silicate chains and the formation of a more polymerized C–A–S–H structure, attributable to prolonged curing and sustained pozzolanic reaction. Despite these differences in chain length and Al substitution, the SiCL values remain similar across all three systems, suggesting that the primary structural distinction arises from Al incorporation and chain extension rather than changes in silicate chain topology.

4.2.2. Effect of drying de-coupled from carbonation on C-A-S-H

Upon transitioning from the undried to the 4MR (dried) condition, the influence of drying becomes evident and appears to vary depending on the system as shown in Figure 5 and Figure 4. In OPC, drying results in a clear increase in Q^1 intensity (from 51% to 57%) alongside a reduction in both Q^2 and $Q^2(1Al)$ components. This shift is indicative of partial depolymerization of silicate chains, possibly due to drying-induced reorganization. In the 30C system, the changes are more modest as Q^1 slightly increases while Q^2 decreases, yet the $Q^2(1Al)$ contribution remains relatively stable. This suggests that Al substitution within the silicate network is retained even after drying. Interestingly, in the 30CLC system, drying leads to an increase in Q^1 and a corresponding decrease in $Q^2(1Al)$. This evolution may reflect a more polymerized and stable C-A-S-H structure, likely resulting from the extended curing duration (56 days) compared to the 30C sample (28 days). These observations suggest that longer curing enhances structural development and mitigates drying induced depolymerization, particularly in clay-containing binders.

4.2.3. Effect of carbonation coupled with drying on hydrate phase assemblage

Preprint not peer reviewed

This preprint research paper has not been peer reviewed. Electronic copy available at: https://ssrn.com/abstract=6205146

In the carbonated OPC sample, the Q^1 peak is significantly reduced in intensity, while the sharp Q^2 peak observed in the uncarbonated state becomes noticeably broader upon carbonation. In 30C the Q^1 peak completely disappeared after carbonation indicating the polymerization of silicate chains and transformations of C-S-H into more polymerized structure. However, in case of 30CLC Q^1 is retained even after 4 months of carbonation exposure, which means that longer curing has been proven beneficial in providing resistance to carbonation.

In the carbonated 30C and 30CLC samples, two new resonances emerge at −93.4 ppm and −103.0 ppm for 30C, and at −93.5 ppm and −102.5 ppm for 30CLC, corresponding to Q^3 and Q^4 environments, respectively [68]. The appearance of these Q^3 and Q^4 resonances indicates the formation of more highly polymerized silicate structures during carbonation. Q^3 species reflect silicate units with three bridging oxygens, while Q^4 species represent fully polymerized silica networks.

To provide an integrated perspective, and to enhance interpretation these spectral changes, we evaluated key structural parameters of the C–S–H including: chain length (CL) in Figure 5(b); silicate chain length (SiCL) in Figure 5(d); and Al/Si molar ratio for Al are incorporated into silicate chains of the C-S-H structure in Figure 5(c). Drying does not appear to substantially influence the chain length for any of the binders, as moderate drying alone does not significantly reorganize the silicate network. After carbonation, the OPC system shows a notable increase in CL, consistent with the earlier observation of enhanced Q^2 connectivity. In the 30C system, CL could not be calculated for the 30C4MC sample because extensive decalcification of the C–A–S–H leads to the complete loss of the Q^1 environment. For 30CLC, chain length increases after carbonation, again reflecting the development of more polymerized silicate structures. For OPC and 30C, carbonation results in an increase in the Al/Si ratio, suggesting greater incorporation of Al into the silicate chains. In contrast, 30CLC shows a reduction in Al/Si after carbonation, pointing to a different carbonation pathway and possibly a more selective decalcification process. Silicate chain length (SiCL) increases after carbonation across all binders; however, the increase is most pronounced for the 30CLC system, in line with its greater structural polymerization observed in the ^{29}Si spectra

To complement the structural interpretation from the NMR spectra, the level of decalcification (Ld) was quantified and given in Figure 5(e). OPC 4MC exhibited Ld of 9%, indicating moderate decalcification in comparison to 30C which reached Ld of 92%, confirming that the C–S–H in 30C is highly vulnerable to Ca depletion, leading to extensive restructuring of the silicate network. 30CLC however, showed a Ld of 34% and thus much lower than 30C, despite being higher than OPC, reflecting the protective effect of extended curing. [67].

Preprint not peer reviewed

This preprint research paper has not been peer reviewed. Electronic copy available at: https://ssrn.com/abstract=6205146

A semi-quantitative evaluation of silicate polymerization is presented in Figure 5(f). The 30C binder shows a B/A ratio of 9.29, reflecting an extensive increase in silicate polymerization that aligns with its very high level of decalcification. In contrast, 30CLC exhibits a much lower B/A ratio of 1.32, indicating only limited polymerization, which is consistent with its substantially reduced degree of decalcification.

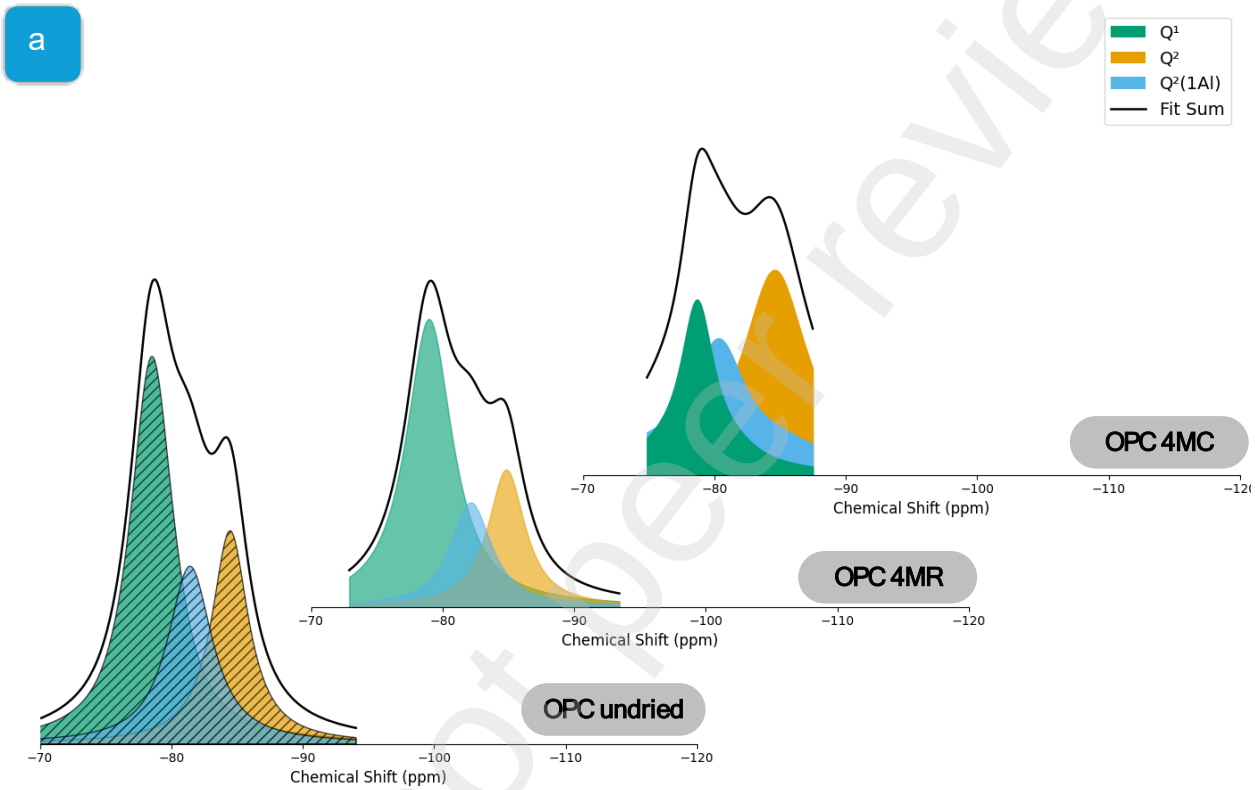

Preprint not peer reviewed

This preprint research paper has not been peer reviewed. Electronic copy available at: https://ssrn.com/abstract=6205146

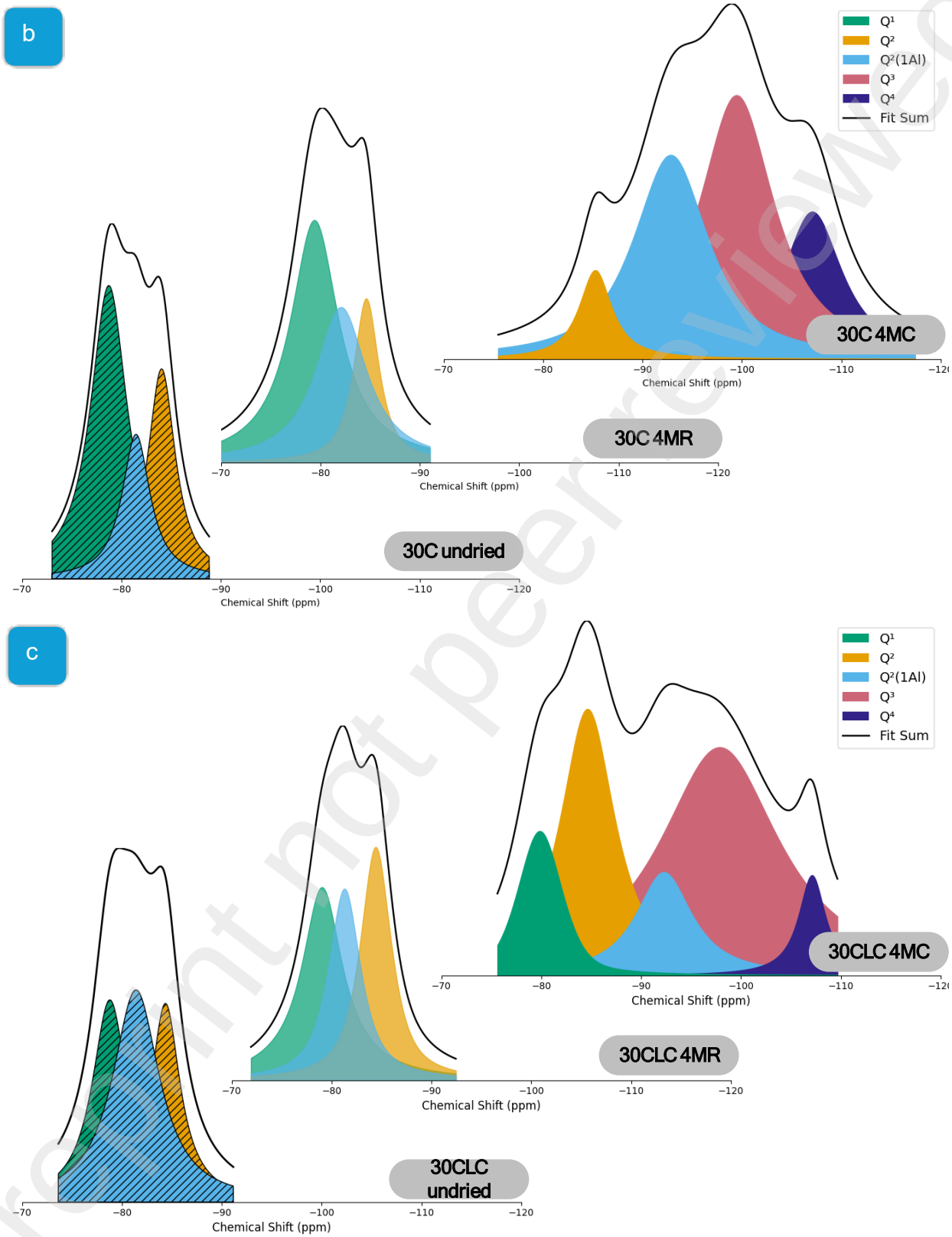

Figure 4. ^{29}Si MAS NMR (a) OPC undried, uncarbonated and carbonated samples (b) 30C undried, uncarbonated and carbonated samples (c) 30CLC undried, uncarbonated and carbonated samples

Preprint not peer reviewed

This preprint research paper has not been peer reviewed. Electronic copy available at: https://ssrn.com/abstract=6205146

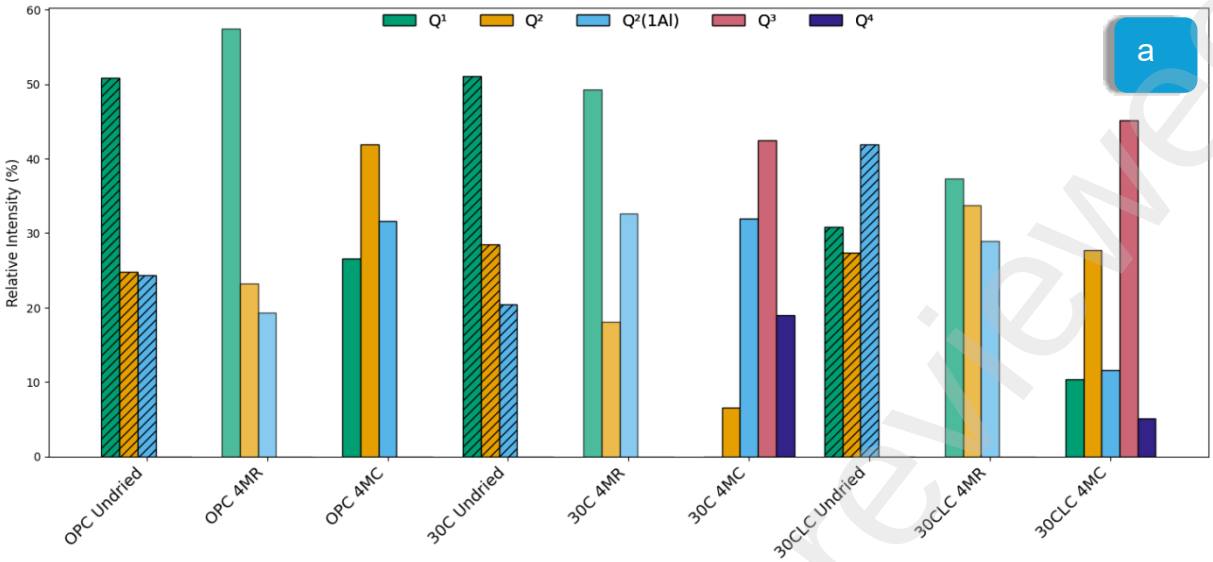

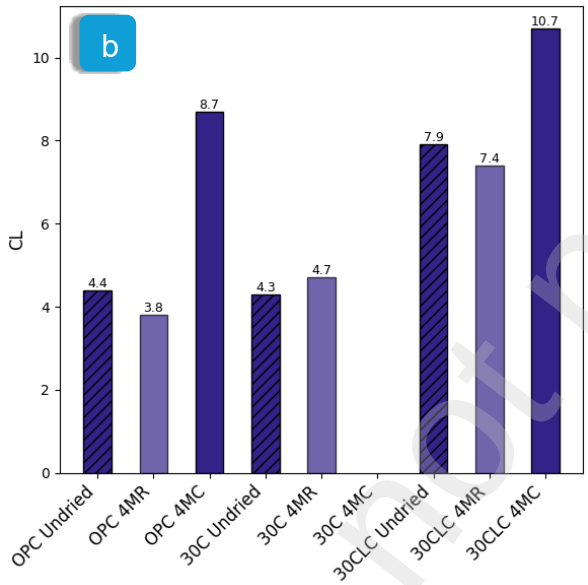

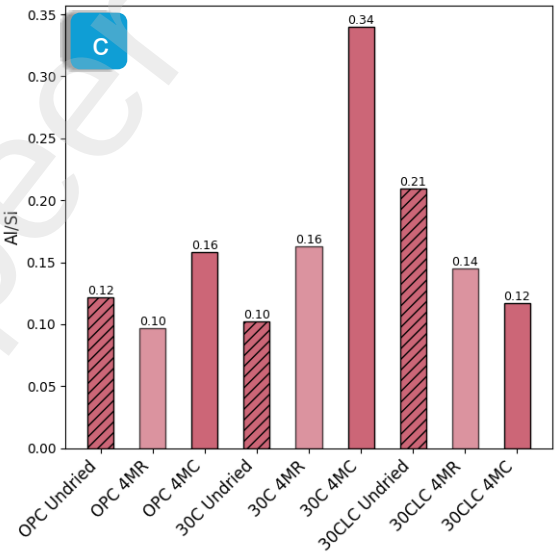

Preprint not peer reviewed

This preprint research paper has not been peer reviewed. Electronic copy available at: https://ssrn.com/abstract=6205146

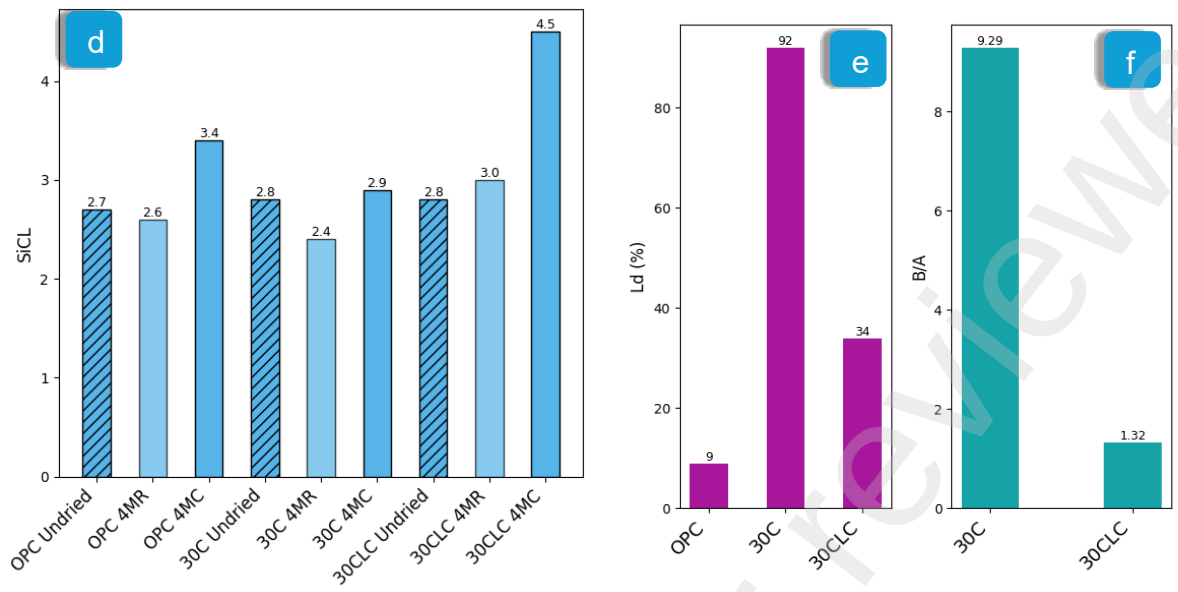

Figure 5. (a) Q^n intensities, (b) chain lengths, (c) Al/Si Ratios, (d) silicate chain lengths, (e) level of decalcification & (f) B/A

4.3. Does of structural changes of C–A-S–H affects re-distribution of Al in hydrate phase systems? and are these similar in OPC systems compared to when low kaolinite mix layer activated clays are incorporated?

The ^{27}Al MAS NMR of the undried, 4MR and 4MC samples for OPC, 30C and 30CLC samples are shown in Figure 6, Figure 7 and Figure 8. As expected, aluminum in octahedral coordination (Al^{VI}) is observed in the chemical shift range of 0–20 ppm, while tetrahedrally coordinated aluminum (Al^{IV}) appears between 50–90 ppm [71]. In all samples, sharp resonances at ~10 ppm and ~15 ppm are attributed to AFm [72] and AFt phases, respectively.

4.3.1. AFm and AFt at prior to carbonation stage

The undried OPC sample displays broad Al^{IV} peak centered at 60 and 71 ppm (Figure 6a) reflects moderate Al incorporation into the C-A-S-H gel. Also, it displays a strong Al^{VI} signal (Figure 6b) , consistent with the presence of AFm and AFt phases at early hydration. In the undried 30C (Figure 6a) sample, the Al^{VI} intensity is even higher than in OPC, reflecting rapid formation of AFm/AFt from the reactive fraction of calcined clay [76]. This aligns with the high early Al/Si ratio (0.16) and the dominant $Q^2(1Al)$ contribution in the ^{29}Si spectrum. In contrast, the undried 30CLC sample exhibits a more balanced distribution between Al^{VI} and Al^{IV}, suggesting that extended hydration promotes gradual transformation of AFm into Al-incorporated C–(A)–S–H.

Preprint not peer reviewed

This preprint research paper has not been peer reviewed. Electronic copy available at: https://ssrn.com/abstract=6205146

4.3.2. Effect of drying on AFm and AFt de-coupled from carbonation

In the 4MR condition, both binders largely preserve the aluminum coordination environments observed in the undried state, indicating that drying at 57% RH introduces only limited structural alteration. OPC remains dominated by Al^{VI}, reflecting the continued presence of AFm and AFt phases, while the broad Al^{IV} signal around 60–70 ppm shows only minor changes.

The 30C sample similarly retains its strong Al^{VI} contribution, consistent with the continued influence of calcined clay on AFm formation. The Al^{IV} region becomes marginally more defined, but the overall balance between Al^{VI} and Al^{IV} remains close to that of the undried state. This is in line with the small drop in Al/Si ratio and the largely unchanged chain length, confirming that moderate drying does not significantly disturb Al incorporation in 30C.

For 30CLC the Al^{VI} (Figure 8b) and Al^{IV} (Figure 7b) distribution remains more even, reflecting the more mature hydrate assemblage produced by extended curing. Only subtle reductions in Al^{VI} intensity appear after drying, accompanied by minimal changes in the Al^{IV} envelope. These trends are consistent with the very stable Al/Si ratio and chain length derived from the ^{29}Si spectra.

4.3.3. Effect of carbonation on AFm and AFt coupled with drying

Upon carbonation, both binders show a clear shift in Al coordination as the intensity of octahedral Al^{VI} is markedly reduced, and in the case of 30C it disappears entirely. The complete loss of Al^{VI} in 30C indicates that the remaining AFm/AFt phases are fully destabilized, which is consistent with the expected breakdown of ettringite once the pore solution pH falls below 10 [13]. This interpretation is supported by the accompanying XRD and TGA results, both of which show the disappearance of AFt after carbonation. The depletion of Al^{VI} and the simultaneous rise in tetrahedral Al^{IV} is in line with earlier observations by Skibsted et al. [73], who reported that carbonation drives the conversion of Al^{VI} to Al^{IV}, promoting Al incorporation into the silicate chains of C-A-S-Hor the formation of poorly crystalline aluminosilicate gels.

Carbonation also produces a modest but systematic shift of the Al^{IV} resonances toward lower chemical shifts appearing at ~58 and 68 ppm in OPC (Figure 6a), ~58 ppm in 30C (Figure 7a), and ~59, 68, and 74 ppm in 30CLC (Figure 7b). Such shifts are typically associated with changes in local Al environments toward more disordered, gel-like aluminosilicate structures [67, 74]. The increased Al^{IV} intensity after carbonation, observed consistently in all systems, further indicates that tetrahedrally coordinated Al becomes increasingly integrated into the reorganized silicate framework as decalcification progresses.

Preprint not peer reviewed

This preprint research paper has not been peer reviewed. Electronic copy available at: https://ssrn.com/abstract=6205146

This evolution in the ^{27}Al spectra mirrors the trends seen in the ^{29}Si MAS NMR data, where carbonation enhances chain polymerization and promotes the formation of Q^3 and Q^4 environments. Together, the Si and Al NMR signatures point to a coupled decalcification–repolymerization process in which the loss of Ca not only collapses AFm/AFt phases but also redistributes Al into the silicate network, giving rise to more polymerized C-A-S-H or secondary aluminosilicate gels.

Owing to relatively lower availability of aluminum content in low kaolinite mix layer calcined clays, the 30C and 30CLC systems, have limited formation of AFm phases, which are known to act as an initial carbonation buffer by preferentially reacting with CO_2. The lower abundance of AFm consequently accelerates the exposure of the C-A-S-H phase to carbonation [3, 73]. This reduced buffering capacity allows carbonation to proceed more rapidly towards the decalcification and structural reorganization of the silicate chains, as confirmed by the evolution of Q^3 and Q^4 species in the ^{29}Si NMR spectra and the increase in tetrahedrally coordinated Al in ^{27}Al NMR. It is also important to take into consideration the role of curing duration for the clay blended binder in carbonation resistance. 30C (28 days cured samples) exhibited a sharper decline in Al^{VI} and more pronounced silicate chain reorganization compared to 30CLC (100 days cured samples). The extended curing period allowed better hydration of calcined clay and formation of C-A-S-H and Afm phases, which improved the ability of matrix to resist carbonation. This contrasts with kaolinitic (1:1) calcined clays, such as metakaolin, which release substantially higher amounts of reactive Si and Al during hydration—up to four times more silicon and twelve times more aluminum than montmorillonite [75]. The higher Al availability in such systems promotes AFm formation and Al^{IV} incorporation into C–A–S–H, leading to greater silicate chain polymerization and a more cross-linked aluminosilicate network that enhances resistance to carbonation [10, 76].

Preprint not peer reviewed

This preprint research paper has not been peer reviewed. Electronic copy available at: https://ssrn.com/abstract=6205146

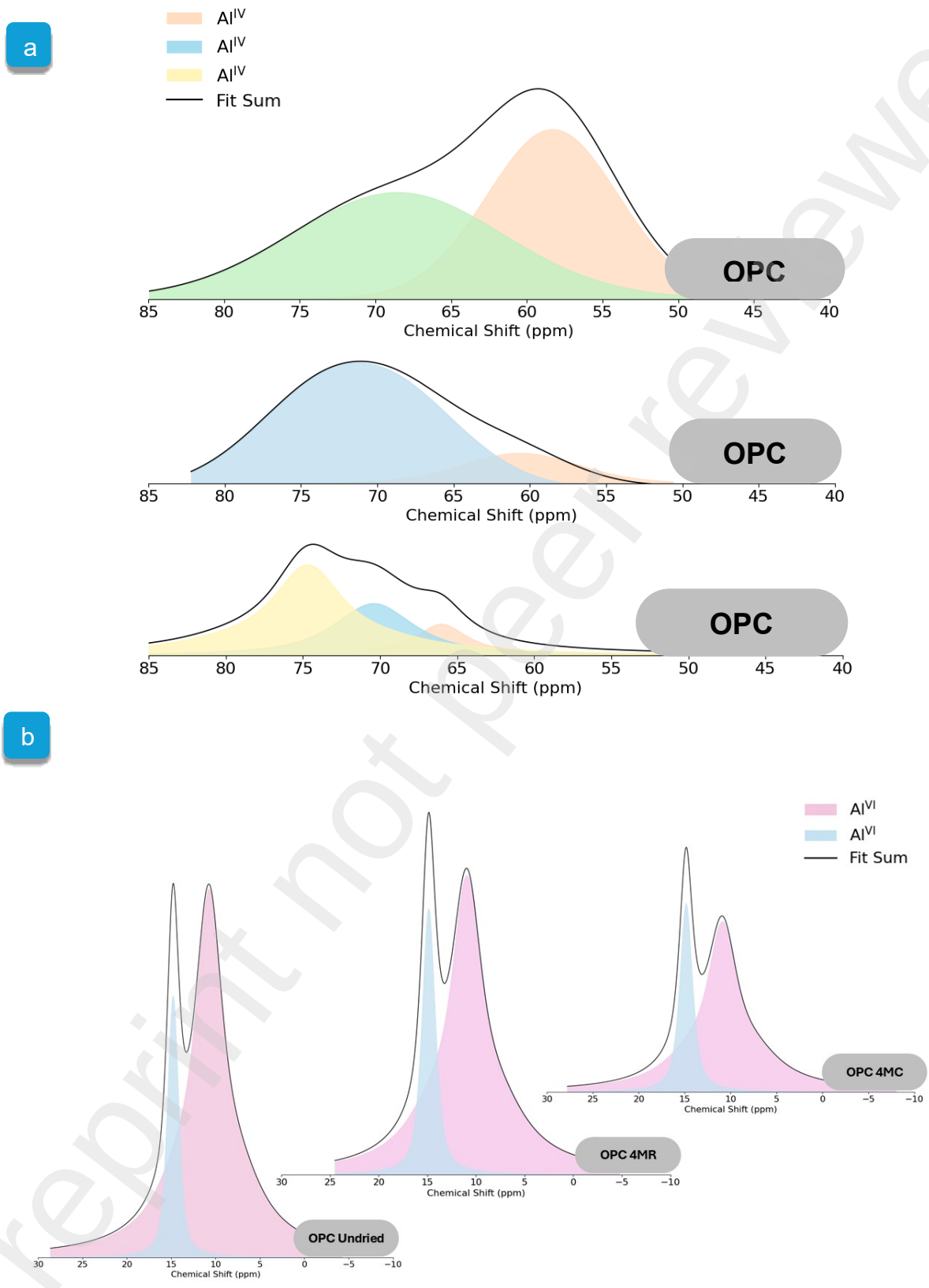

Figure 6. ^{27}Al MAS NMR spectra (a) Al^{IV} for OPC undried, uncarbonated and carbonated samples (b) Al^{VI} for OPC undried, uncarbonated and carbonated samples

Preprint not peer reviewed

This preprint research paper has not been peer reviewed. Electronic copy available at: https://ssrn.com/abstract=6205146

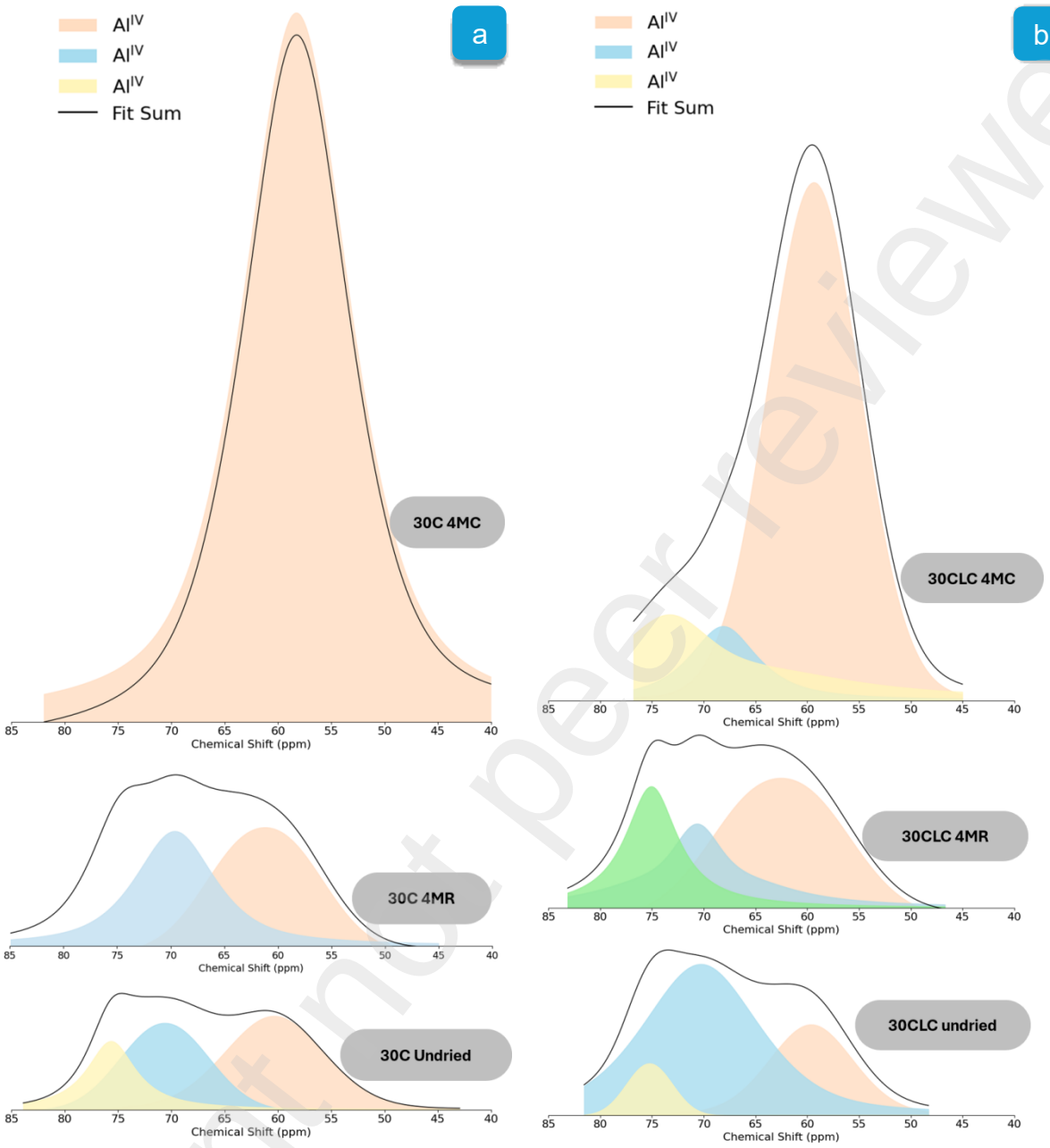

Figure 7. ^{27}Al MAS NMR spectra (a) Al^{IV} for 30C undried, uncarbonated and carbonated samples (b) Al^{IV} for 30CLC undried, uncarbonated and carbonated samples

Preprint not peer reviewed

This preprint research paper has not been peer reviewed. Electronic copy available at: https://ssrn.com/abstract=6205146

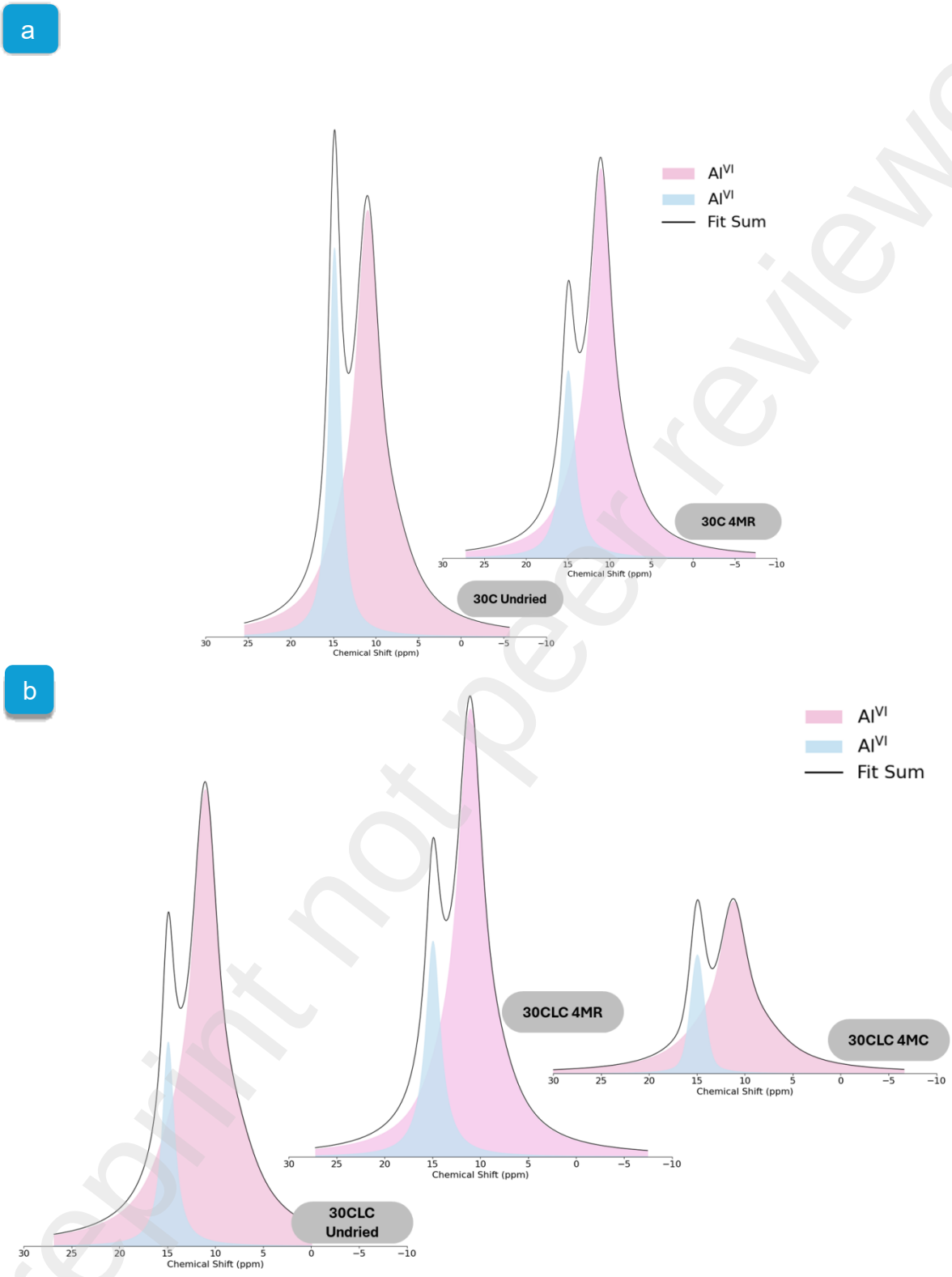

Figure 8. 27Al MAS NMR (a) Al^{VI} for 30C undried, uncarbonated and carbonated (b) Al^{VI} for 30CLC undried, uncarbonated and carbonated samples

Preprint not peer reviewed

This preprint research paper has not been peer reviewed. Electronic copy available at: https://ssrn.com/abstract=6205146

4.4. How do the changes in hydrate phase assemblage and CASH structural modifications cause re-distribution of pore structure in OPC system in comparison to in binders with incorporation of low kaolinite mix layer activated clays?

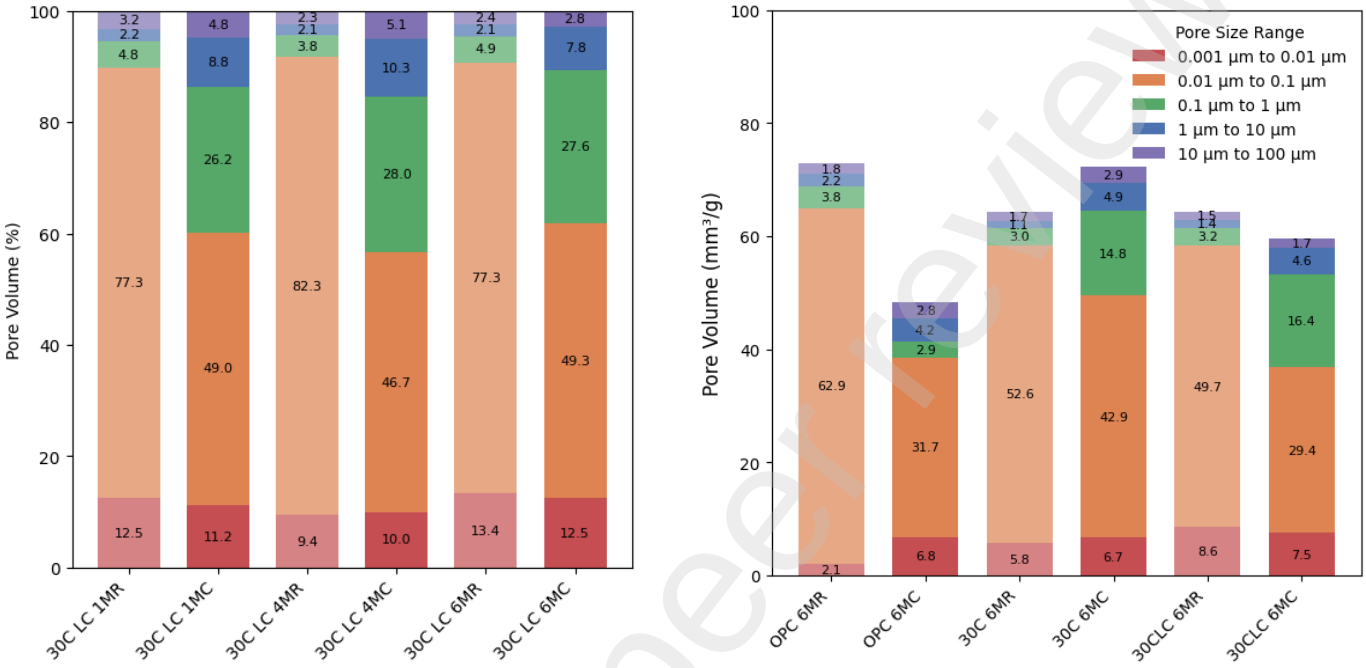

Figure 9Figure 9 gives normalized mercury intrusion porosimetry (MIP) results showing the relative pore size distribution within each sample and Figure 10, shows differential pore volumes across different exposure durations (1, 4, and 6 months).

4.4.1. Effect of drying de-coupled from carbonation on re-distribution of pore structure

Under drying conditions, in OPC, the fraction of small capillary pores (0.01–0.1 µm) gradually increases from 1 to 6 months, while the gel pore fraction with range < 0.01 µm slightly decreases. This indicates a slight coarsening of the pore structure during prolonged drying, likely caused by shrinkage of the C–S–H gel. As moisture is lost, part of the gel porosity may transform into slightly larger capillary pores due to microstructural rearrangement and partial pore merging. The proportion of pores larger than 1 µm remains very small throughout.

In the case of 30C, the overall pattern resembles that of OPC, though the system generally contains a higher share of capillary pores, reflecting its coarser and more open microstructure at 28 days of curing.

For 30CLC, which was cured 100 days, the fraction of gel pores is slightly higher, and capillary pores are less prominent compared to OPC and 30C. This reflects that extended

Preprint not peer reviewed

This preprint research paper has not been peer reviewed. Electronic copy available at: https://ssrn.com/abstract=6205146

curing resulted in continued pozzolanic activity leading to a denser pore structure, and more cohesive gel network that better resists coarsening.

4.4.2. Effect of carbonation coupled with drying on re-distribution of pore structure

A clear reduction in total porosity is observed in OPC after carbonation in comparison with reference samples in the same temperature and RH conditions as shown in Figure 10d. The reduction in porosity is attributed to carbonation of portlandite, as the molar volume of calcium carbonated is higher than that of portlandite, irrespective of the type of polymorph of calcium carbonate precipitate [77]. Therefore, the additional solid volume fills the empty pore volume in the microstructure which results in reduction of overall porosity. In contrast, the 30C system the carbonated sample exhibits a slightly higher cumulative pore volume than the reference. This supports the idea that the limited availability of portlandite in high-clay systems shifts carbonation toward the decalcification of C-S-H, potentially coarsening the pore structure instead of refining it [36, 78-80]. For 30CLC, the difference in total pore volume between 6MR and 6MC is minimal. This reflects the fact that prolonged curing has already resulted in a relatively dense microstructure through continued hydration and pore filling, thereby limiting the extent of further densification induced by carbonation.

In the case of OPC, carbonation causes a clear shift toward finer pores. The fraction of gel pore volume (Figure 9a) increases after carbonation while the proportion of small capillary pores (0.01–0.1 μm) decreases [81]. This trend is consistent throughout all exposure durations i.e. 1, 4, and 6 months. The reduction observed in small capillary pore range corresponds to partial clogging of pores corresponding to medium capillary pores, which are associated with outer C-S-H clusters [41, 82] as reported in literature [83]. The increase in gel pores after carbonation can be attributed to the release of chemically bound water during carbonation, which, along with moisture available at the carbonation front, may facilitate continued hydration of unreacted clinker phases. As a result, the formation of additional C–S–H could contribute to the observed rise in gel porosity.

Moreover, as portlandite dissolves during carbonation, it leaves voids that can locally merge into slightly larger pores, while carbonation products preferentially precipitate within the finer pore ranges [27]. This simultaneous formation and filling process explains the appearance of new pores around 0.1-0.2 μm and the reduction in those near 0.03 μm, as also seen in the differential intrusion curves in Figure 10.

In comparison with OPC, the clay blended binders exhibited somewhat different responses. Although, in case of both 30C and 30CLC the volume of small capillary pores (0.01–0.1 μm) decreases consistently after carbonation across all exposure durations, yet the proportion of medium capillary pores (0.1–1 μm) increases, which reflects coarsening of porosity. Although the total porosity in 30CLC remains almost the same

Preprint not peer reviewed

This preprint research paper has not been peer reviewed. Electronic copy available at: https://ssrn.com/abstract=6205146

between the 30CLC 6MR and 30CLC 6MC samples, the internal pore size distribution still indicates coarsening. Previous studies have reported that carbonation can lead to coarsening of mesopores, mainly due to the formation of porous silica gel, microcracking in the $CaCO_3$ layer around portlandite, and shrinkage-induced cracking. This effect is particularly evident in binders with low Ca/Si ratios, such as those containing fly ash, slag, or silica fume, where limited portlandite and the decalcification of C-A-S-H promote higher porosity and a shift toward larger pores [37, 84].

As confirmed by the TGA results, carbonation in 30C and 30CLC proceeds beyond portlandite consumption and involves the carbonation of sulfoaluminate hydrates (AFt and AFm) [30, 66]. Following the early exhaustion of CH in these systems, the destabilisation and decomposition of these pore-filling phases contribute directly to the observed pore coarsening. In addition to C–A–S–H decalcification, carbonation of ettringite (AFt) plays an important role in microstructural evolution. Ettringite is a highly voluminous, pore-filling hydrate, and its destabilisation during carbonation leads to dissolution and partial replacement by calcite, gypsum, and Al-rich amorphous phases [66]. The dissolution of AFt locally increases pore volume and pore connectivity, particularly within the capillary and mesopore ranges.

Similarly, carbonation of AFm phases reduces their pore-filling efficiency through progressive decalcification and transformation into carbonate-bearing or Al-rich residual phases. Although some carbonation products may precipitate within finer pores, the net effect of AFt and AFm decomposition is a redistribution of porosity toward the medium capillary pore range (0.1–1 μm), consistent with the MIP results for both 30C (Figure 9b) and 30CLC (Figure 9c) [66]. This mechanism is particularly relevant in systems with limited portlandite availability, where early CH exhaustion accelerates sulfoaluminate carbonation and promotes pore coarsening even when changes in total porosity are small, as observed for 30CLC. The involvement of AFt and AFm carbonation is further supported by the NMR results, which showed structural changes associated with aluminate-bearing hydrates during carbonation.

In 30C, the gel-pore fraction (<0.01 μm) remains almost unchanged, which leads to the idea that no later hydration is going on in 30C. On the other hand, 30CLC shows a slight increase in gel pores, especially in the 6-month carbonated sample. This could be related to secondary hydration supported by the moisture available during carbonation. Studies have reported that the decrease in micro-pores is attributed to clogging by $CaCO_3$ from C–S–H carbonation, while the reduction of macro-pores is mainly attributed to pore clogging by $CaCO_3$ from portlandite carbonation [27, 30, 78, 85].

Further insight into microstructural evolution is provided by the differential intrusion curves shown in Figure 10. In the reference (MR) samples, two distinct peaks appear within the 0.01–0.1 μm range, which correspond to the medium capillary pores typically associated

Preprint not peer reviewed

This preprint research paper has not been peer reviewed. Electronic copy available at: https://ssrn.com/abstract=6205146

with outer C–S–H clusters [86]. Upon carbonation, the intensity of these peaks decreases in all three binder systems, indicating partial blockage and densification of the capillary network. In some cases, the main peak shifts slightly toward smaller diameters, suggesting mild pore refinement [87].

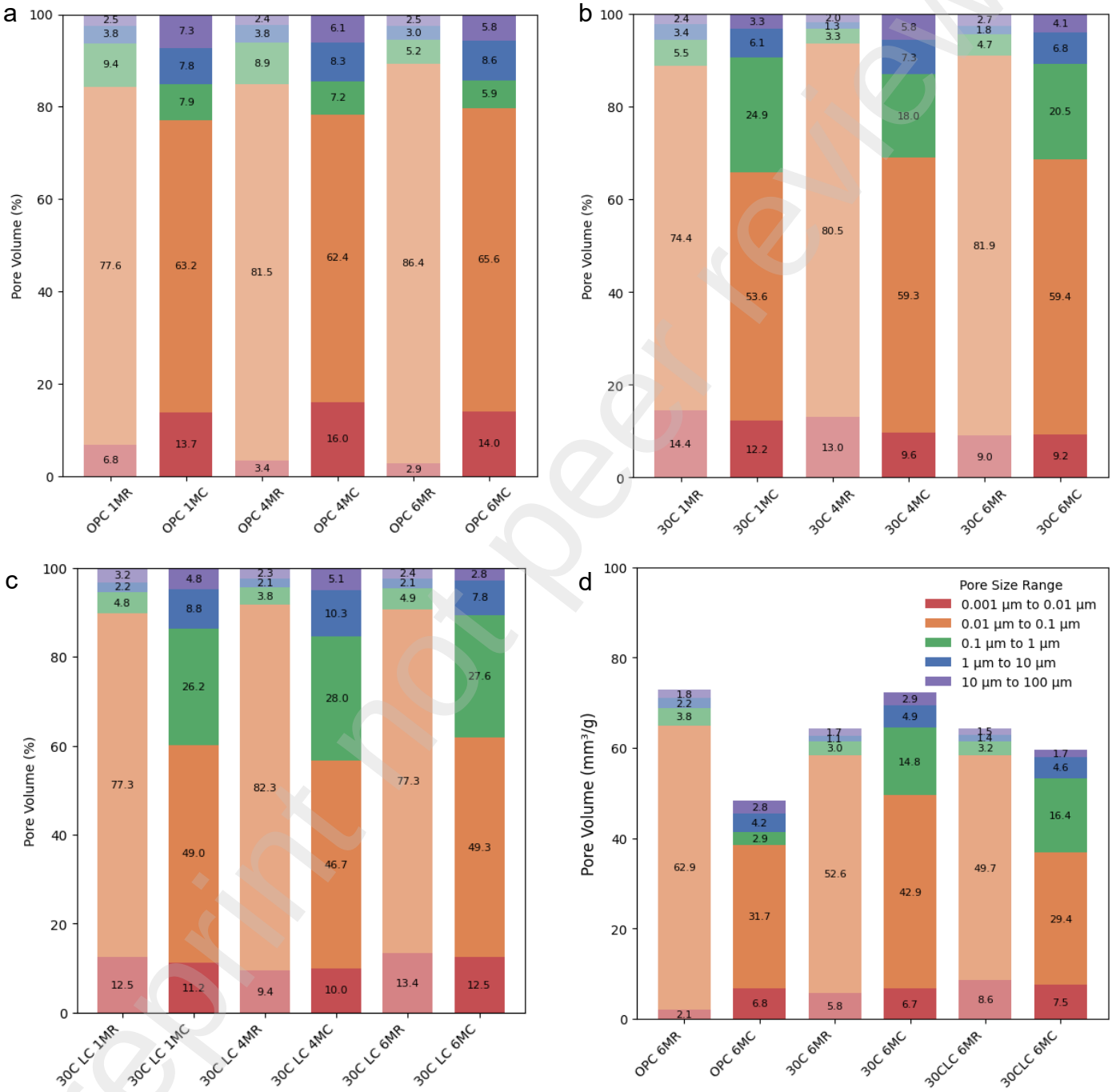

Figure 9. Mercury intrusion porosimetry – Pore structure evolution under drying and carbonation (a) OPC over 1, 4 and 6 months of age (b) 30C over 1, 4 and 6 months of age (c) 30CLC over 1, 4 and 6 months of age (d) Total porosity of OPC, 30C and 30CLC

Preprint not peer reviewed

This preprint research paper has not been peer reviewed. Electronic copy available at: https://ssrn.com/abstract=6205146

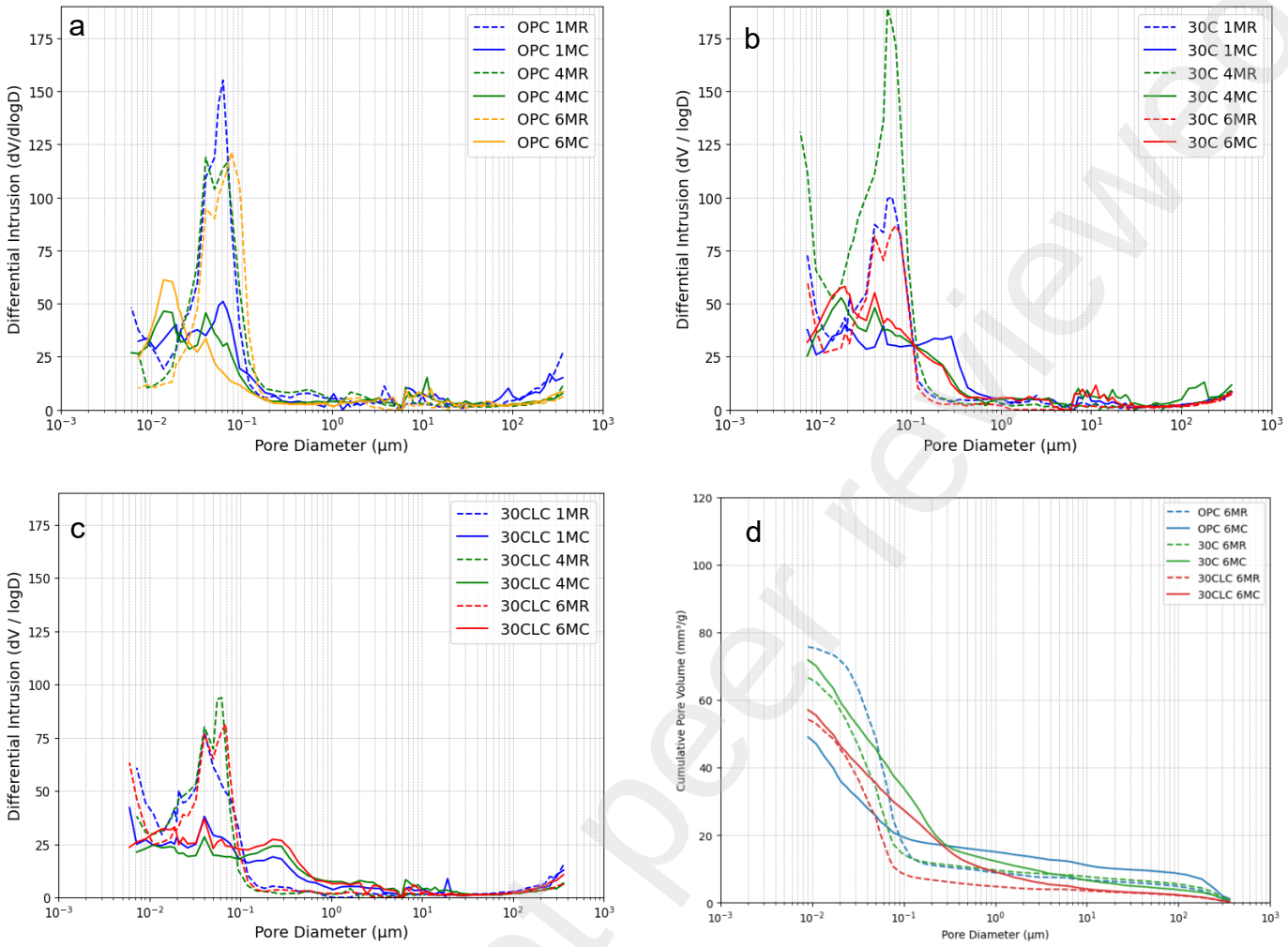

Figure 10. Mercury intrusion porosimetry – Differential porosity under drying and carbonation (a) OPC over 1, 4 and 6 months of age (b) 30C over 1, 4 and 6 months of age (c) 30CLC over 1, 4 and 6 months of age (d) Total porosity of OPC, 30C and 30CLC

5. Mechanistic Reflections: Understanding Carbonation Resistance in Low-Kaolinite Systems

The findings of this study invite a deeper examination of the mechanisms underlying carbonation resistance in low-kaolinite clay blended binders. At first glance, one might attribute the improved performance of the extended-cured system (30CLC) to a higher portlandite content, given its role as the primary carbonation buffer. However, our results challenge this assumption: despite prolonged curing, the portlandite content remained nearly unchanged compared to the 28-day cured system (30C). This observation indicates that the enhanced resistance of 30CLC cannot be explained by CH availability alone.

Instead, the key lies in the evolution of the hydrate assemblage and the chemistry of the C–A–S–H gel. Extended curing promotes the transformation of AFt into AFm and

Preprint not peer reviewed

This preprint research paper has not been peer reviewed. Electronic copy available at: https://ssrn.com/abstract=6205146

facilitates greater incorporation of aluminum into the silicate chains of C–A–S–H. These changes are subtle but significant. AFm phases, though often considered secondary, provide an additional buffering capacity once CH is depleted, delaying the onset of aggressive decalcification. Simultaneously, aluminum incorporation increases the polymerization and cross-linking of the C–A–S–H network, enhancing its structural stability under carbonation. This mechanistic link between curing, gel chemistry, and durability represents a critical insight for systems based on low-reactivity clays.

While AFm phases provide an intermediate buffering capacity, the long-term resistance to carbonation ultimately depends on the stability of the C–A–S–H gel. Once AFm and CH are consumed, the gel becomes the primary target for carbonation, and its chemistry, particularly the degree of polymerization and aluminum incorporation, determines how severely decalcification progresses. This highlights that, beyond AFm buffering, which is a known key parameters in designing LC3 cement, the structural resilience of C–A–S–H is a critical factor for durability in low-kaolinite systems.

The choice of 30% clay replacement further underscores this point. By retaining some portlandite, the system allowed observation of the full carbonation sequence—CH depletion, AFm buffering, and eventual C–A–S–H transformation. At higher replacement levels, where CH would be nearly absent, carbonation would proceed directly to gel decalcification, obscuring the intermediate buffering effects and the role of curing in hydrate evolution.

Microstructural analysis reinforces this interpretation. OPC exhibited the expected pore refinement due to $CaCO_3$ precipitation, whereas the clay systems displayed contrasting behavior. Severe pore coarsening in 30C correlates with extensive gel decalcification (Ld = 92%), while the minimal changes in 30CLC reflect the stabilizing influence of a denser matrix and a chemically mature gel. Prolonged curing promotes further incorporation of Al into the C–A–S–H structure, leading to the development of a more chemically mature gel that is less susceptible to decalcification during carbonation. As a result, improved carbonation resistance is achieved despite the lower portlandite content in the clay-blended binders, indicating that hydrate chemistry and gel maturity play a more decisive role than CH availability alone.

From a broader perspective, these observations suggest that carbonation resistance in low-kaolinite clay systems is influenced by factors beyond portlandite content, particularly the evolution of secondary hydrates and the chemistry of C–A–S–H during hydration. While the fundamental mechanisms align with those reported for other SCM systems, the sensitivity to curing duration highlights an area that merits further attention. Future studies could explore how curing protocols and binder design adjustments optimize these characteristics, ensuring that low-kaolinite clays can be effectively incorporated into durable cementitious materials.

Preprint not peer reviewed

This preprint research paper has not been peer reviewed. Electronic copy available at: https://ssrn.com/abstract=6205146

6. Conclusions

This study investigated carbonation in low-kaolinite mixed-layer calcined clay blended binders, focusing on hydrate phase evolution, C–A–S–H structure, and pore characteristics, while differentiating the effects of curing and drying. The main conclusions are:

1. Carbonation induces interconnected changes in hydrate assemblage, C–A–S–H structure, and pore network in both binders, but the progression differs significantly with curing duration.
    - In OPC, C–S–H remains stable under carbonation, with limited decalcification (Ld ≈ 9%). Carbonation is mainly accommodated by portlandite consumption and $CaCO_3$ precipitation, with the presence of portlandite providing a natural buffering capacity against CO_2 ingress. Consequently, the silicate connectivity of C–S–H remains dominated by Q^1, Q^2, and $Q^2(1Al)$ species before and after carbonation, and carbonation-induced degradation of the hydrated matrix is limited.
    - In 30C, the immature hydrate assemblage and limited Al incorporation in C–A–S–H led to early CH depletion, rapid destabilization of AFm and AFt, and severe gel decalcification (Ld ≈ 92%). This resulted in extensive structural reorganization, formation of highly polymerized silicate species (Q^3/Q^4), and pronounced pore coarsening.
    - In contrast, 30CLC benefitted from extended curing, which promoted AFm formation, greater Al incorporation into C–A–S–H, and a denser microstructure. These changes delayed deep decalcification (Ld ≈ 34%), preserved Q^1 species, and minimized pore redistribution, as confirmed by NMR and MIP results.
    - These findings indicate that curing improves carbonation resistance primarily through hydrate chemistry and microstructural maturity rather than portlandite content alone.
2. Drying at 57% RH produced only minor changes compared to carbonation.
    - Crystalline hydrates (CH, AFm, AFt) remained stable, and the silicate network showed only slight depolymerization and gel contraction.
    - Pore structure changes were limited to minor densification, without the redistribution toward larger pores observed under carbonation.
    - While drying alone does not induce the same chemical transformations as carbonation, it may influence the internal relative humidity of the material, which in turn can affect CO_2 transport. Differences in moisture retention between OPC and SCM-containing binders may therefore contribute to variations in carbonation behavior, even under similar external exposure conditions.
3. Microstructural implications and practical relevance:

Preprint not peer reviewed

This preprint research paper has not been peer reviewed. Electronic copy available at: https://ssrn.com/abstract=6205146

- OPC exhibited pore refinement due to $CaCO_3$ precipitation, whereas clay systems showed coarsening linked to C–A–S–H collapse. The extended curing constrained CO_2 ingress and the negative effects it causes by densifying the pore network.
- While carbonation mechanisms align with those reported for pozzolanic SCM binders, the sensitivity to curing duration highlights an important consideration for durability design. Future work should validate these findings and explore binder formulations, including higher clay substitution levels, that promote AFm formation and effective Al incorporation into C–A–S–H. In this context, an important direction is the development of binder chemistries that achieve a mature hydrate assemblage without relying on extended curing, for example through approaches inspired by lime–aluminosilicate systems reported in the literature.

Acknowledgements

The authors acknowledge the grant offered by Family Thomas Foundation for project: Evolution of pozzolan incorporated concrete: resistance to carbonation (Carbo-crete). The authors would like to acknowledge NMR support from the NMR Core Facility at the Swedish NMR Centre (SwedNMR, Umeå node), Umeå University and SciLifeLab. Additionally, the authors are grateful to Haitao Gu for facilitating the MIP measurements, and student assistants at Chalmers Building Materials Lab – Archanath Dickwella, Sunil Gautam, Suriyaprakash Saravanan and Amith Adhikari for helping with material preparations and experiments.

Preprint not peer reviewed

This preprint research paper has not been peer reviewed. Electronic copy available at: https://ssrn.com/abstract=6205146

7. References

1. Scrivener, K.L., V.M. John, and E.M. Gartner, *Eco-efficient cements: Potential economically viable solutions for a low-CO2 cement-based materials industry.* Cement and concrete Research, 2018. **114**: p. 2-26.
2. Snellings, R., P. Suraneni, and J. Skibsted, *Future and emerging supplementary cementitious materials.* Cement and concrete research, 2023. **171**: p. 107199.
3. Scrivener, K., et al., *Calcined clay limestone cements (LC3).* Cement and concrete research, 2018. **114**: p. 49-56.
4. Antoni, M., et al., *Cement substitution by a combination of metakaolin and limestone.* Cement and concrete research, 2012. **42**(12): p. 1579-1589.
5. Gonthier, J.N., et al., *Advanced characterization of chloride binding in OPC and LC³ pastes.* 2021.
6. Zunino, F., et al., *Hydration and mixture design of calcined clay blended cements: review by the RILEM TC 282-CCL.* Materials and Structures, 2022. **55**(9): p. 234.
7. Hanein, T., et al., *Clay calcination technology: state-of-the-art review by the RILEM TC 282-CCL.* Materials and Structures, 2022. **55**(1): p. 3.
8. Alujas Diaz, A., et al., *Properties and occurrence of clay resources for use as supplementary cementitious materials: a paper of RILEM TC 282-CCL.* Materials and Structures, 2022. **55**(5): p. 139.
9. Rashid, K., et al., *Synergistic mechanical and chemical activation of kaolin clays for enhanced reactivity in limestone calcined clay cement (LC3).* Sustainable Materials and Technologies, 2026: p. e01876.
10. Avet, F. and K. Scrivener, *Investigation of the calcined kaolinite content on the hydration of Limestone Calcined Clay Cement (LC3).* Cement and Concrete Research, 2018. **107**: p. 124-135.
11. Fernandez, R., F. Martirena, and K.L. Scrivener, *The origin of the pozzolanic activity of calcined clay minerals: A comparison between kaolinite, illite and montmorillonite.* Cement and concrete research, 2011. **41**(1): p. 113-122.
12. Sisomphon, K. and L. Franke, *Carbonation rates of concretes containing high volume of pozzolanic materials.* Cement and Concrete Research, 2007. **37**(12): p. 1647-1653.
13. Lothenbach, S.v.G.-D.B., et al., *Understanding the carbonation of concrete with supplementary cementitious materials: a critical review by RILEM TC 281-CCC.* Materials and Structures, 2020. **53**: p. 136.
14. Lothenbach, B., et al., *Influence of limestone on the hydration of Portland cements.* Cement and concrete research, 2008. **38**(6): p. 848-860.
15. Lilkov, V., et al., *Long term study of hardened cement pastes containing silica fume and fly ash.* Construction and Building Materials, 2014. **60**: p. 48-56.
16. Gruyaert, E., P. Van den Heede, and N. De Belie, *Carbonation of slag concrete: Effect of the cement replacement level and curing on the carbonation coefficient – Effect of carbonation on the pore structure.* Cement and Concrete Composites, 2013. **35**(1): p. 39-48.

Preprint not peer reviewed

This preprint research paper has not been peer reviewed. Electronic copy available at: https://ssrn.com/abstract=6205146

17. Borges, P.H.R., et al., *Carbonation of CH and C–S–H in composite cement pastes containing high amounts of BFS.* Cement and Concrete Research, 2010. **40**(2): p. 284-292.
18. Beuntner, N., R. Sposito, and K.-C. Thienel, *Potential of calcined mixed-layer clays as pozzolans in concrete.* ACI Materials Journal, 2019. **116**(4): p. 19-29.
19. Tole, I., *Enhancing the Pozzolanic Activity of Three Natural Clays from Sweden by Mechanochemical Activation Process.* Available at SSRN 4100172, 2022.
20. Alujas, A., et al., *Pozzolanic reactivity of low grade kaolinitic clays: Influence of calcination temperature and impact of calcination products on OPC hydration.* Applied Clay Science, 2015. **108**: p. 94-101.
21. Alujas, A., et al. *Pozzolanic reactivity of low grade kaolinitic clays: influence of mineralogical composition*. in *Calcined Clays for Sustainable Concrete: Proceedings of the 1st International Conference on Calcined Clays for Sustainable Concrete*. 2015. Springer.
22. Marsh, A.T., S. Krishnan, and S.A. Bernal, *Structural features of thermally or mechano-chemically treated montmorillonite clays as precursors for alkali-activated cements production.* Cement and Concrete Research, 2024. **181**: p. 107546.
23. Hazarika, A., L. Huang, and A. Babaahmadi, *Characterisation, activation, and reactivity of heterogenous natural clays.* Materials and Structures, 2024. **57**(4): p. 68.
24. Hazarika, A., et al., *Evolution of hydration in cement blends with incorporation of activated low-kaolinite clays: Insights into the preferred aluminum uptake by C-(A)-SH.* Cement and Concrete Research, 2026. **201**: p. 108086.
25. Dhandapani, Y., et al., *The meta-kaolinite content of the calcined clay source impacts the mechanical and durability performance of blended Portland concrete.* Cement and Concrete Research, 2025. **196**: p. 107922.
26. Flegar, M., et al., *Regional waste streams as potential raw materials for immediate implementation in cement production.* Materials, 2020. **13**(23): p. 5456.
27. Wu, B. and G. Ye, *Development of porosity of cement paste blended with supplementary cementitious materials after carbonation.* Construction and Building Materials, 2017. **145**: p. 52-61.
28. Peter, M.A., et al., *Competition of several carbonation reactions in concrete: A parametric study.* Cement and concrete research, 2008. **38**(12): p. 1385-1393.
29. Ngala, V. and C. Page, *Effects of carbonation on pore structure and diffusional properties of hydrated cement pastes.* Cement and concrete research, 1997. **27**(7): p. 995-1007.
30. von Greve-Dierfeld, S., et al., *Understanding the carbonation of concrete with supplementary cementitious materials: a critical review by RILEM TC 281-CCC.* Materials and structures, 2020. **53**(6): p. 136.
31. Anstice, D.J., C.L. Page, and M.M. Page, *The pore solution phase of carbonated cement pastes.* Cement and Concrete Research, 2005. **35**(2): p. 377-383.
32. Visser, J., *Influence of the carbon dioxide concentration on the resistance to carbonation of concrete.* Construction and Building Materials, 2014. **67**: p. 8-13.

Preprint not peer reviewed

This preprint research paper has not been peer reviewed. Electronic copy available at: https://ssrn.com/abstract=6205146

33. Chang, J. and Y. Fang, *Quantitative analysis of accelerated carbonation products of the synthetic calcium silicate hydrate(C–S–H) by QXRD and TG/MS.* Journal of Thermal Analysis and Calorimetry, 2015. **119**(1): p. 57-62.
34. El-Hassan, H. and Y. Shao, *Early carbonation curing of concrete masonry units with Portland limestone cement.* Cement and Concrete Composites, 2015. **62**: p. 168-177.
35. Georget, F., J.H. Prévost, and B. Huet, *Impact of the microstructure model on coupled simulation of drying and accelerated carbonation.* Cement and concrete research, 2018. **104**: p. 1-12.
36. Morandeau, A., M. Thiéry, and P. Dangla, *Impact of accelerated carbonation on OPC cement paste blended with fly ash.* Cement and concrete research, 2015. **67**: p. 226-236.
37. Pham, S.T. and W. Prince, *Effects of carbonation on the microstructure of cement materials: influence of measuring methods and of types of cement.* International Journal of Concrete Structures and Materials, 2014. **8**(4): p. 327-333.
38. Morandeau, A., M. Thiery, and P. Dangla, *Investigation of the carbonation mechanism of CH and CSH in terms of kinetics, microstructure changes and moisture properties.* Cement and concrete research, 2014. **56**: p. 153-170.
39. Black, L., et al., *Structural features of C–S–H (I) and its carbonation in air—a Raman spectroscopic study. Part II: carbonated phases.* Journal of the American Ceramic Society, 2007. **90**(3): p. 908-917.
40. Soja, W., et al., *Evolution of microstructural changes in cement paste during environmental drying.* Cement and Concrete Research, 2020. **134**: p. 106093.
41. Song, H.-W. and S.-J. Kwon, *Permeability characteristics of carbonated concrete considering capillary pore structure.* Cement and Concrete Research, 2007. **37**(6): p. 909-915.
42. Auroy, M., et al., *Impact of carbonation on unsaturated water transport properties of cement-based materials.* Cement and Concrete Research, 2015. **74**: p. 44-58.
43. Saetta, A.V. and R.V. Vitaliani, *Experimental investigation and numerical modeling of carbonation process in reinforced concrete structures: Part I: Theoretical formulation.* Cement and concrete research, 2004. **34**(4): p. 571-579.
44. Drouet, E., et al., *Carbonation of hardened cement pastes: Influence of temperature.* Cement and Concrete Research, 2019. **115**: p. 445-459.
45. Shah, V. and S. Bishnoi, *Carbonation resistance of cements containing supplementary cementitious materials and its relation to various parameters of concrete.* Construction and Building Materials, 2018. **178**: p. 219-232.
46. Ruixia, H., *A study on carbonation for low calcium fly ash concrete under different temperature and relative humidity.* The Electronic Journal of Geotechnical Engineering (EJGE), 2010. **15**: p. 1871-1877.
47. Leemann, A. and F. Moro, *Carbonation of concrete: the role of CO2 concentration, relative humidity and CO2 buffer capacity.* Materials and Structures, 2017. **50**(1): p. 30.
48. Ekolu, S., *A review on effects of curing, sheltering, and CO2 concentration upon natural carbonation of concrete.* Construction and Building Materials, 2016. **127**: p. 306-320.

Preprint not peer reviewed

This preprint research paper has not been peer reviewed. Electronic copy available at: https://ssrn.com/abstract=6205146

49. Hyvert, N., et al., *Dependency of C–S–H carbonation rate on CO2 pressure to explain transition from accelerated tests to natural carbonation.* Cement and concrete research, 2010. **40**(11): p. 1582-1589.
50. Standardization, E.C.f., *EN 12390-12:2020 — Testing hardened concrete – Part 12: Determination of the carbonation resistance of concrete: Accelerated carbonation method*. 2020: Brussels, Belgium.
51. Fung, B.M.K., A. K.; Ermolaev, K., *An improved broadband decoupling sequence for liquid crystals and solids.* Journal of Magnetic Resonance, 2000. **142**: p. 97–101.
52. O'Haver, T., *ipf(arg1,arg2,arg3,arg4)*. 2025, MATLAB Central File Exchange.
53. Dai, Z., T.T. Tran, and J. Skibsted, *Aluminum Incorporation in the C–S–H phase of white Portland cement–metakaolin blends studied by 27 Al and 29 Si MAS NMR spectroscopy.* Journal of the American Ceramic Society, 2014. **97**(8): p. 2662-2671.
54. Liu, W., et al., *XRD and 29Si MAS NMR study on carbonated cement paste under accelerated carbonation using different concentration of CO2.* Materials Today Communications, 2019. **19**: p. 464-470.
55. Gonçalves, B., et al., *X-ray diffraction study of the early hydration of Portland cements containing calcium carbonate by in-situ and ex-situ approaches.* Construction and Building Materials, 2023. **365**: p. 129947.
56. Lu, B., et al., *Effects of carbonated hardened cement paste powder on hydration and microstructure of Portland cement.* Construction and Building Materials, 2018. **186**: p. 699-708.
57. Gastaldi, D., et al., *Hydration products in sulfoaluminate cements: Evaluation of amorphous phases by XRD/solid-state NMR.* Cement and Concrete Research, 2016. **90**: p. 162-173.
58. Hay, R., L. Li, and K. Celik, *Shrinkage, hydration, and strength development of limestone calcined clay cement (LC3) with different sulfation levels.* Cement and concrete composites, 2022. **127**: p. 104403.
59. Zunino, F. and K. Scrivener, *Microstructural developments of limestone calcined clay cement (LC3) pastes after long-term (3 years) hydration.* Cement and Concrete Research, 2022. **153**: p. 106693.
60. Bahman-Zadeh, F., A.A. Ramezanianpour, and A. Zolfagharnasab, *Effect of carbonation on chloride binding capacity of limestone calcined clay cement (LC3) and binary pastes.* Journal of Building Engineering, 2022. **52**: p. 104447.
61. Lothenbach, B., K. Scrivener, and R. Hooton, *Supplementary cementitious materials.* Cement and concrete research, 2011. **41**(12): p. 1244-1256.
62. Huang, Z. and T. Liang, *Experimental studies on durability performances of ultra-lightweight low-carbon LC3 cement composites against chloride ingression and carbonation.* Construction and Building Materials, 2023. **395**: p. 132340.
63. Deschner, F., et al., *Hydration of Portland cement with high replacement by siliceous fly ash.* Cement and Concrete Research, 2012. **42**(10): p. 1389-1400.
64. Herterich, J., *Microstructure and phase assemblage of low-clinker cements during early stages of carbonation*. 2017, University of Leeds.

Preprint not peer reviewed

This preprint research paper has not been peer reviewed. Electronic copy available at: https://ssrn.com/abstract=6205146

65. Dubina, E., et al., *Influence of water vapour and carbon dioxide on free lime during storage at 80 C, studied by Raman spectroscopy.* Spectrochimica Acta Part A: Molecular and Biomolecular Spectroscopy, 2013. **111**: p. 299-303.
66. Yang, H., et al., *Carbonation of ettringite and monosulfate: product evolution, microstructure, and comparison.* Cement and Concrete Composites, 2025: p. 106297.
67. Auroy, M., et al., *Comparison between natural and accelerated carbonation (3% CO2): Impact on mineralogy, microstructure, water retention and cracking.* Cement and Concrete Research, 2018. **109**: p. 64-80.
68. Zhuo Dai, T.T.T., and Jørgen Skibsted†,*, *Aluminum Incorporation in the C–S–H Phase of White Portland Cement– Metakaolin Blends Studied by 27Al and 29Si MAS NMR Spectroscopy.* 2014.
69. Ikeda, Y., et al., *29Si MAS NMR study on structural change of silicate anions with carbonation of synthetic 11Å tobermorite.* Journal of the Ceramic Society of Japan, 1992. **100**(1165): p. 1098-1102.
70. Skibsted, J., J. Hjorth, and H.J. Jakobsen, *Correlation between 29Si NMR chemical shifts and mean Si□ O bond lengths for calcium silicates.* Chemical physics letters, 1990. **172**(3-4): p. 279-283.
71. Neto, F.M., R. Snellings, and J. Skibsted, *Aqueous carbonation of aged blended Portland cement pastes: Impact of the Al/Si ratio on the structure of the alumina-silica gel.* Cement and Concrete Research, 2024. **177**: p. 107428.
72. Neto, F.M., R. Snellings, and J. Skibsted, *Reactivity of aqueous carbonated cement pastes: Effect of chemical composition and carbonation conditions.* Journal of CO2 Utilization, 2024. **89**: p. 102970.
73. Maia Neto, F. and J. Skibsted, *Characterization of aqueous carbonated cement-based materials by multinuclear solid-state NMR spectroscopy.* Journal of Sustainable Cement-Based Materials, 2025. **14**(6): p. 1191-1206.
74. Sevelsted, T.F. and J. Skibsted, *Carbonation of C–S–H and C–a–S–H samples studied by 13C, 27Al and 29Si MAS NMR spectroscopy.* Cement and concrete research, 2015. **71**: p. 56-65.
75. Souayfan, F., et al., *29Si and 27Al MAS NMR spectroscopic studies of activated metakaolin-slag mixtures.* Construction and Building Materials, 2022. **322**: p. 126415.
76. Jaskulski, R., D. Jóźwiak-Niedźwiedzka, and Y. Yakymechko, *Calcined Clay as Supplementary Cementitious Material.* Materials (Basel), 2020. **13**(21).
77. Lagerblad, B., *Carbon dioxide uptake during concrete life cycle: State of the art*. 2005: Swedish Cement and Concrete Research Institute Stockholm.
78. Shah, V., et al., *Changes in microstructure characteristics of cement paste on carbonation.* Cement and Concrete Research, 2018. **109**: p. 184-197.
79. Shi, Z., et al., *Experimental studies and thermodynamic modeling of the carbonation of Portland cement, metakaolin and limestone mortars.* Cement and Concrete Research, 2016. **88**: p. 60-72.
80. Villain, G. and M. Thiery. *Impact of carbonation on microstructure and transport properties of concrete*. in *Proceedings of*. 2005.

Preprint not peer reviewed

This preprint research paper has not been peer reviewed. Electronic copy available at: https://ssrn.com/abstract=6205146

81. Chen, T. and X. Gao, *Effect of carbonation curing regime on strength and microstructure of Portland cement paste.* Journal of CO2 Utilization, 2019. **34**: p. 74-86.
82. Matsusato, H., et al. *Studies on the carbonation of hydrated cement and its effect on microstructure and strength*. in *9th International Congress on the Chemistry of Cement*. 1992. National Council for Cement and Building Materials New Dehli.
83. Pihlajavaara, S., *Some results of the effect of carbonation on the porosity and pore size distribution of cement paste.* Matériaux et Construction, 1968. **1**(6): p. 521-527.
84. Chen, J.J., J.J. Thomas, and H.M. Jennings, *Decalcification shrinkage of cement paste.* Cement and concrete research, 2006. **36**(5): p. 801-809.
85. Kim, J.-S., et al., *Effect of carbonation on cement paste microstructure characterized by micro-computed tomography.* Construction and Building Materials, 2020. **263**: p. 120079.
86. Young, J.F., *The science and technology of civil engineering materials.* (No Title), 1998.
87. Cook, R.A. and K.C. Hover, *Mercury porosimetry of hardened cement pastes.* Cement and Concrete research, 1999. **29**(6): p. 933-943.

Preprint not peer reviewed

This preprint research paper has not been peer reviewed. Electronic copy available at: https://ssrn.com/abstract=6205146

Supplementary Data

Deconvoluted DTG Peaks for Undried OPC

Peak Analysis

Data Set:[Book6]"OPC undried"!E"Inv deriv" Date:2025-12-03

BaseLine:Straight

Chi^2=8.17500E-07 Adj. R-Square=8.33071E-01 # of Data Points=1941

SS=1.58513E-03 Degrees of Freedom=1939

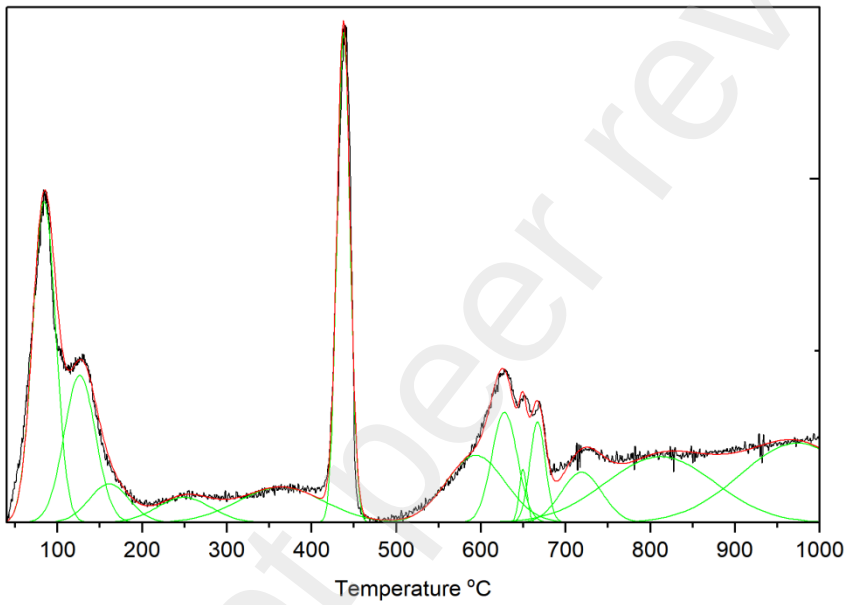

Fitting Results

Peak Index	Peak Type	Area Intg	FWHM	Max Height	Center Grvty	Area IntgP
1	Gaussian	0.31778	31.97538	0.00934	84.19946	15.23949
2	Gaussian	0.19897	43.65952	0.00428	126.38366	9.54183
3	Gaussian	0.06678	55.81005	0.00112	161.01968	3.2024
4	Gaussian	0.0588	75.54493	7.31258E-4	249.35923	2.82002
5	Gaussian	0.13099	118.84756	0.00104	363.75011	6.28172
6	Gaussian	0.2755	18.15272	0.01426	437.77944	13.21186
7	Gaussian	0.1708	82.04702	0.00196	593.71819	8.19106
8	Gaussian	0.12078	35.42182	0.0032	627.85768	5.79202
9	Gaussian	0.01748	10.64831	0.00154	649.56172	0.83842
10	Gaussian	0.06703	21.53316	0.00292	666.82469	3.21464
11	Gaussian	0.08787	56.38198	0.00146	718.61179	4.21401
12	Gaussian	0.26203	158.46429	0.00231	973.49159	12.56586
13	Gaussian	0.31042	152.57731	0.00191	811.9474	14.88665

Preprint not peer reviewed

This preprint research paper has not been peer reviewed. Electronic copy available at: https://ssrn.com/abstract=6205146

List of Figures:

Preprint not peer reviewed

This preprint research paper has not been peer reviewed. Electronic copy available at: https://ssrn.com/abstract=6205146

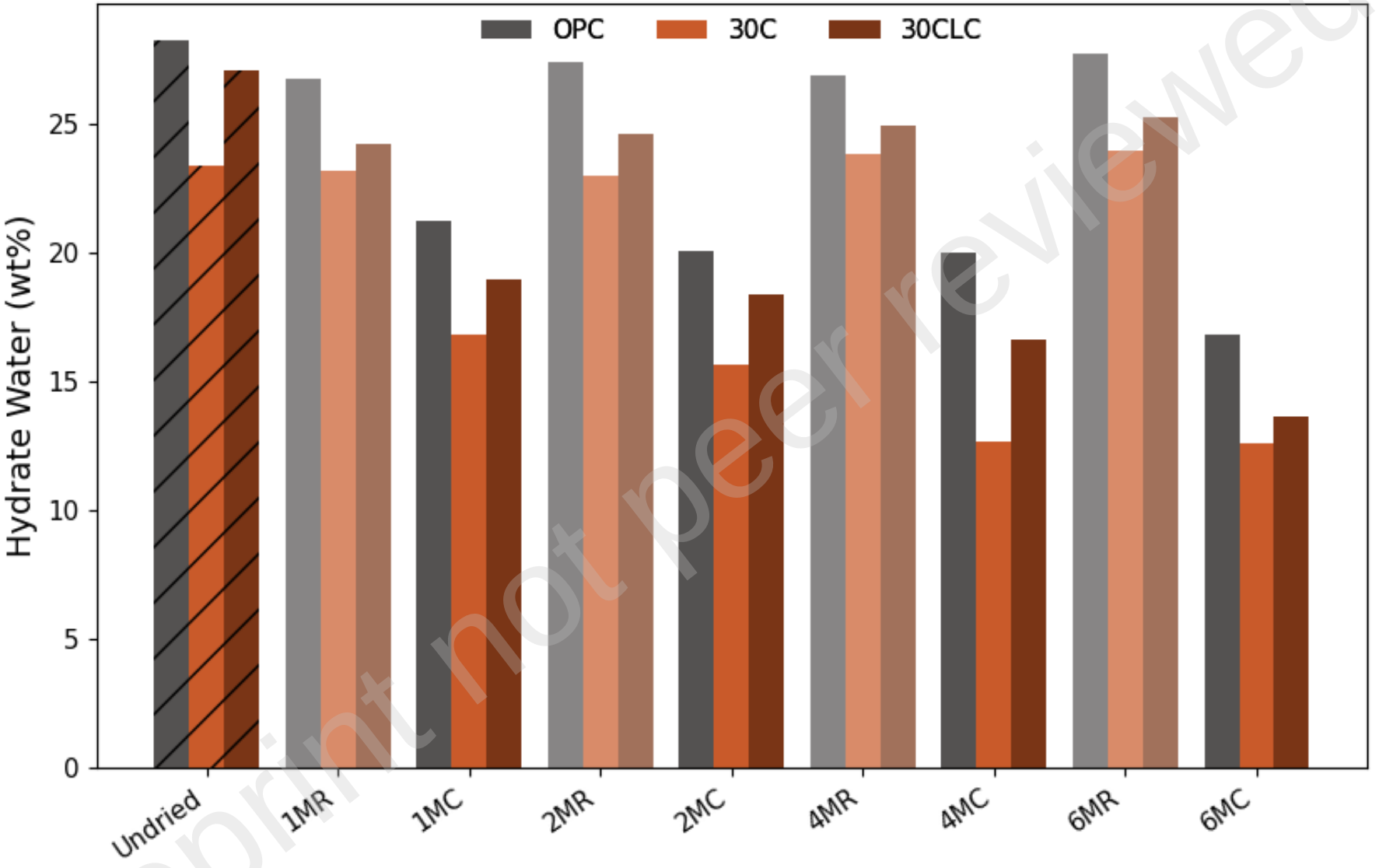

Preprint not peer reviewed

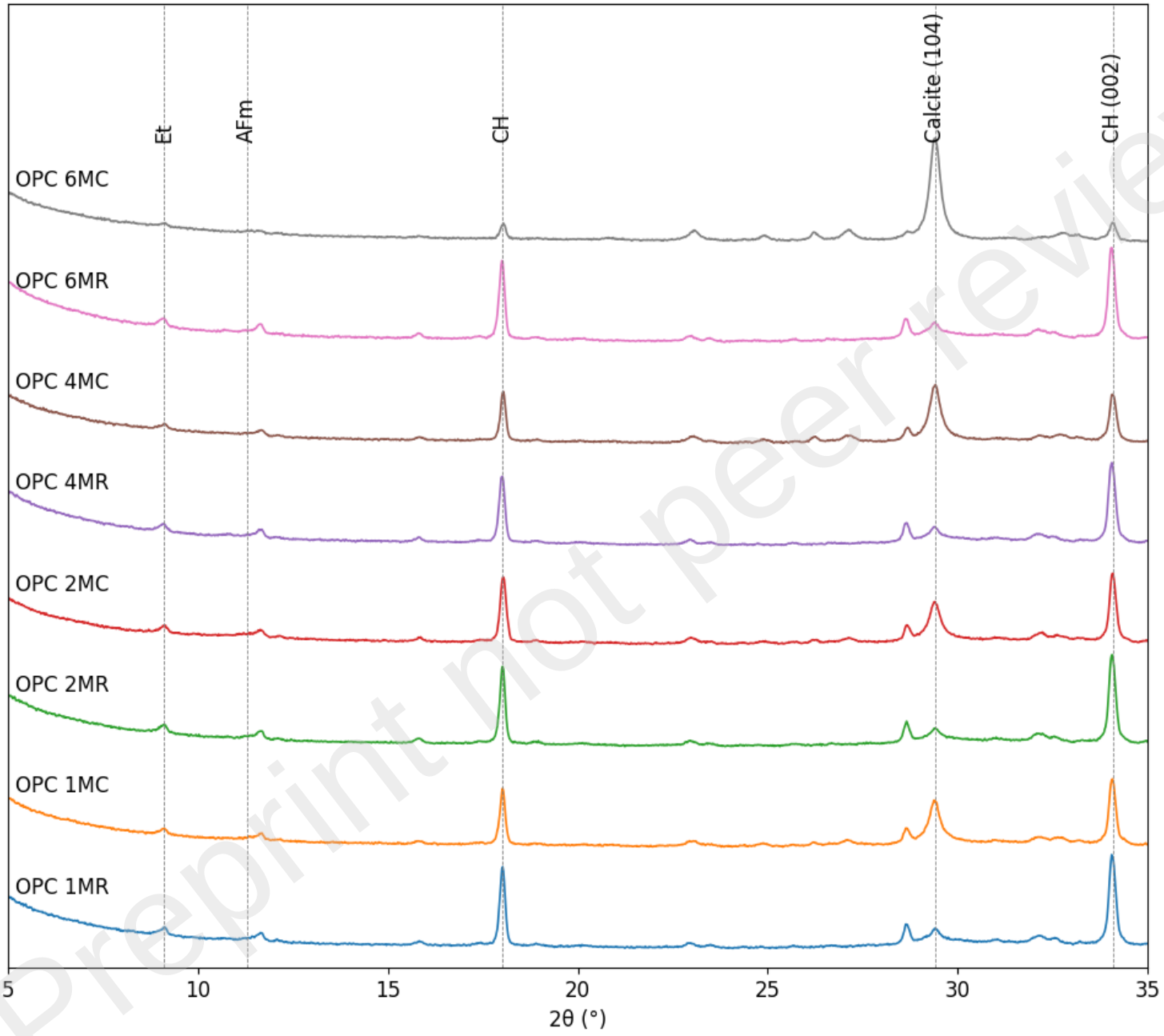

Preprint not peer reviewed

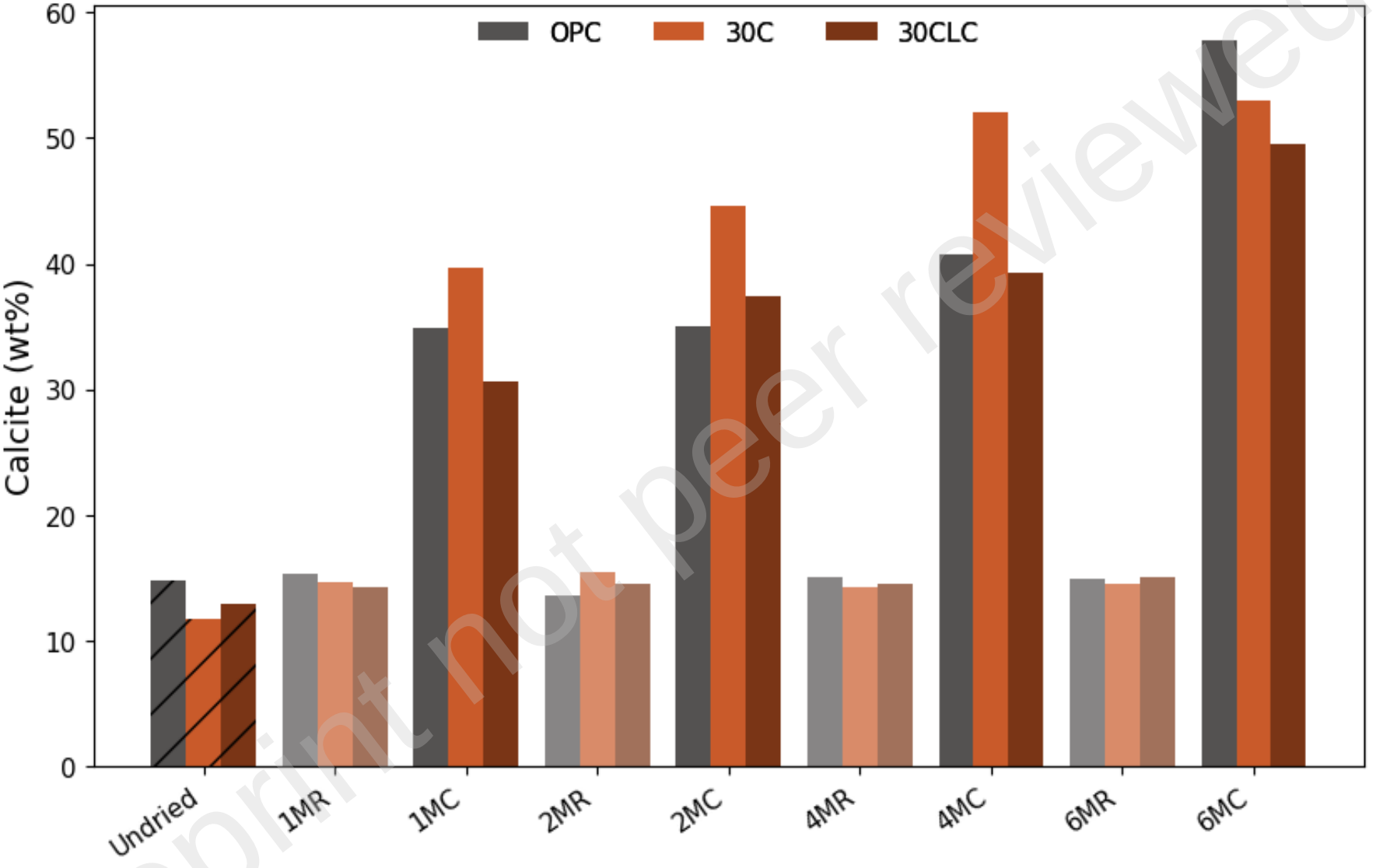

Preprint not peer reviewed

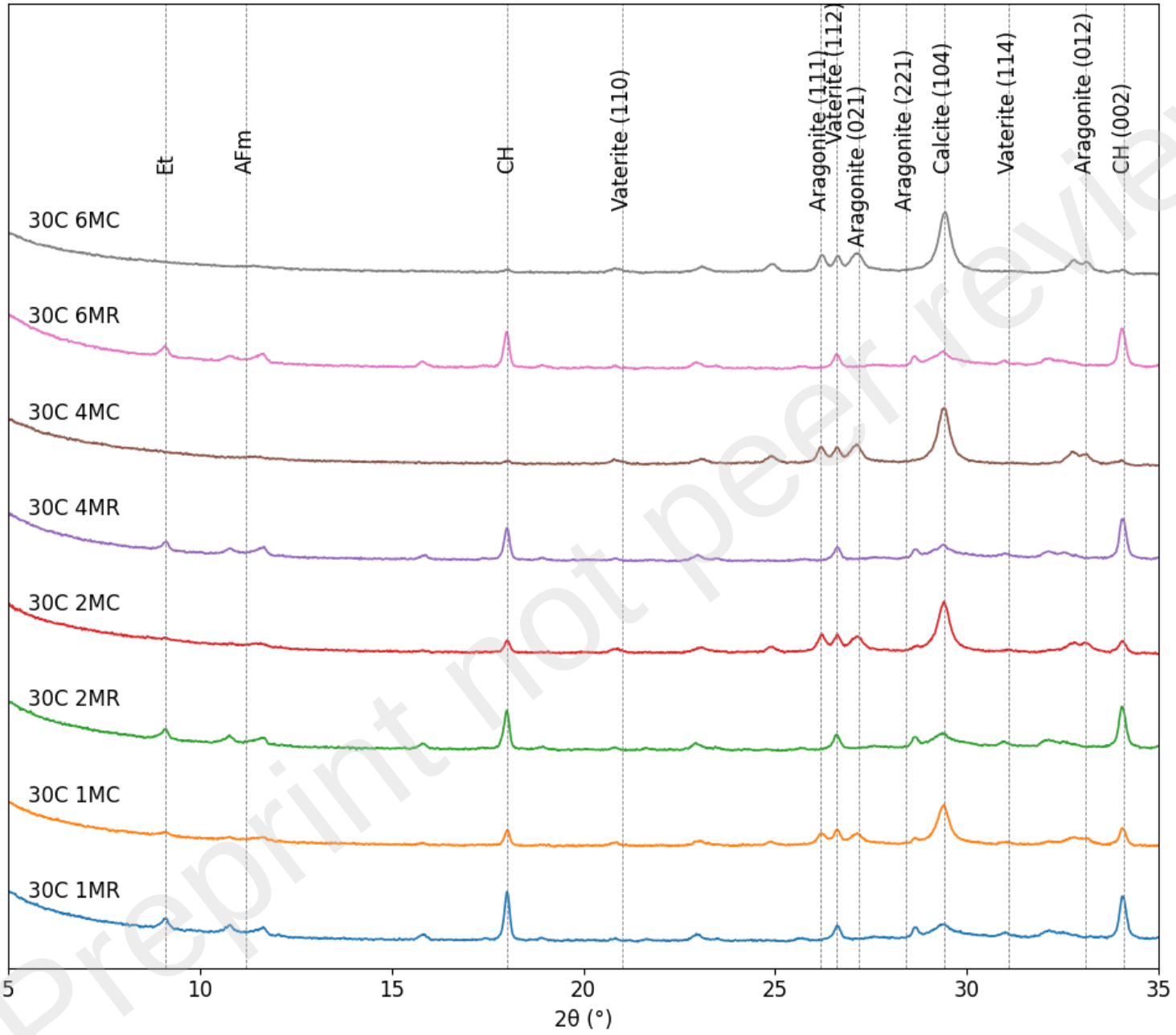

Preprint not peer reviewed

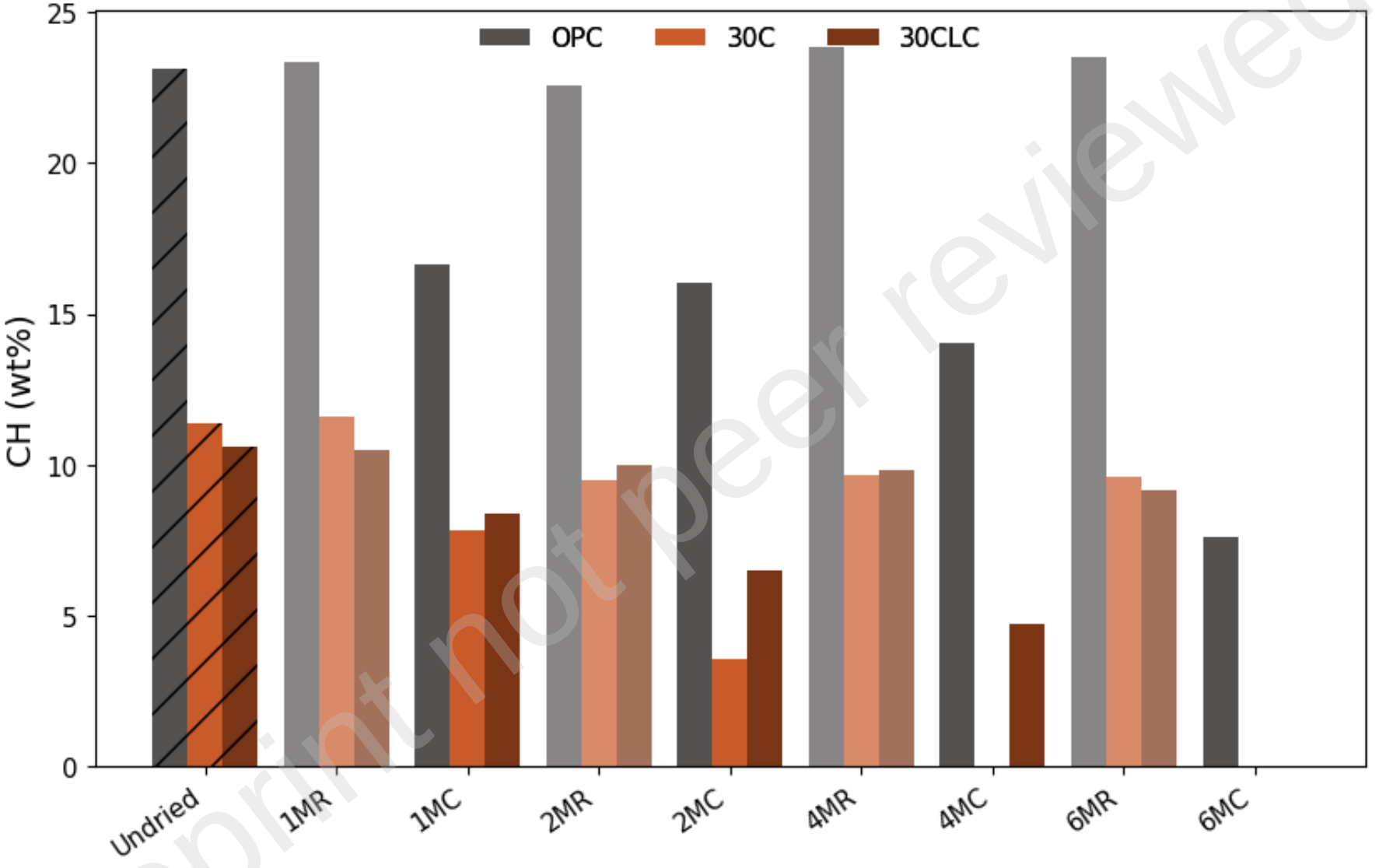

Preprint not peer reviewed

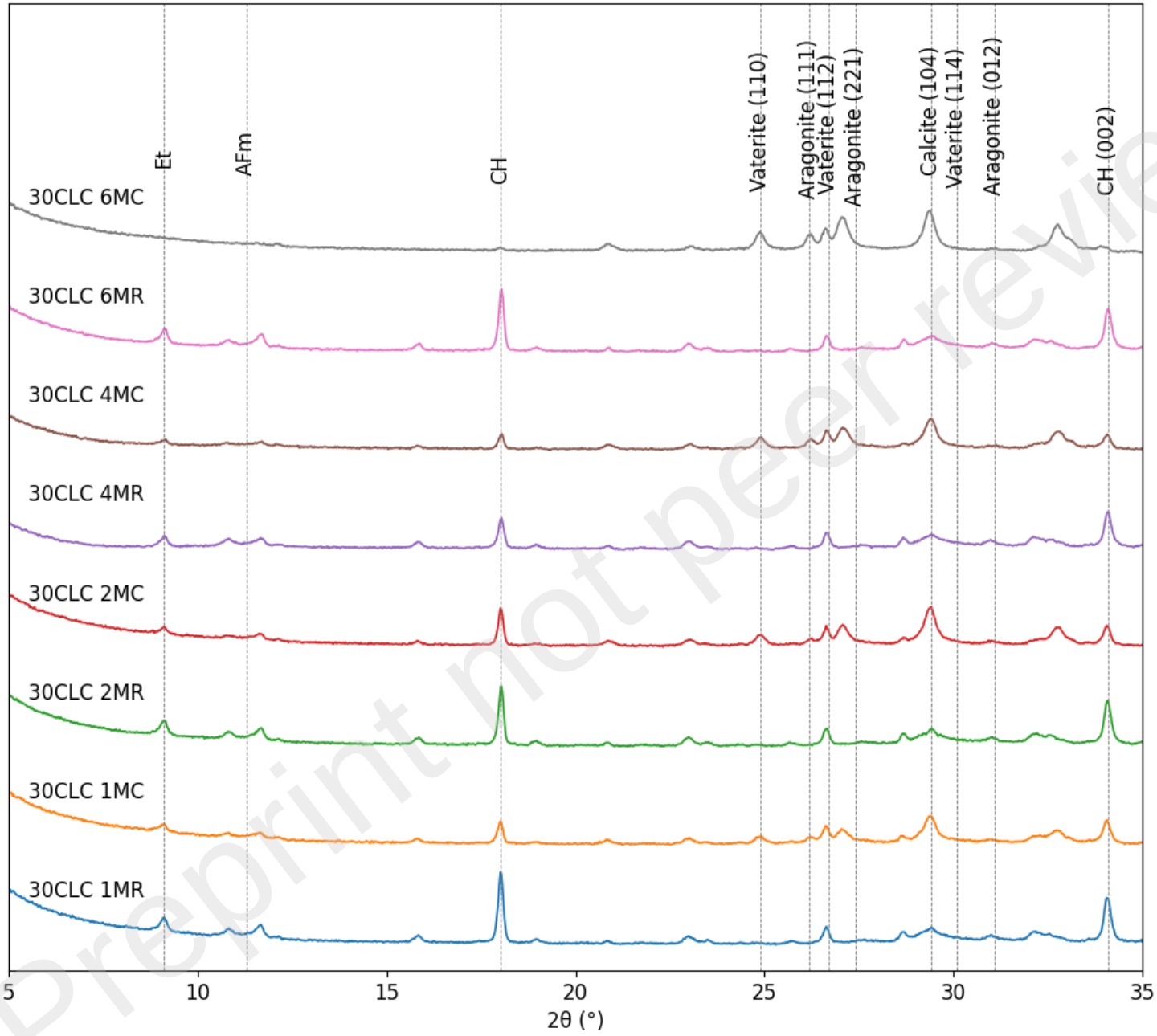

Preprint not peer reviewed

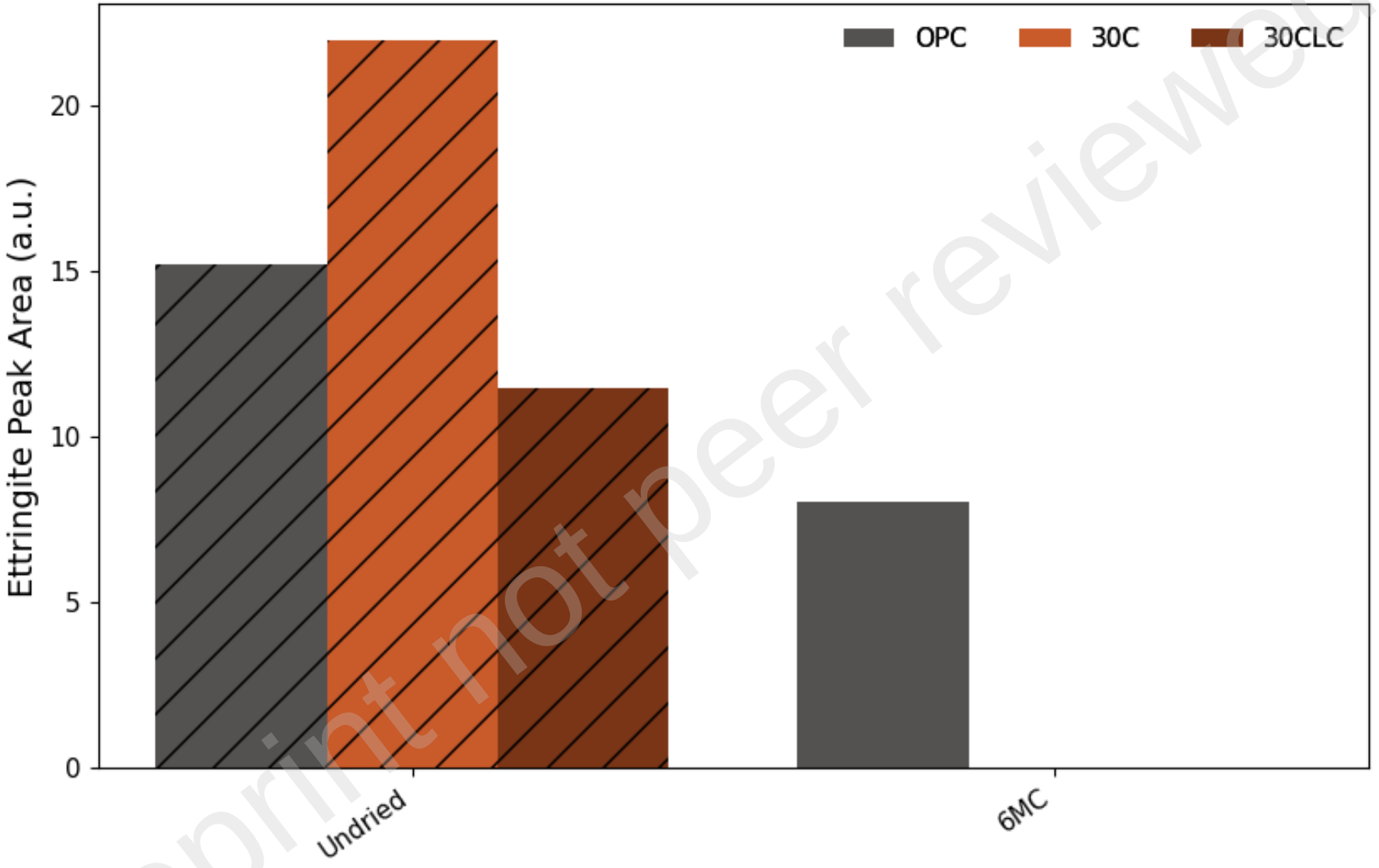

Preprint not peer reviewed

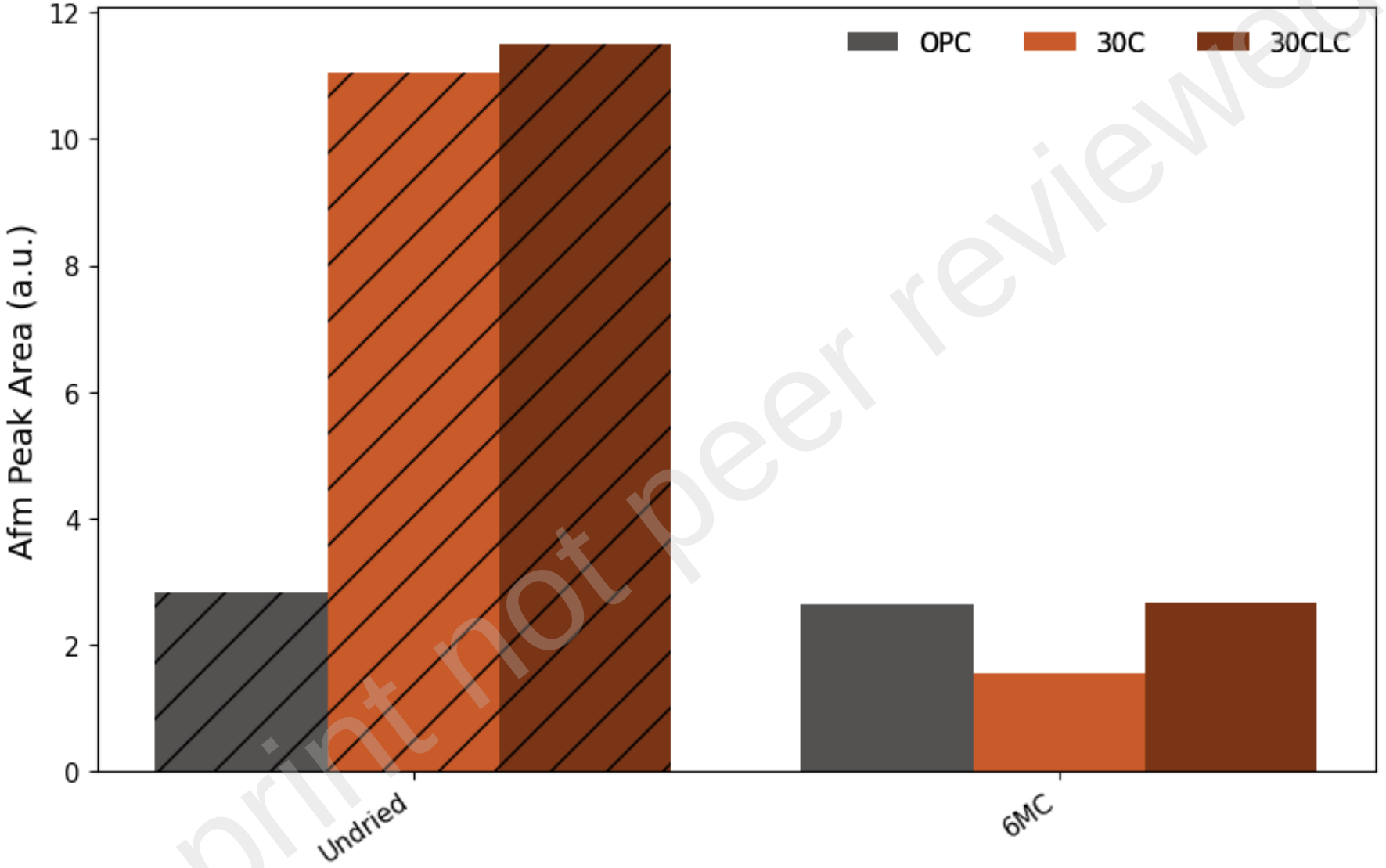

Preprint not peer reviewed

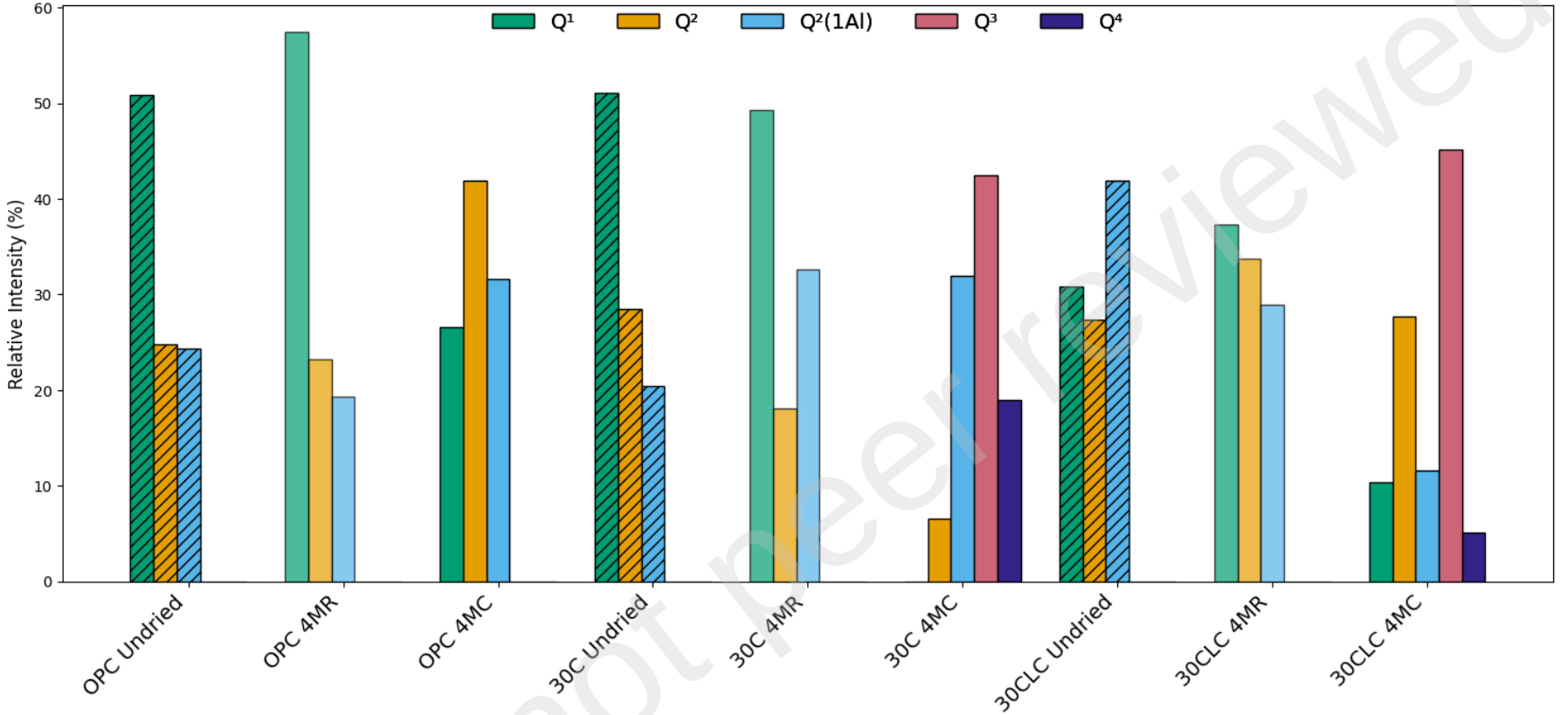

Preprint not peer reviewed

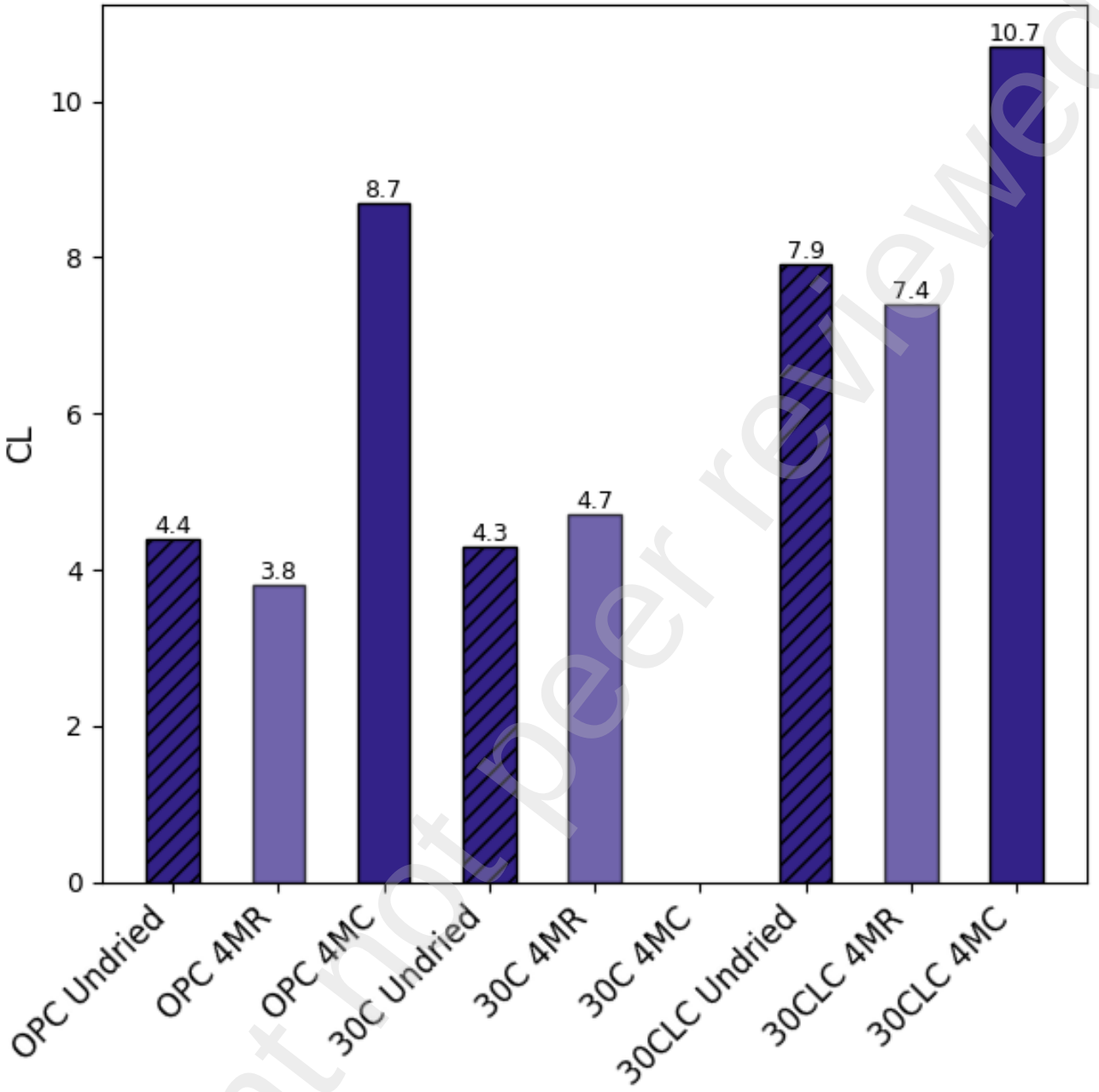

Preprint not peer reviewed

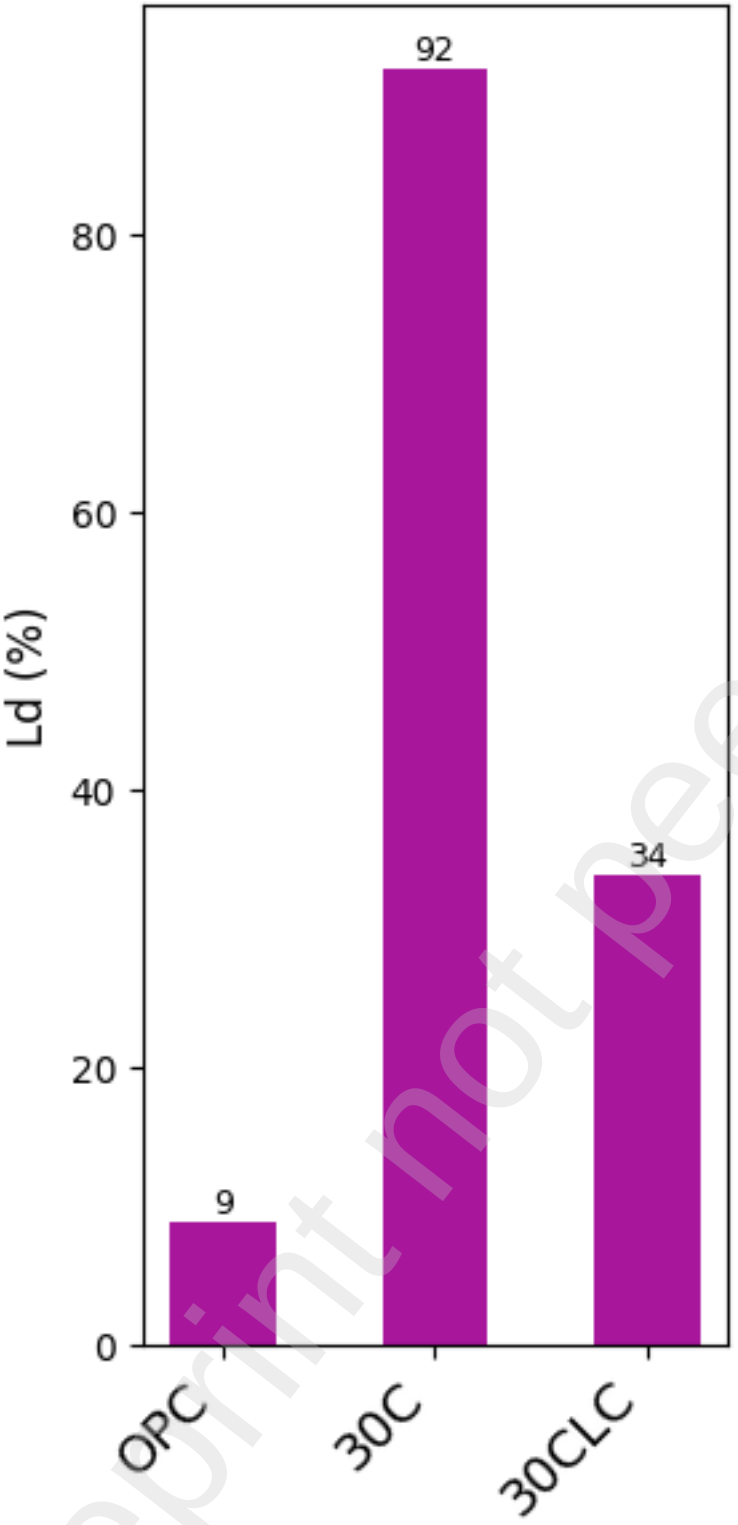

Preprint not peer reviewed

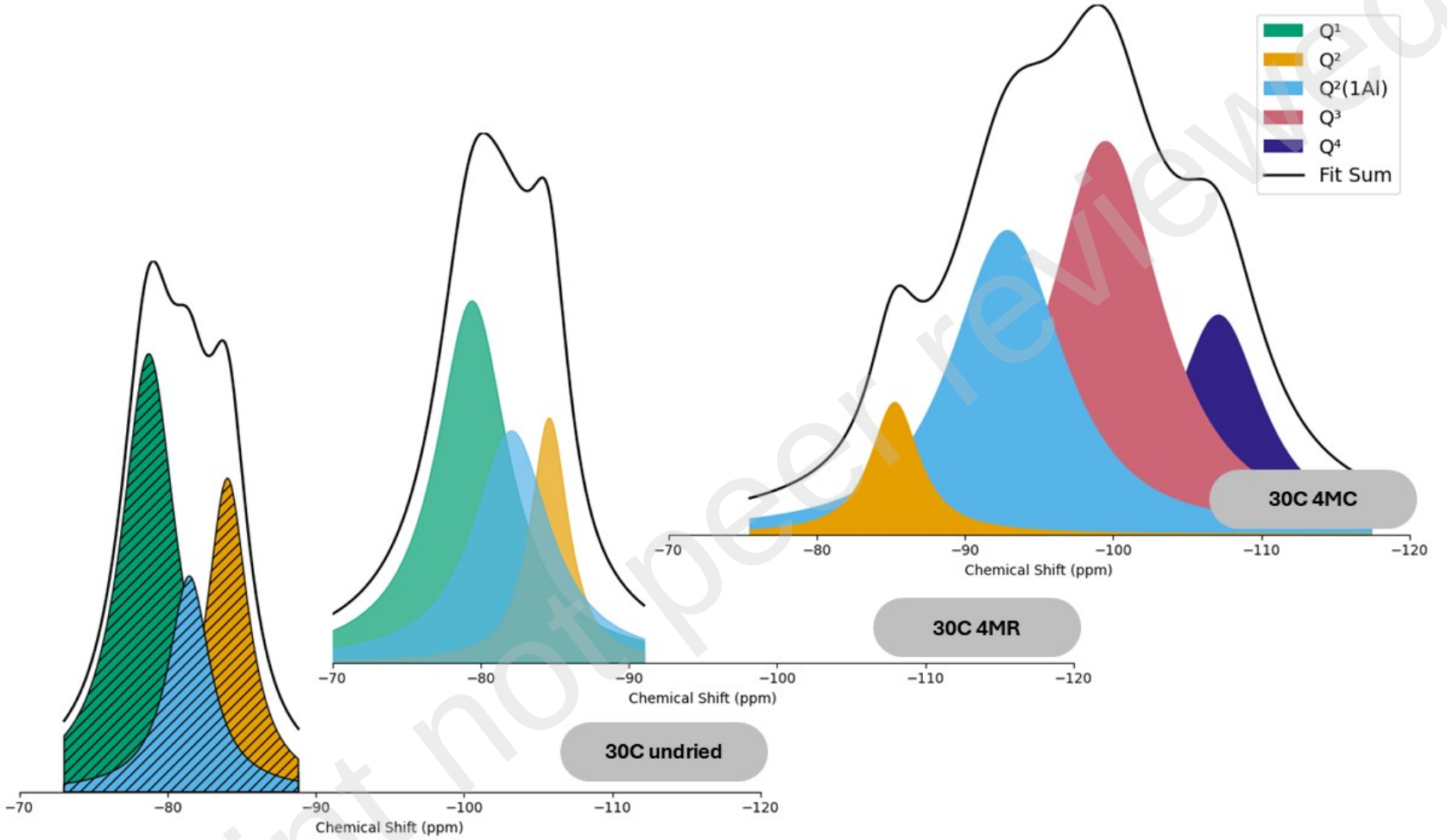

Preprint not peer reviewed

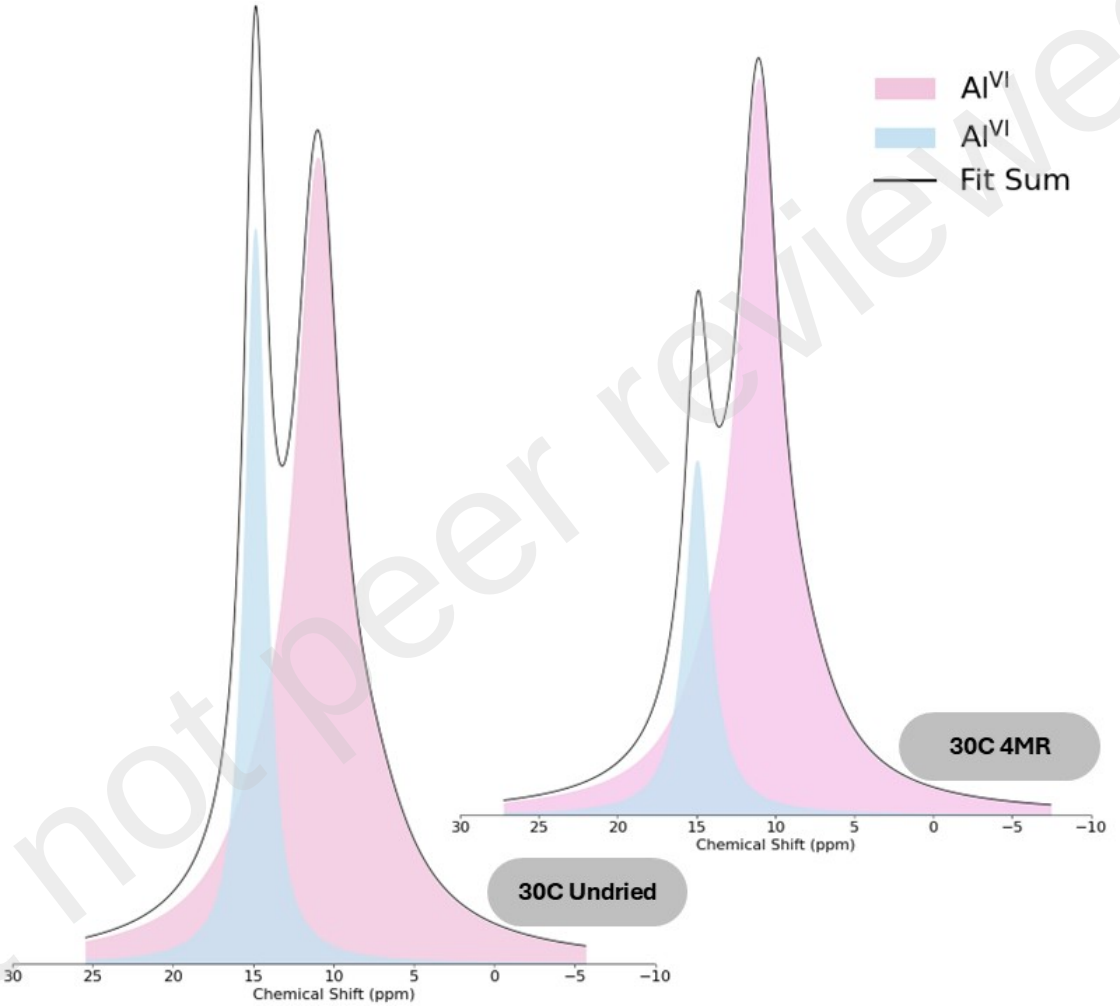

Preprint not peer reviewed

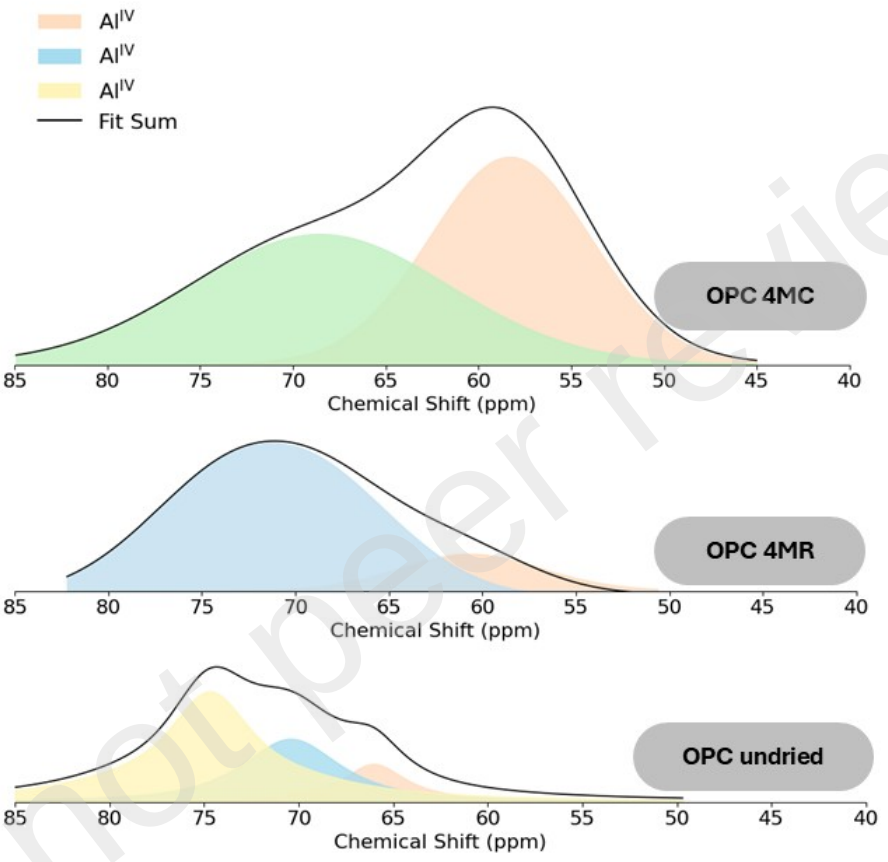

Preprint not peer reviewed

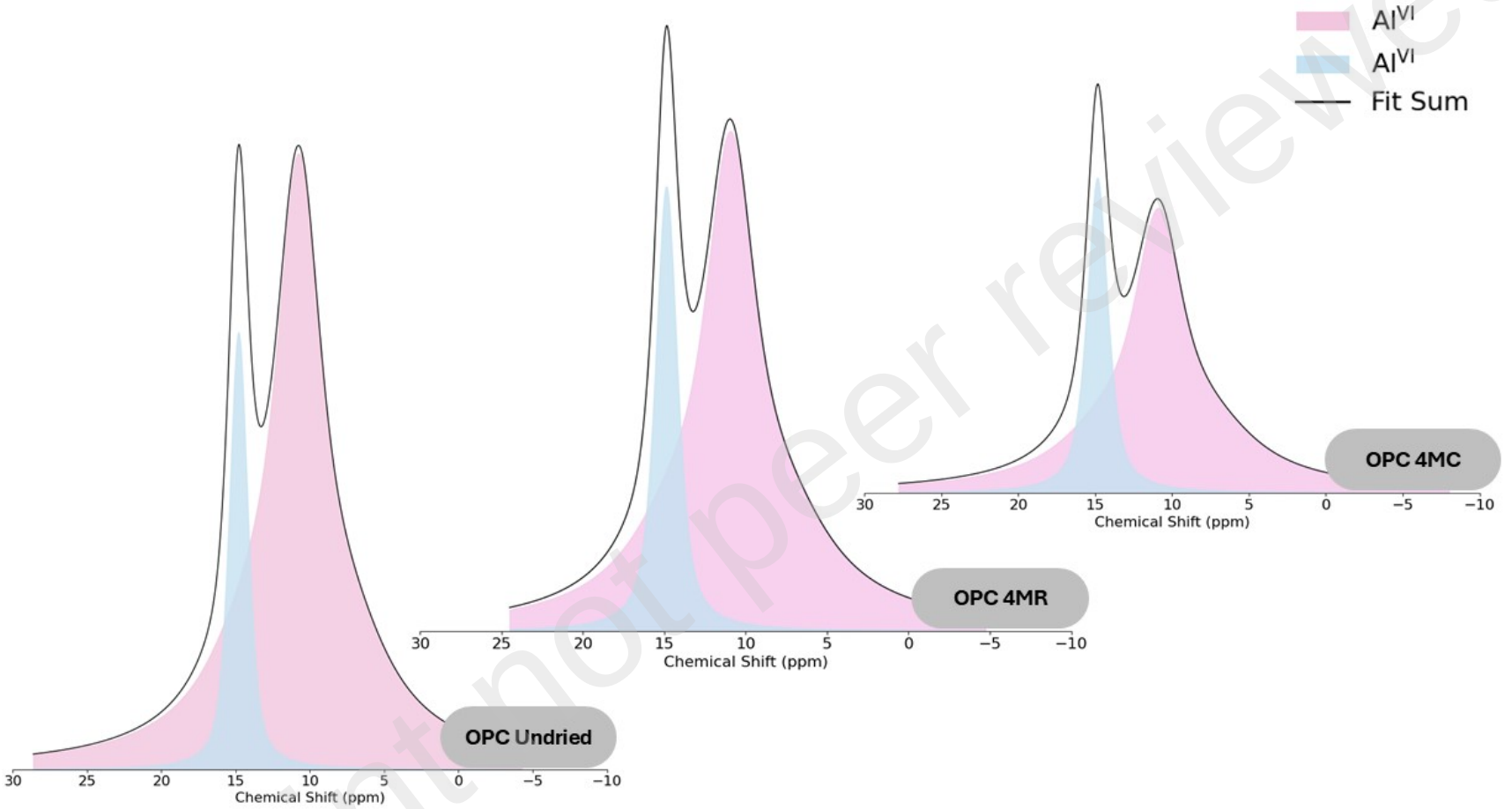

Preprint not peer reviewed

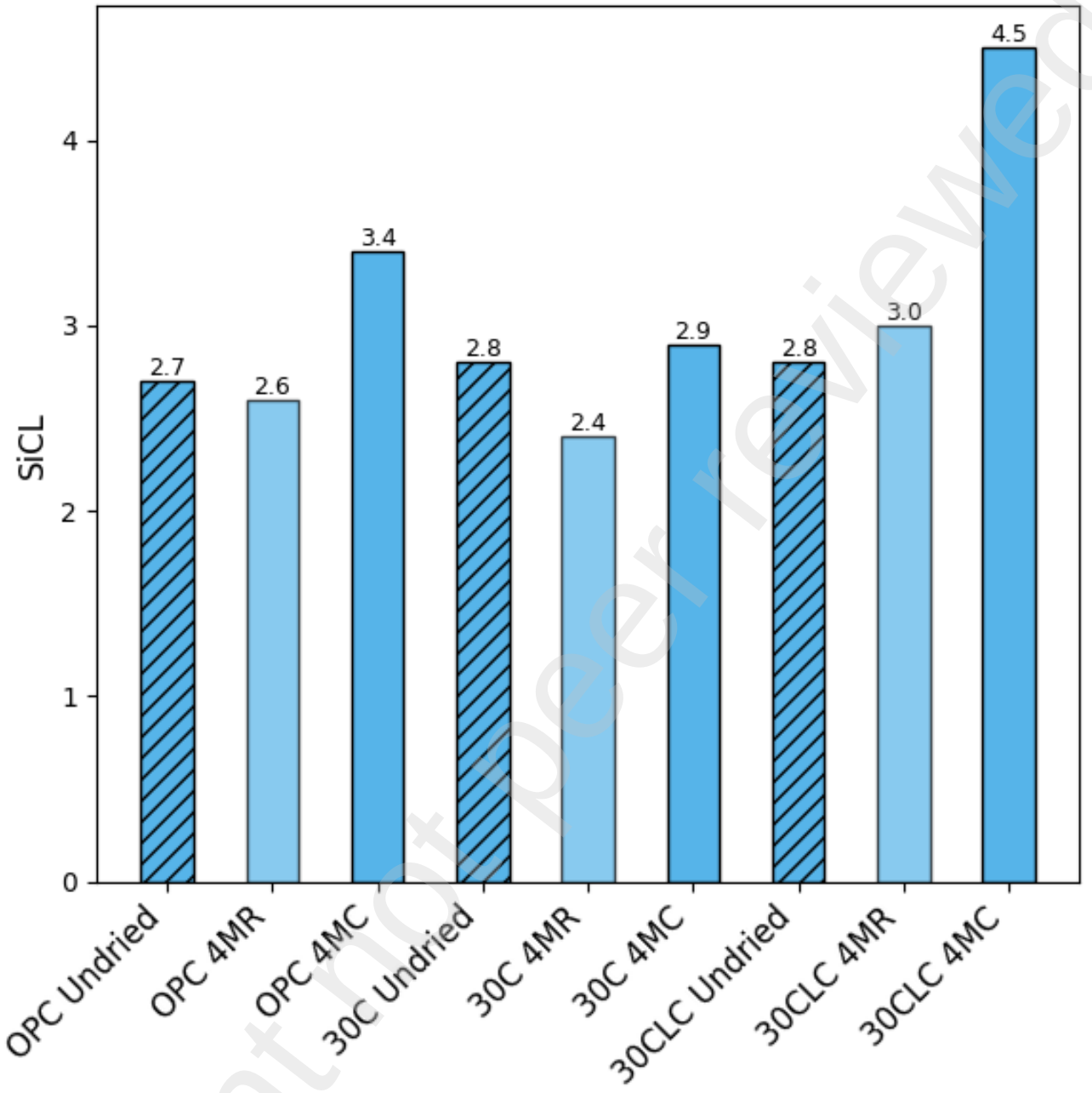

Preprint not peer reviewed

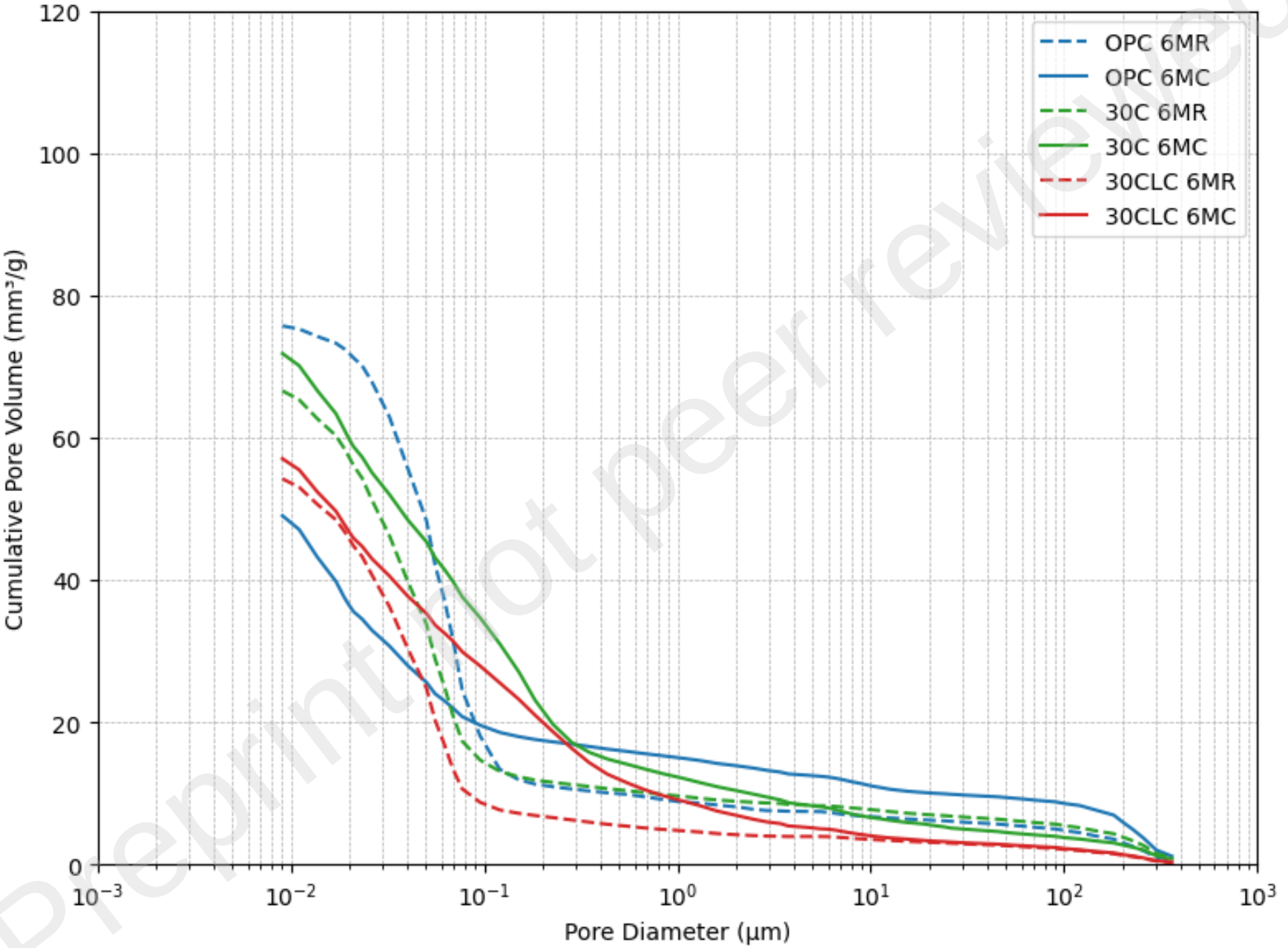

Preprint not peer reviewed

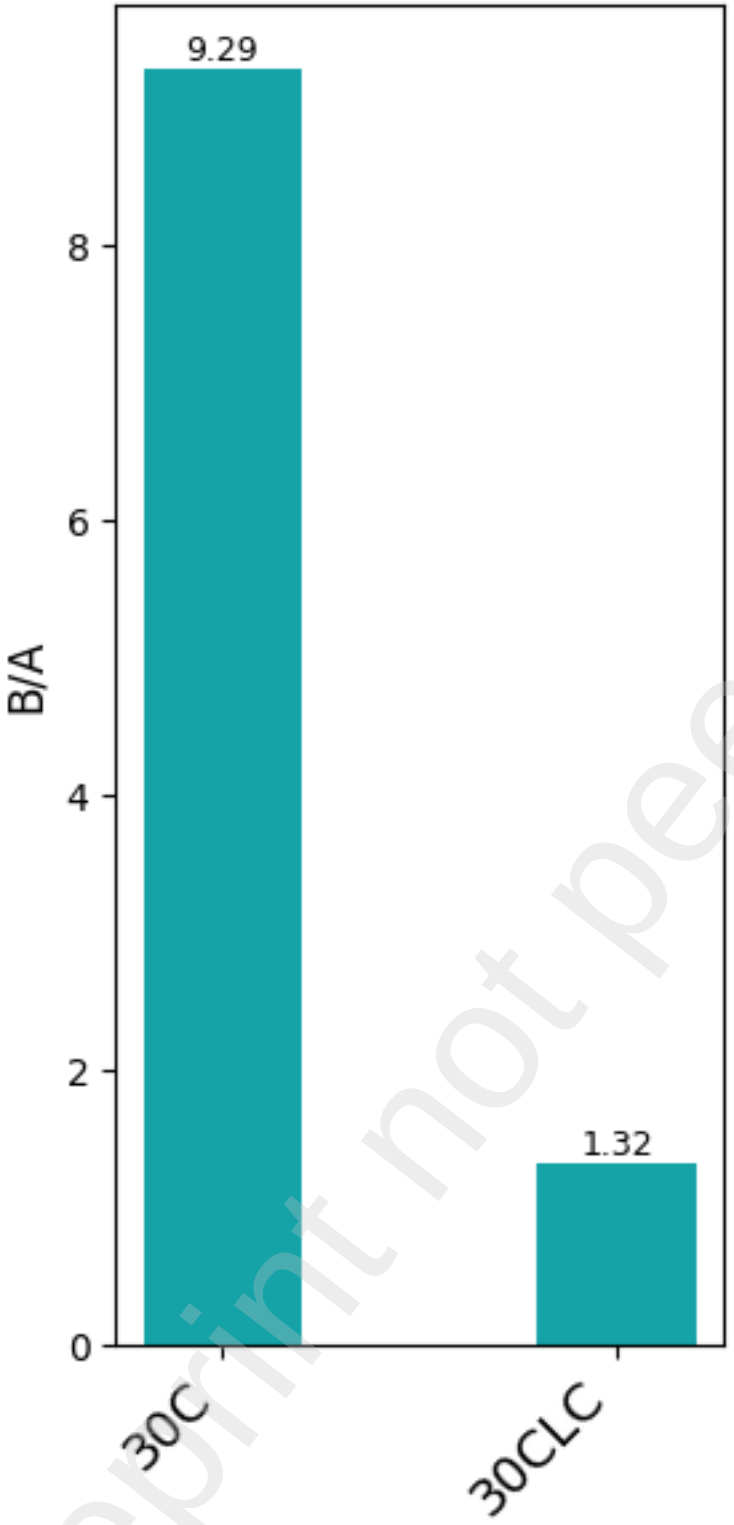

Preprint not peer reviewed

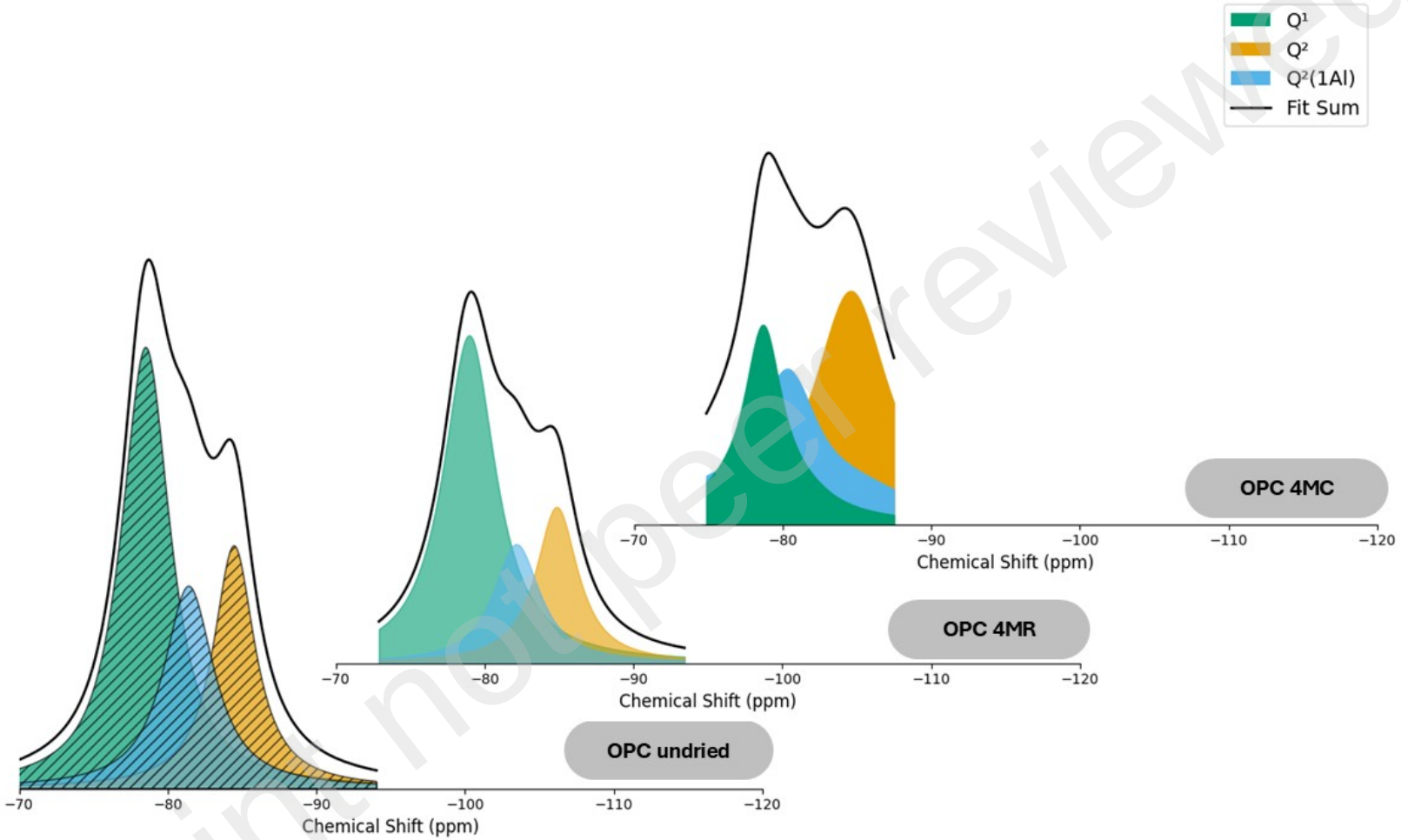

Preprint not peer reviewed

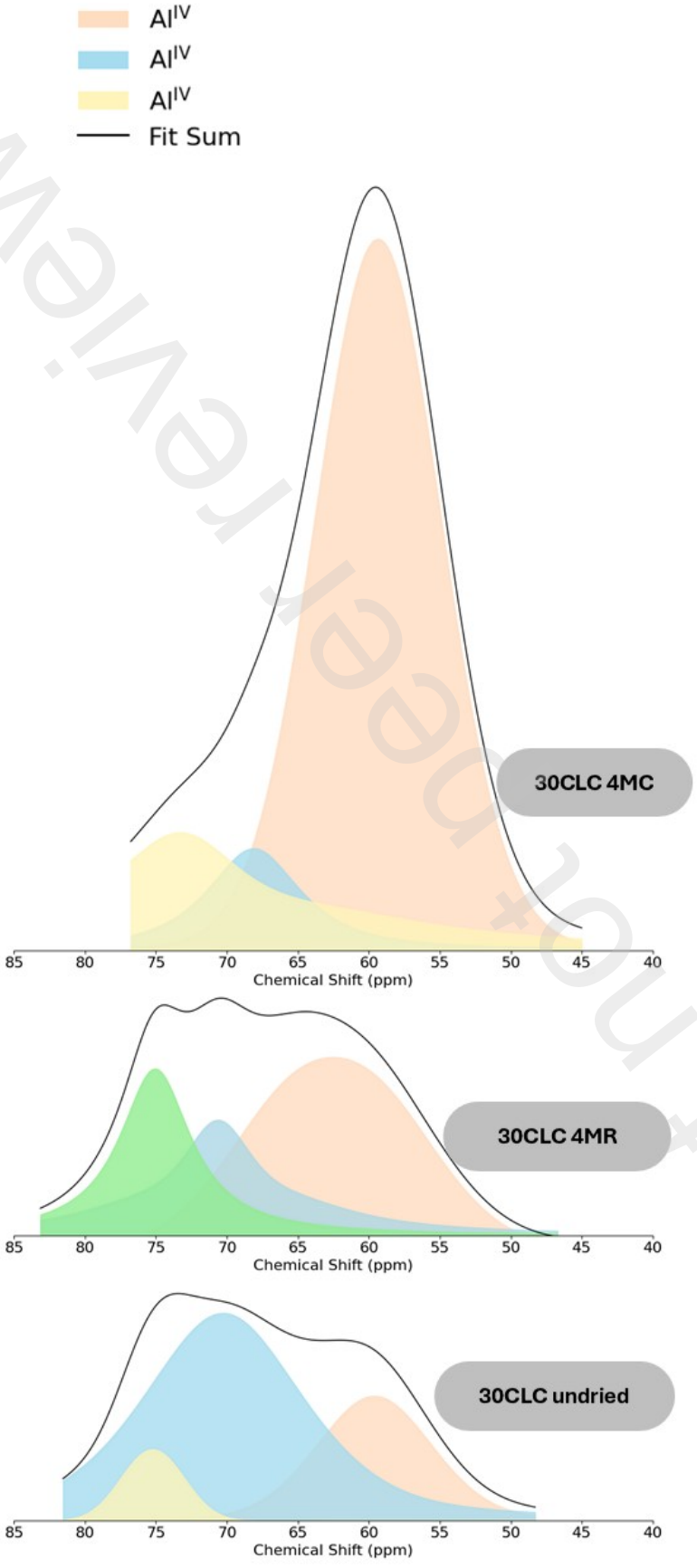

Preprint not peer reviewed

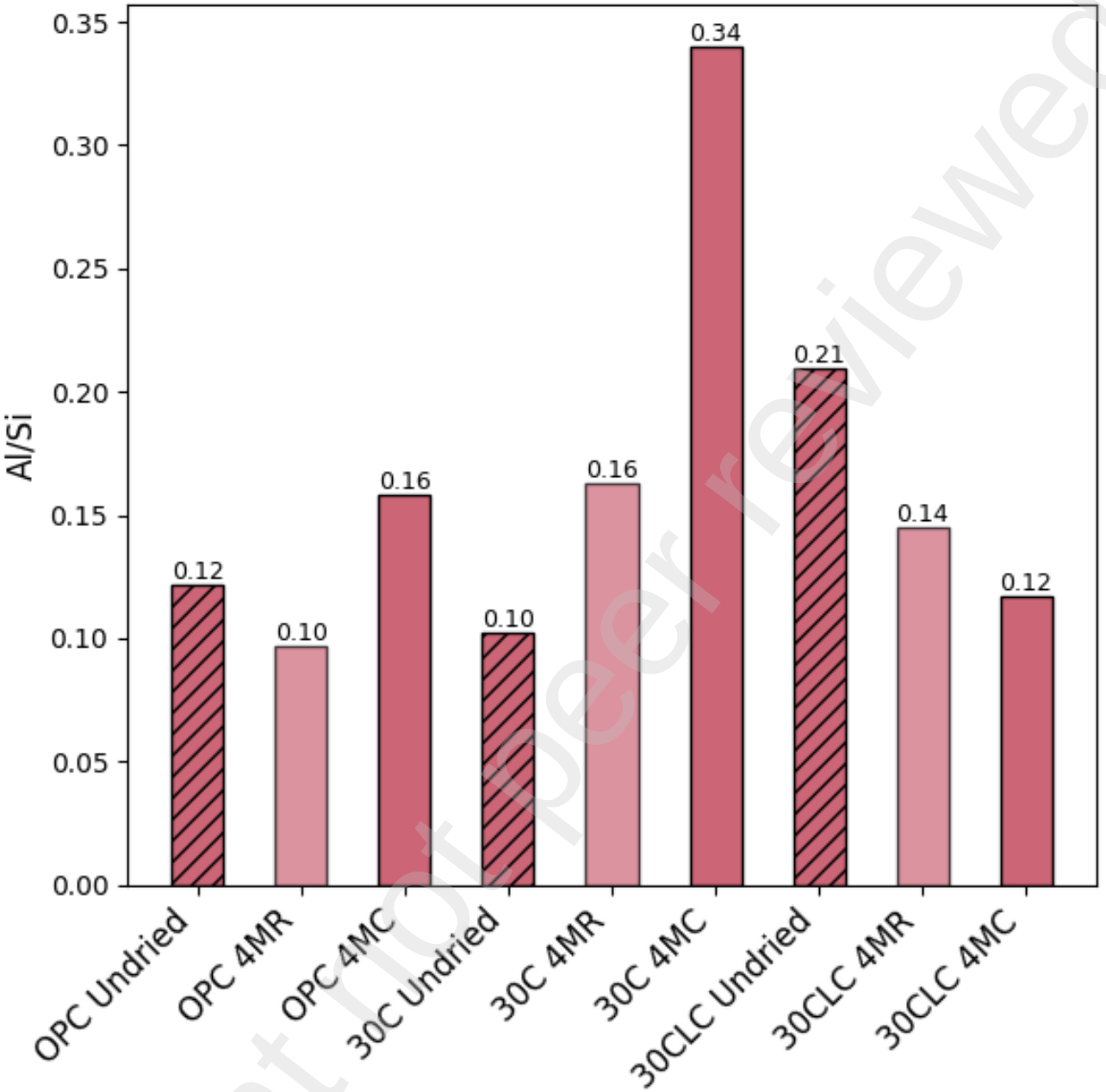

Preprint not peer reviewed

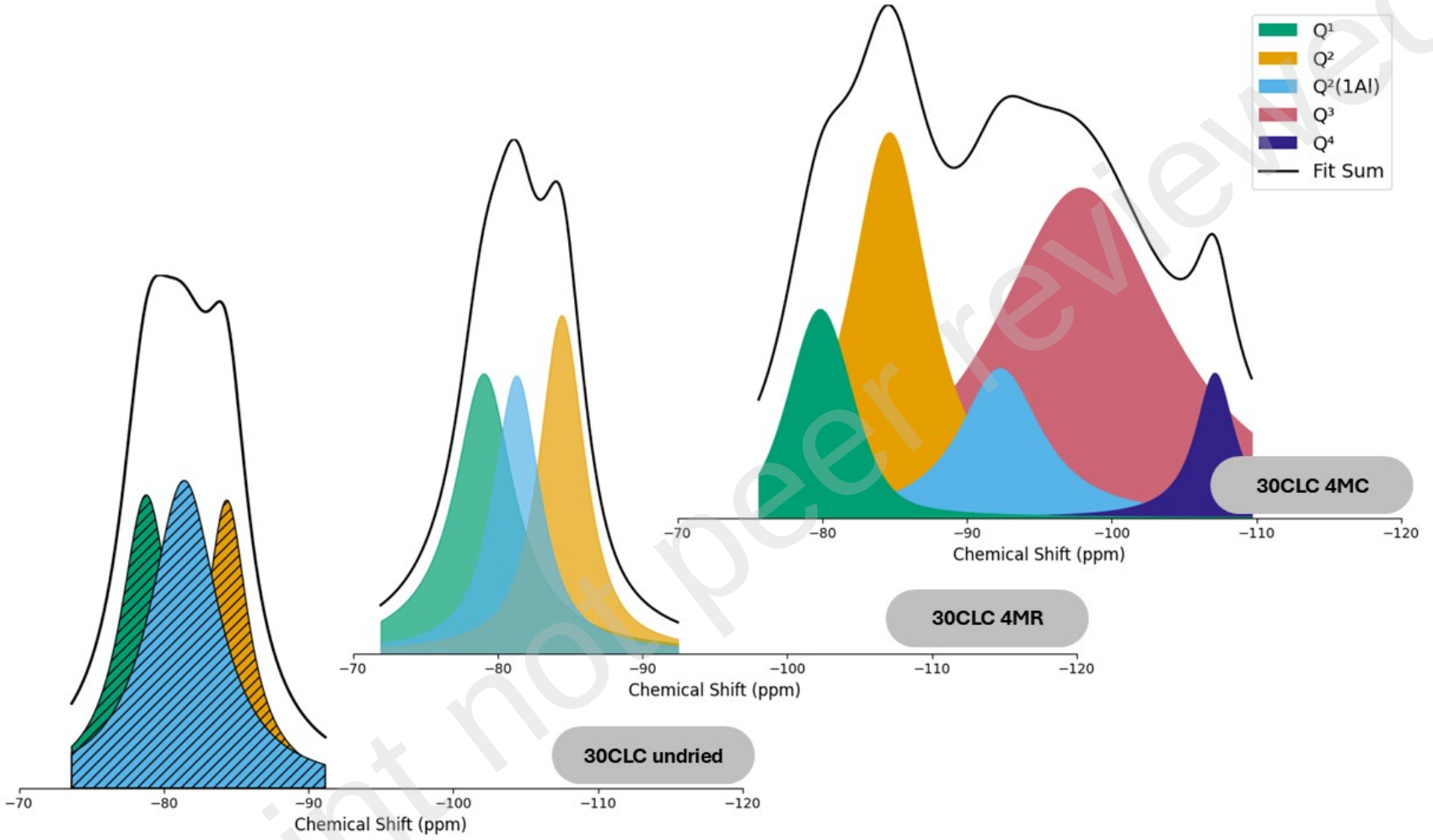

Preprint not peer reviewed

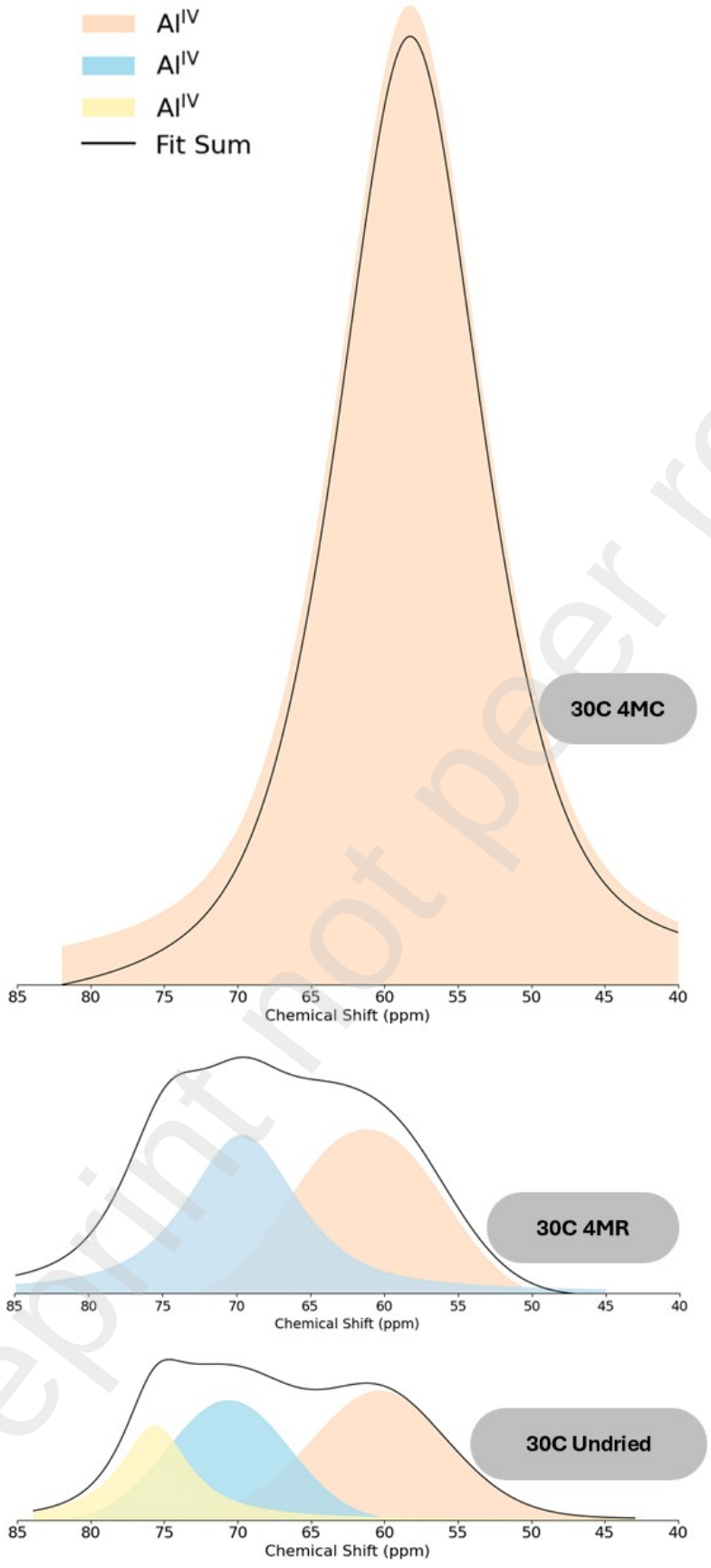

Preprint not peer reviewed

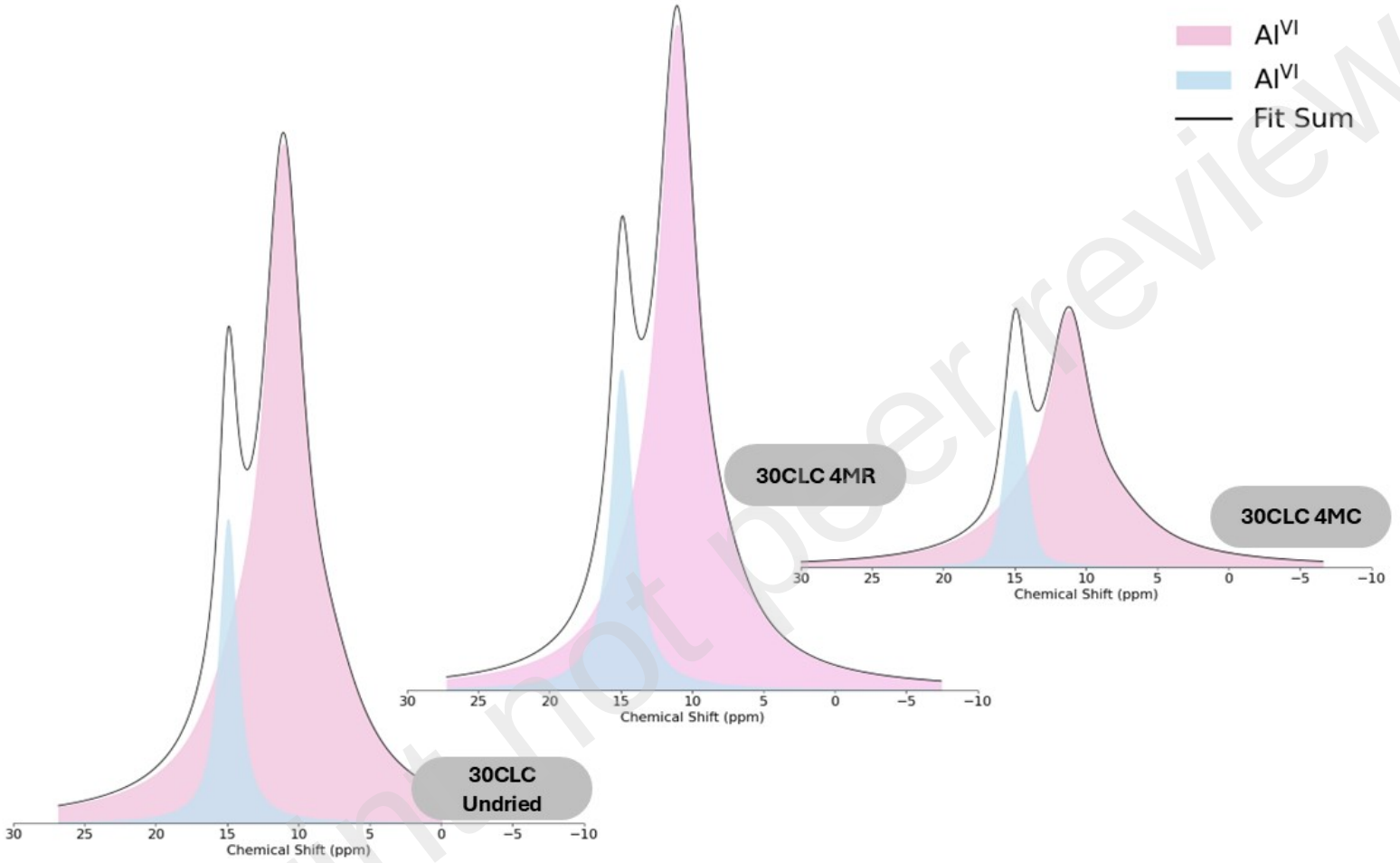

Preprint not peer reviewed

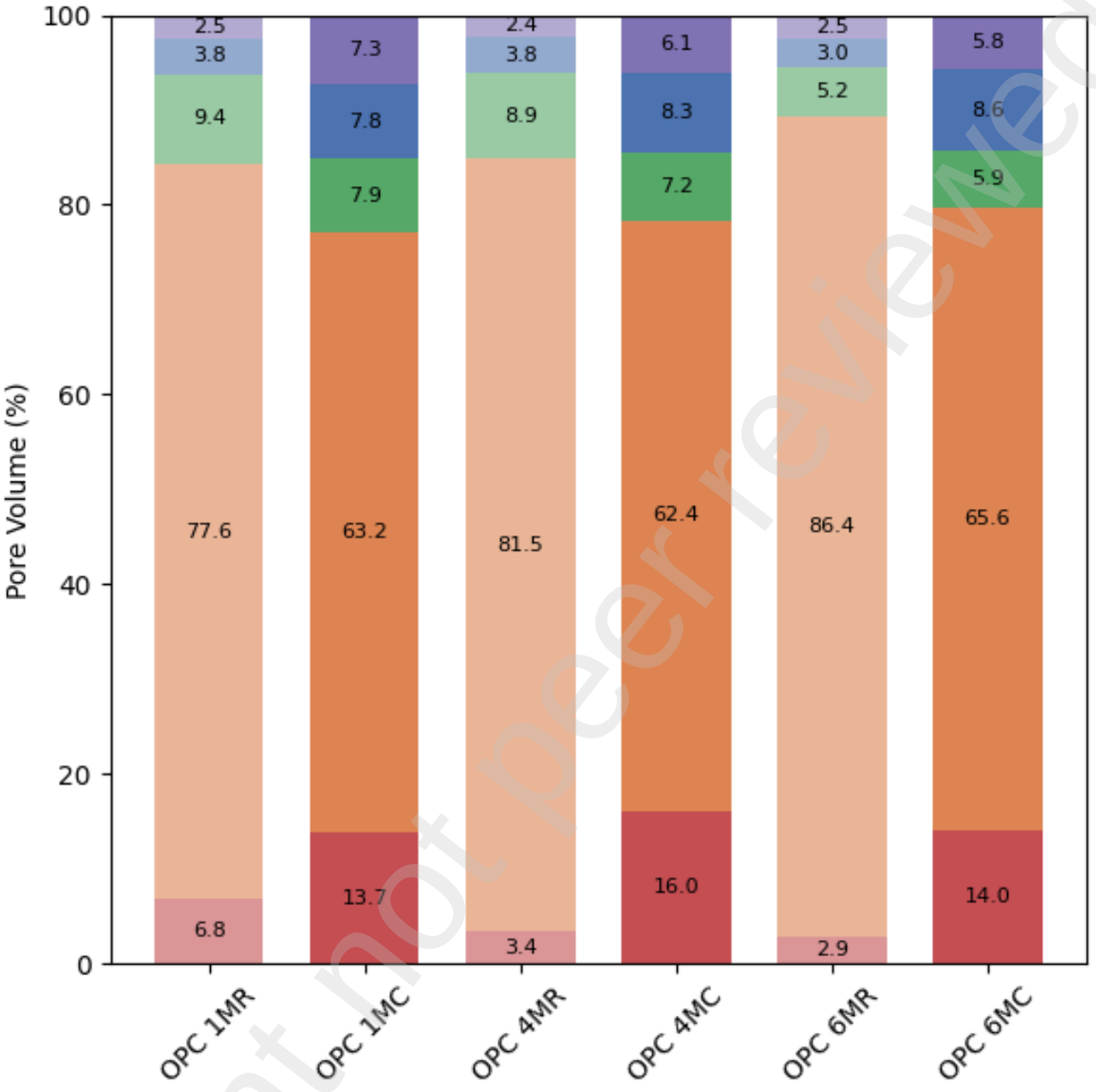

Preprint not peer reviewed

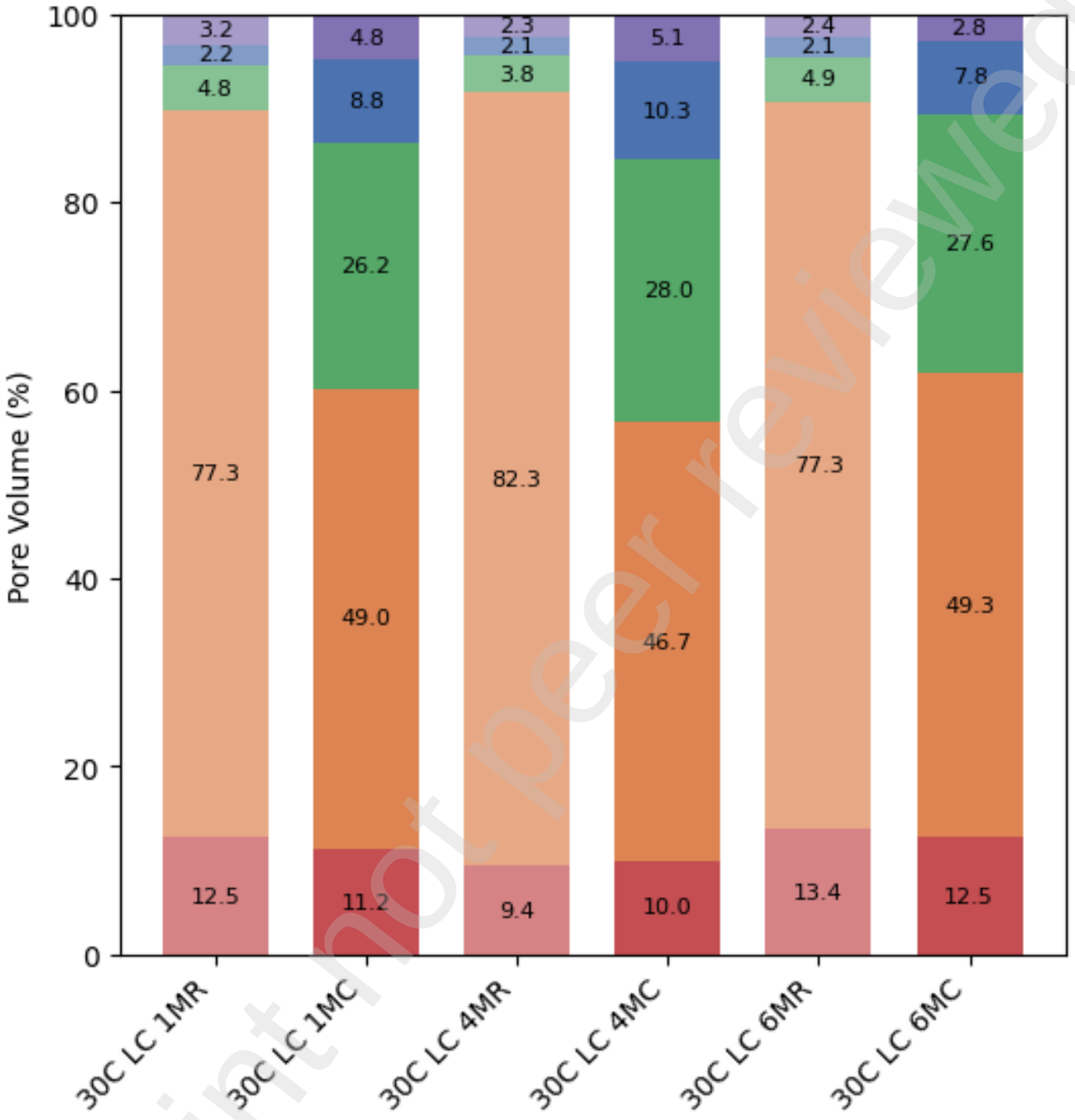

Preprint not peer reviewed

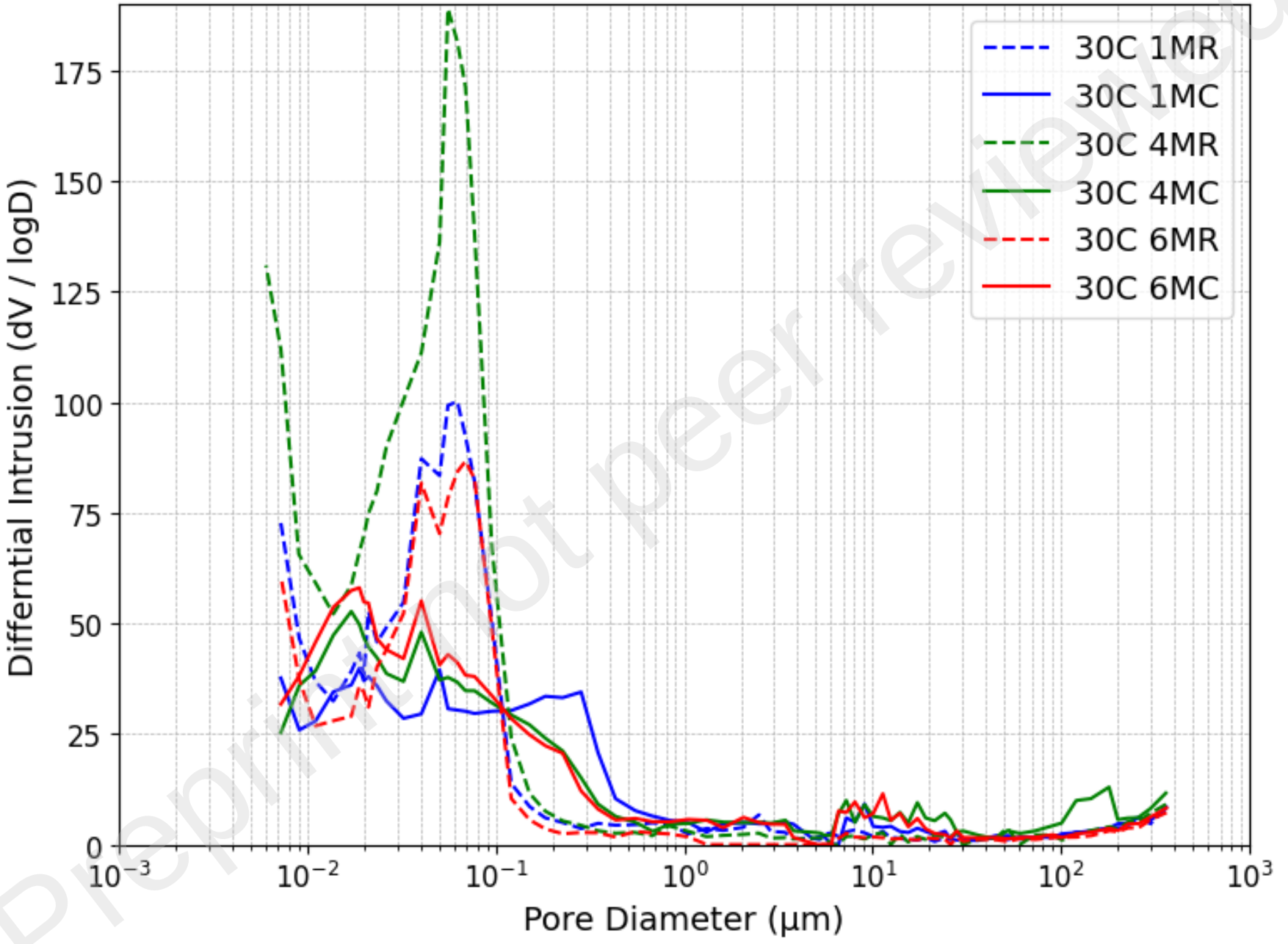

Preprint not peer reviewed

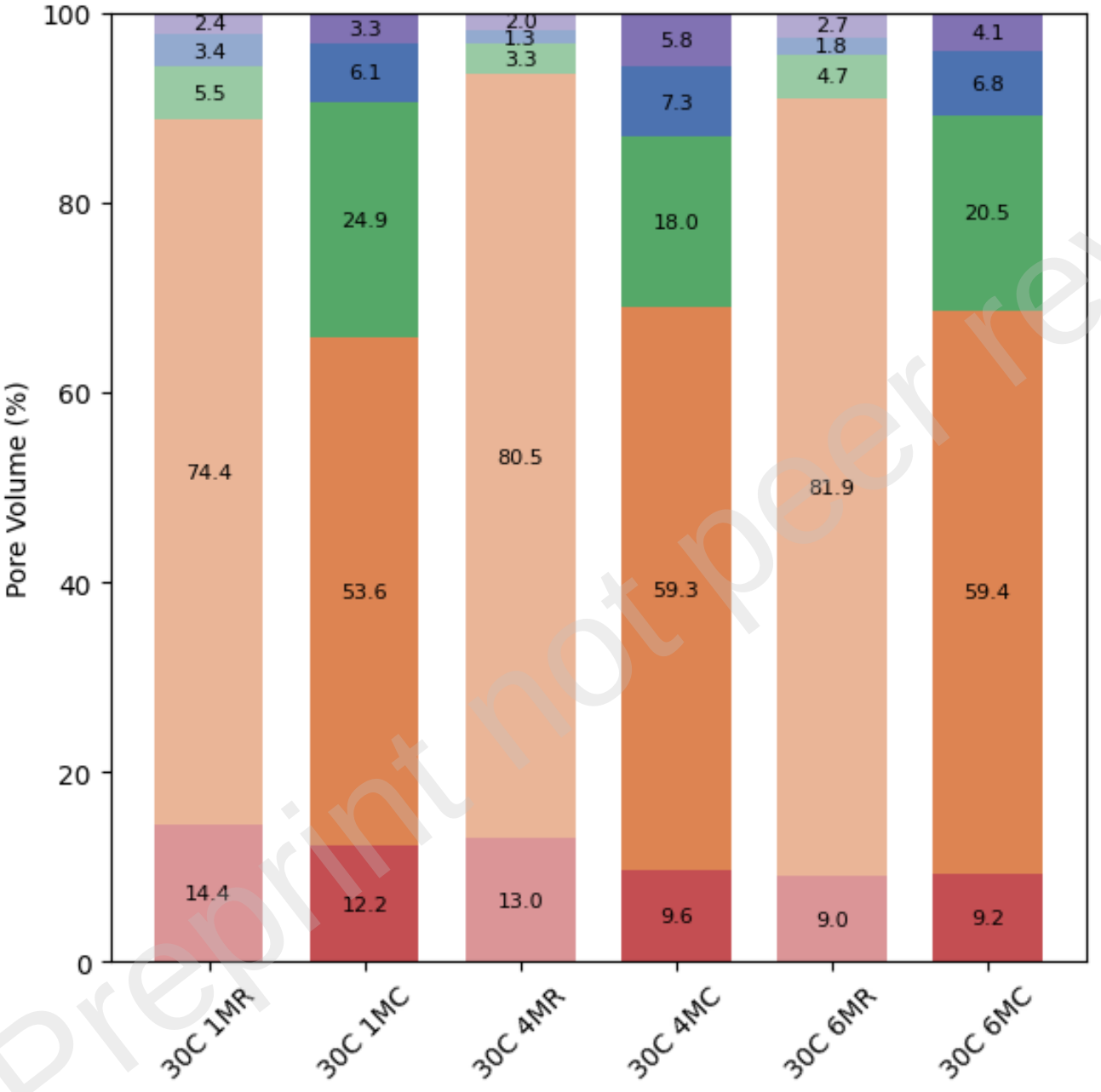

Preprint not peer reviewed

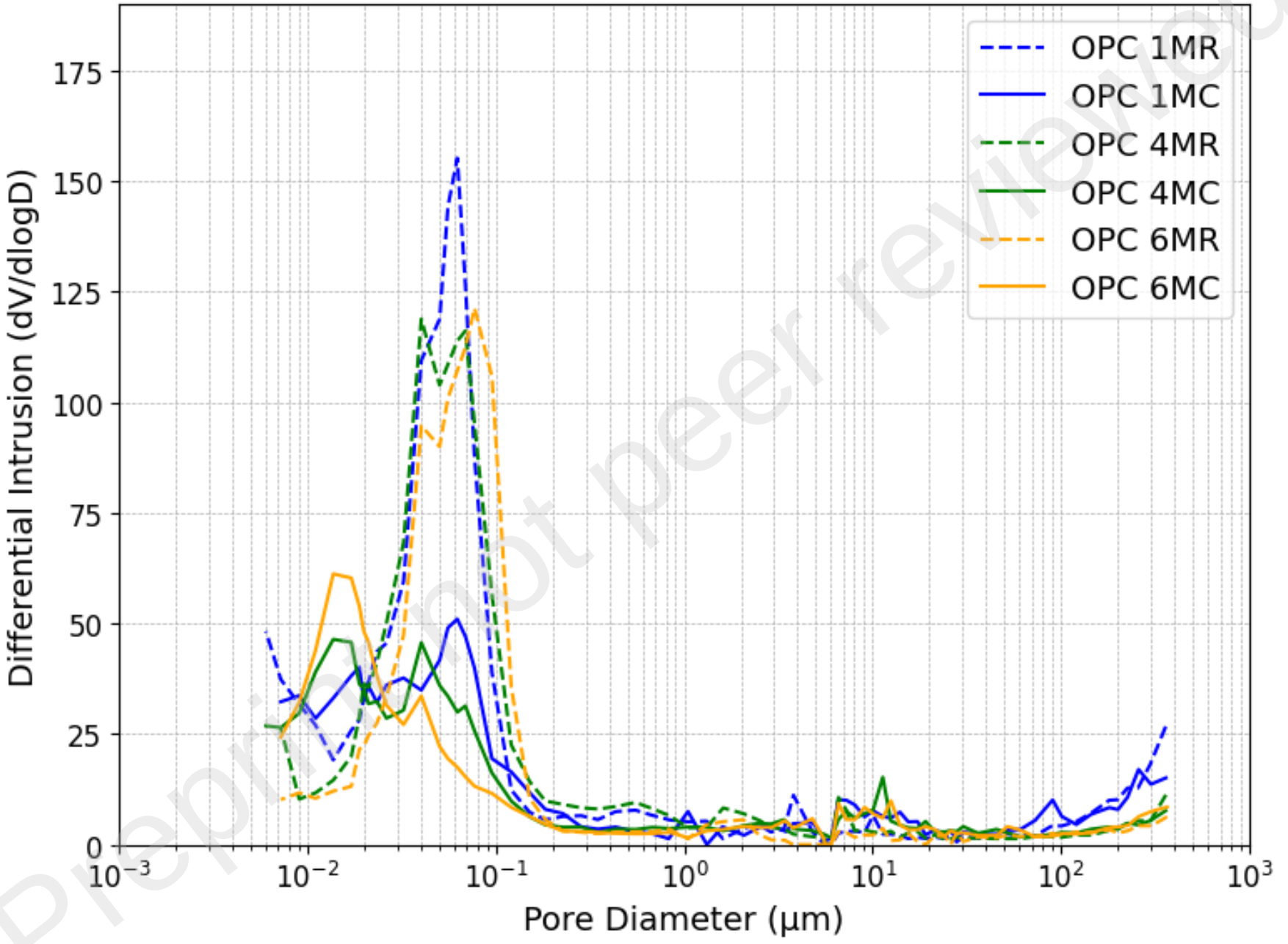

Preprint not peer reviewed

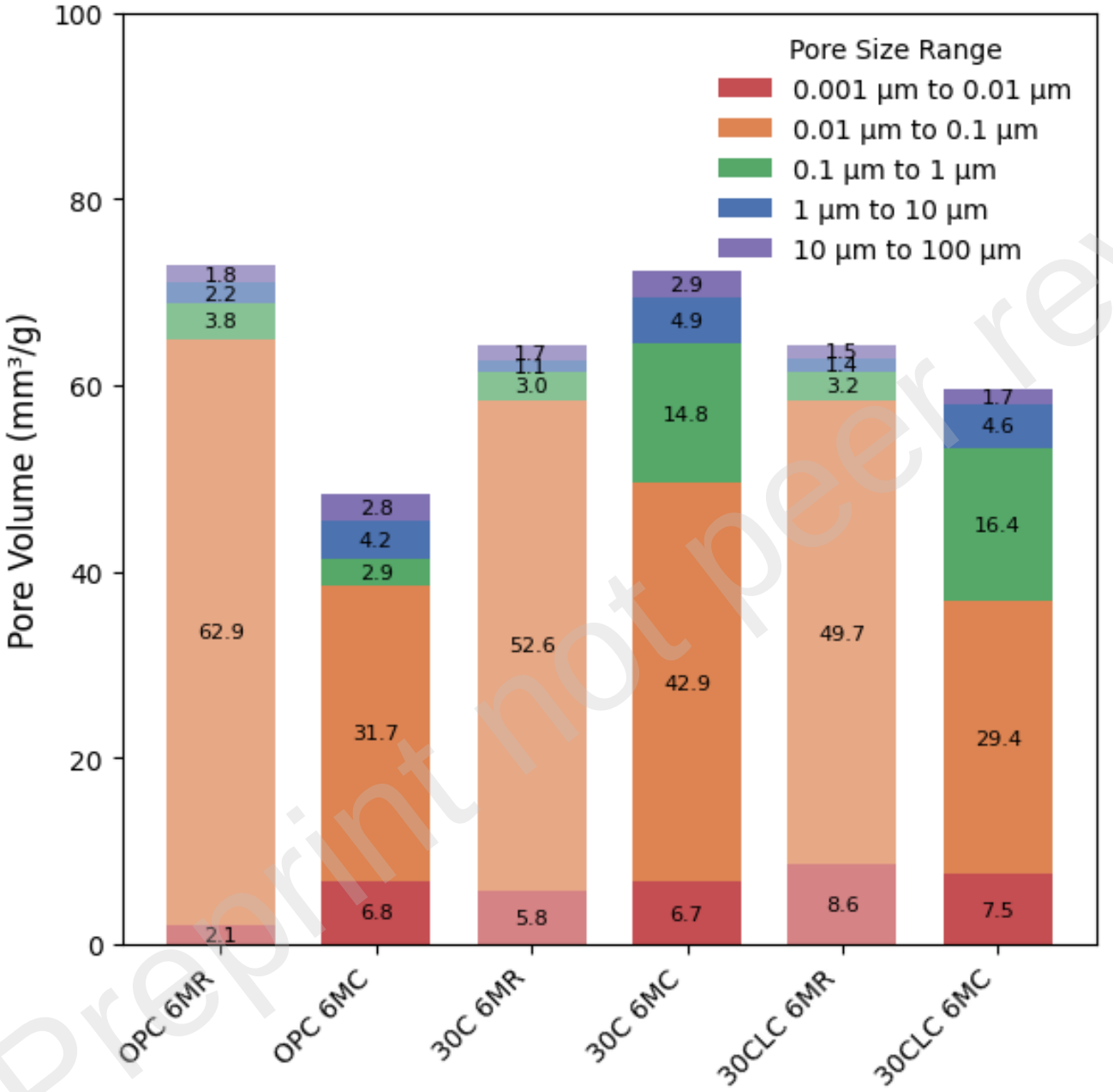

Preprint not peer reviewed

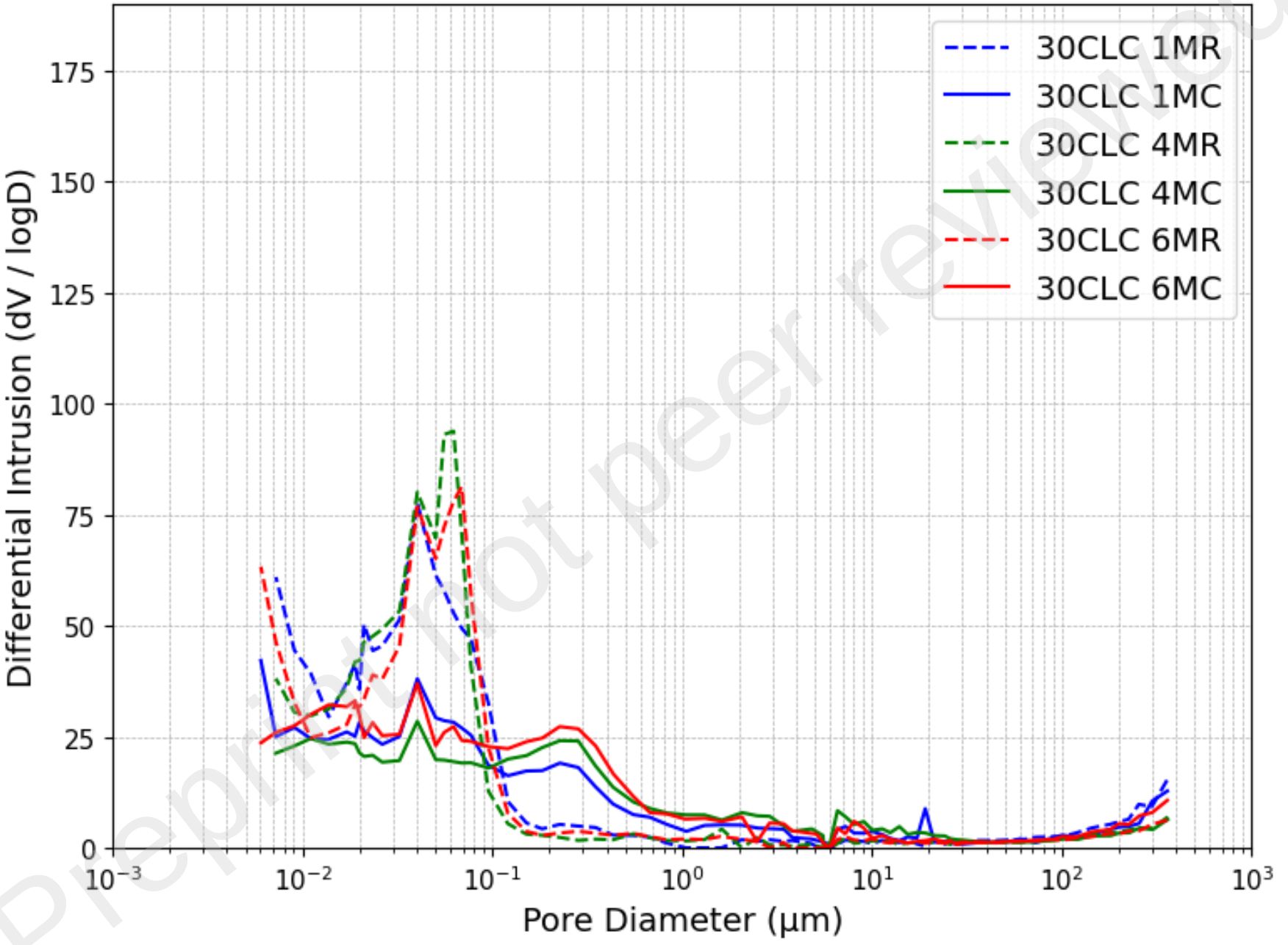

Preprint not peer reviewed

Table 1. Chemical composition of ordinary Portland cement and calcined clay

wt.%	SiO_2	Al_2O_3	Fe_2O_3	CaO	MgO	Na_2O	K_2O	TiO_2	SO_3	MnO	P_2O_5	SrO	BaO	LOI	Total
OPC	19.60	4.50	3.00	62.20	3.50	0.27	1.01	-	3.50	-	-	-	-	2.50	100.08
C	51.80	18.35	9.55	1.32	3.34	1.70	4.42	0.87	-	0.11	0.15	0.01	0.08	8.15	99.86

Table 2. Binder composition and curing durations

Sample Designation	SCM	Curing
OPC	-	28 days
30C	30% Clay	28 days
30CLC	30% Clay	100 days

Preprint not peer reviewed

This preprint research paper has not been peer reviewed. Electronic copy available at: https://ssrn.com/abstract=6205146